UNCLASSIFIED

AD NUMBER

AD857647

NEW LIMITATION CHANGE

TO

Approved for public release, distribution unlimited

FROM

Distribution authorized to U.S. Gov't. agencies and their contractors; Administrative/Operational Use; 24 JUL 1969. Other requests shall be referred to Army Missile Command, Attn: AMSMI-RER, Redstone Arsenal, AL 35809.

AUTHORITY

USAMC ltr, 29 Nov 1972

THIS PAGE IS UNCLASSIFIED

AD857647

ELECTRICAL

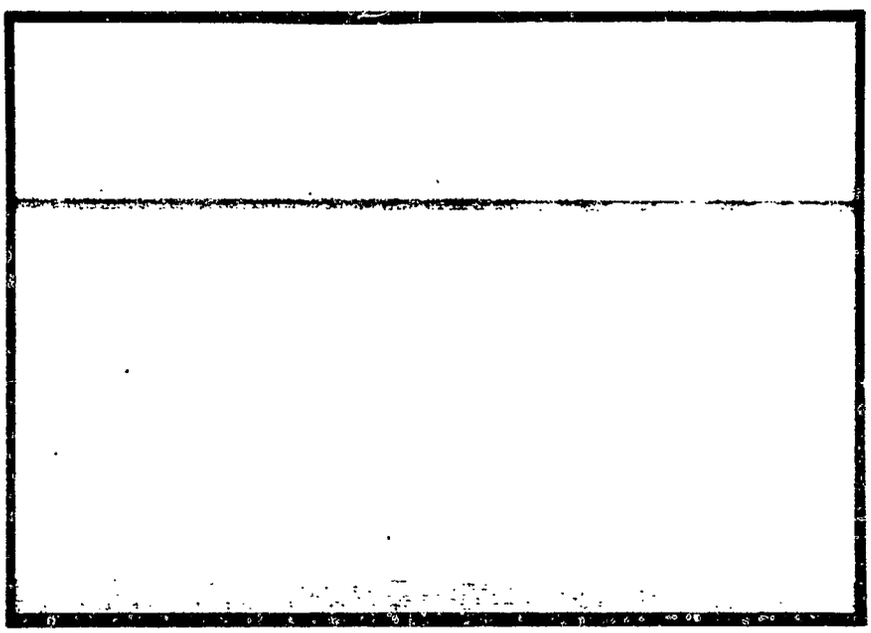

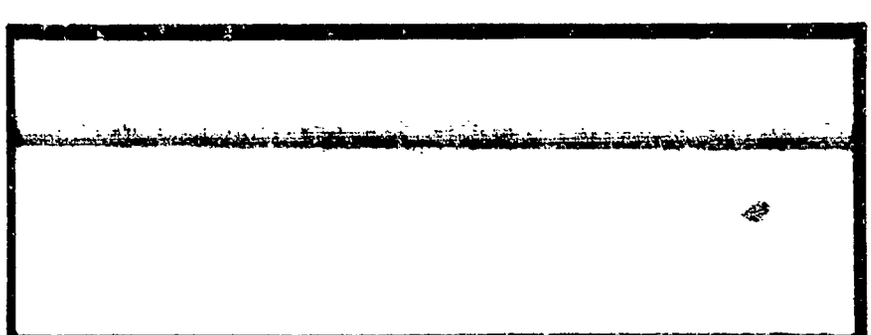

Reproduced by
NATIONAL TECHNICAL
INFORMATION SERVICE
U S Department of Commerce
Springfield VA 22151

DDC
SEP 2 1969
B

ENGINEERING EXPERIMENT STATION

AUBURN UNIVERSITY

AUBURN, ALABAMA

STATEMENT #2 UNCLASSIFIED

This document is subject to special export controls and each transmittal to foreign governments or foreign nationals may be made only with prior approval of ARMY MISSILE COMMAND
attn: AMSMI-RER
Redstone Arsenal, Ala. 35809

FINAL REPORT

CONTRACT DA-01-021-AMC 14525(Z)

VOLUME II: THE DETERMINATION OF GLINT FOR A COMPLEX RADAR TARGET

Prepared by

GUIDANCE SYSTEMS LABORATORY

E. R. GRAF, PROJECT LEADER

24 JULY 1969

This document has been approved for public release and sale; its distribution is unlimited.

This research is part of the project "Computer Smoothed Homing," Sponsored by the Future Missile Systems Division, U. S. Army, Department of Defense. Technical Direction of this effort is under the Army Missile Command.

APPROVED BY:

C. H. Holmes
Head Professor
Electrical Engineering

SUBMITTED BY:

E. R. Graf
Alumni Professor
Electrical Engineering

FOREWORD

This report summarizes part of a study performed by the Auburn University Electrical Engineering Department concerning the glint problem as applied to radar-guided homing missiles.

This volume of the final report describes the unclassified glint literature and a model used in the study of the problem, while Volume I contains a discussion of prior classified glint investigations as well as a summary of other research performed as a part of the project "Computer Smoothed Homing." This work was performed under the asupices of the Engineering Experiment Station, Inc., Auburn, Alabama, and was sponsored by the Future Missile Systems Division, United States Army, Department of Defense. Technical direction of this effort was under the Army Missile Command, Redstone Arsenal, Huntsville, Alabama, under contract DA-01-021-AMC 14525(Z).

ABSTRACT

The unclassified glint literature is described and discussed, with particular emphasis on applications of diversity. A computer-implemented model based upon the concept of coherent summation of contributions from independent scattering complexes is developed. The application of the model is illustrated using synthesized scattering patterns. Data processing techniques for frequency and space diversity are investigated with the model. The results indicate a significant reduction in RMS glint error is possible by the appropriate utilization of diversity techniques.

TABLE OF CONTENTS

LIST OF TABLES

LIST OF FIGURES

FINAL REPORT

CONTRACT DA-01-021-AMC 14525(Z)

VOLUME II: THE DETERMINATION OF GLINT FOR A COMPLEX RADAR TARGET

R. J. Sims and E. R. Graf

INTRODUCTION

As indicated in Volume I of this final report, the research performed under this contract may be divided roughly into three phases. Phase I dealt with the design and parametric study of a dual-mode sequentially-lobed antenna array and its use in a strapped-down radar seeker head, and also with the radar signature of vibrating targets. Phase II included the study of the target-image effect and the glint induced by simple geometric targets which subtend a significant part of a tracking antenna beamwidth. Phase III evolved from the latter part of Phase II. The goal of this effort was to compile a bibliography of the glint literature, analyze these prior investigations with particular emphasis on diversity techniques for reducing glint error, and to use this analysis to guide the formulation of a glint model for a complex radar target. The results of Phase I and Phase II are summarized in Volume I, which also includes a discussion of the classified glint literature analyzed under Phase III. It is the purpose of the present volume to report the unclassified

portion of the Phase III research effort.

Back-scattered wave-interference phenomena, which occur whenever a target of complex shape is illuminated by a radar with radiation wavelength much less than the physical dimensions of the target, can give rise to several different target scintillation effects. Among these are fading of the radar echoes with changing aspect angle, variation of the apparent range to the target, variation of the received radar frequency about the Doppler-shifted value expected from the radial component of the target velocity vector, and variation in the apparent angular location of the target with respect to the radar. This latter effect (glint) can introduce errors of such magnitude as to indicate the angular location of the target to be many target spans outside of the region occupied by the target itself. With the increasing radar precision being demanded by the space and missile age, such errors may soon be intolerable.

This report develops a technique which, with the aid of the modern digital computer, may provide a means of describing the glint phenomenon for a complex radar target. In order to demonstrate the basic glint behavior, a simple example will be enumerated. This will be followed by a review of the techniques and results of various glint investigations in the form of a brief history of the study of the problem. Finally, in the light of the previous investigations, a glint model will be developed. Emphasis will be placed upon maintaining sufficient generality and flexibility in the model to permit the analysis

of both theoretical target configurations and actual complex radar targets. Also, various forms of parameter diversity will be discussed in relation to their applicability in reducing glint errors.

II. AN ILLUSTRATIVE EXAMPLE OF GLINT

A general introduction to the nature of the glint phenomenon can perhaps best be accomplished through presentation of a simple example. It should be pointed out that target glint affects search radar as well as tracking radar, and that conical-scan, lobe-switching, and monopulse tracking techniques are all susceptible to glint-induced errors. However, a convenient case to examine is that of a lobe-switching radar tracking a pair of reflectors illuminated by a plane wave. This example is a classical one, and the development here essentially parallels that of Meade [1].

The lobe-switching tracking technique is the earliest form used for deriving an error signal proportional to the angular deviation of the target return from the boresight axis of the tracking radar. This is accomplished by comparing the received amplitudes of two antennas illuminating slightly different volumes in space. This situation is depicted in the polar diagram in Fig. 2-1. As shown by the linear plot in Fig. 2-2, the crossover of the two antenna patterns coincides with the boresight axis, θ_o, and the angular displacement of the beams from this axis, or squint angle, θ_s, is usually chosen such that the field pattern is down about 2 db from maximum at the crossover point. By restricting the analysis to angles near boresight, the shape of the patterns in this

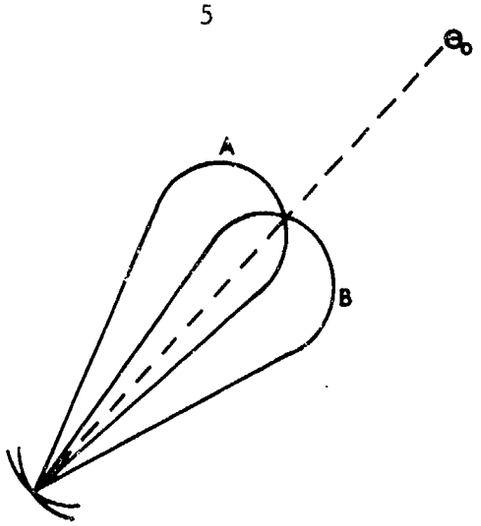

Fig. 2-1.--Polar lobe patterns for a sequentially-lobed tracking radar.

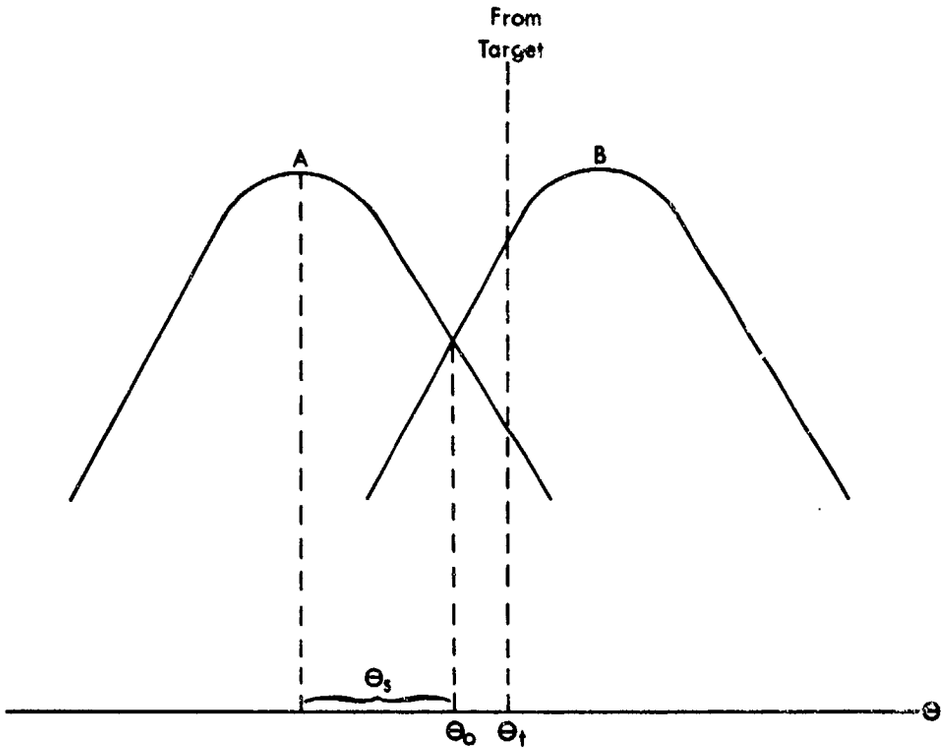

Fig. 2-2.--Linear plot of the patterns of Fig. 2-1.

region may be assumed to be linear functions of θ. (This is equivalent to expanding the pattern in a Taylor's series about θ_o and retaining the first two terms.) Letting the magnitude of the pattern slope in the crossover region be p, the amplitude response may be written

$$E = E_o[1 \pm p(\theta - \theta_o)] \tag{2-1}$$

where E_o is the response at boresight. If a single target reflector is located at an angle θ_T, the response of lobe A is

$$E_A = K[1 - p(\theta_T - \theta_o)]\cos \omega t \tag{2-2}$$

and of lobe B is

$$E_B = K[1 + p(\theta_T - \theta_o)]\cos \omega t \tag{2-3}$$

where ω is the radian radar frequency and K is a constant representing such parameters as target cross section and system gain. The radar receiver derives an angular error signal by sequentially sampling and square-law detecting the outputs of the two antennas, passing the resulting voltages through a low-pass filter which rejects all but the d-c and low-frequency terms, and forming the difference

$$\varepsilon = \overline{E_B^2} - \overline{E_A^2} \tag{2-4}$$

where the bar indicates the filtered value. Carrying out these operations,

$$E_A^2 = K^2[1-2p(\theta_T-\theta_o) + p^2(\theta_T-\theta_o)^2]\cos^2 \omega t$$
$$= K^2[1-2p(\theta_T-\theta_o) + p^2(\theta_T-\theta_o)^2][1/2 + 1/2 \cos 2\omega t]$$

and

$$\overline{E_A^2}=(1/2)K^2[1-2p(\theta_T-\theta_o) + p^2(\theta_T-\theta_o)^2].$$

Similarly,

$$\overline{E_B^2}=(1/2)K^2[1+2p(\theta_T-\theta_o) + p^2(\theta_T-\theta_o)^2]$$

thus,

$$\varepsilon = 2K^2p(\theta_T-\theta_o) \ . \qquad (2\text{-}5)$$

In operation, this error signal is used to command a mechanical positioner which aligns the radar boresight axis with the target return. Thus, when ε is reduced to zero, $\theta_o = \theta_T$ and the radar is properly tracking the target.

Now consider the case of a target comprising two reflectors, located at angles θ_{T1} and θ_{T2}. For a stationary target, the frequency of the two resulting returns will be the same, but the relative phase, α, will depend upon range and aspect angle. Letting a be the amplitude ratio of the two reflectors, the lobe responses are

$$E_A = K[1-p(\theta_{T1}-\theta_o)]\cos\ \omega t + aK[1-p(\theta_{T2}-\theta_o)]\cos\ (\omega t+\alpha) \qquad (2\text{-}6)$$

and

$$E_B = K[1+p(\theta_{T1}-\theta_o)]\cos\ \omega t + aK[1+p(\theta_{T2}-\theta_o)]\cos\ (\omega t+\alpha). \qquad (2\text{-}7)$$

Again carrying out the squaring and filtering operations,

$$\overline{E^2} = (1/2)K^2[1 \pm 2p(\theta_{T1}-\theta_o) + p^2(\theta_{T1}-\theta_o)^2]$$

$$+ aK^2\cos\alpha[1 \pm p(\theta_{T1}-\theta_o) \pm p(\theta_{T2}-\theta_o) + p^2(\theta_{T1}-\theta_o)(\theta_{T2}-\theta_o)]$$

$$+ (1/2)a^2K^2[1 \pm 2p(\theta_{T2}-\theta_o) + p^2(\theta_{T2}-\theta_o)^2] \qquad (2\text{-}8)$$

where the upper and lower signs correspond to lobes B and A respectively. The error signal is then

$$\varepsilon = 2K^2p(\theta_{T1}-\theta_o) + 2a^2K^2p(\theta_{T2}-\theta_o)$$

$$+ 2aK^2\cos\alpha[p(\theta_{T1}-\theta_o) + p(\theta_{T2}-\theta_o)]$$

$$= 2K^2p\{\theta_{T1}(1+a\cos\alpha) + \theta_{T2}(a^2+a\cos\alpha) - \theta_o(1+a^2+2a\cos\alpha)\}. \qquad (2\text{-}9)$$

Letting the angular spacing between the reflectors be $\theta_D = \theta_{T2} - \theta_{T1}$ and letting $\varepsilon = 0$ (an on-target indication), the boresight position becomes

$$\theta_o = \theta_{T1} + \theta_D\left[\frac{a^2 + a\cos\alpha}{1 + a^2 + 2a\cos\alpha}\right]. \qquad (2\text{-}10)$$

An examination of (2-10) for various cases is instructive. If reflector 1 is much larger than reflector 2 ($a \to 0$), then $\theta_o \to \theta_{T1}$, and, conversely, if reflector 2 dominates reflector 1 ($a \to \infty$), $\theta_o \to \theta_{T1} + \theta_D = \theta_{T2}$. These cases are equivalent to accurate tracking of a single reflector as described above. If the ranges to the reflectors are such that the received signals are in phase ($\alpha = 0$), then (2-10) reduces to

$$\theta_o = \theta_{T1} + \theta_D\frac{a}{a + 1} \qquad (2\text{-}11)$$

and the radar accurately tracks the amplitude "center of gravity" of the two reflectors. However, some values of α can lead to erroneous

tracking. Consider the case where the propagation paths from the reflectors is such that $\alpha = 180^{\circ}$. Then (2-10) becomes

$$\theta_o = \theta_{T1} + \theta_D \frac{a}{a - 1} \quad . \tag{2-12}$$

If, for example, a = 0.5, then (2-12) gives $\theta_o = \theta_{T1} - \theta_D$, and the radar tracks a point outside of the region between the reflectors. Thus the boresight position, or balance point, is seen to depend upon relative amplitude, relative phase, and the spacing between the two reflectors. This relationship is depicted in Fig. 2-3, which is a plot of (2-10) with amplitude ratio as a parameter. The boresight position, θ, is plotted in units of the spacing between the two reflectors, i.e., when the balance point is above or below the region defined by $\theta = \pm 1/2$, the tracking point is outside of the region between the reflectors. (Of course, physical limitations, such as antenna beamwidth, would prohibit the very large errors indicated as $a \to 1$.)

While this simple model should not be considered as realistic, it does demonstrate how glint can occur. It is also useful in that it suggests several possibilities for obtaining more accurate tracking information in the presence of glint.

If by some means two or more independent samples of the apparent target position could be obtained by the radar, then it is reasonable to presume that some computer processing or smoothing technique could yield a probable value more accurate than that indicated by a single sample. Because the glint error is strongly influenced by the relative phase between the echoes from the different parts of the target, some

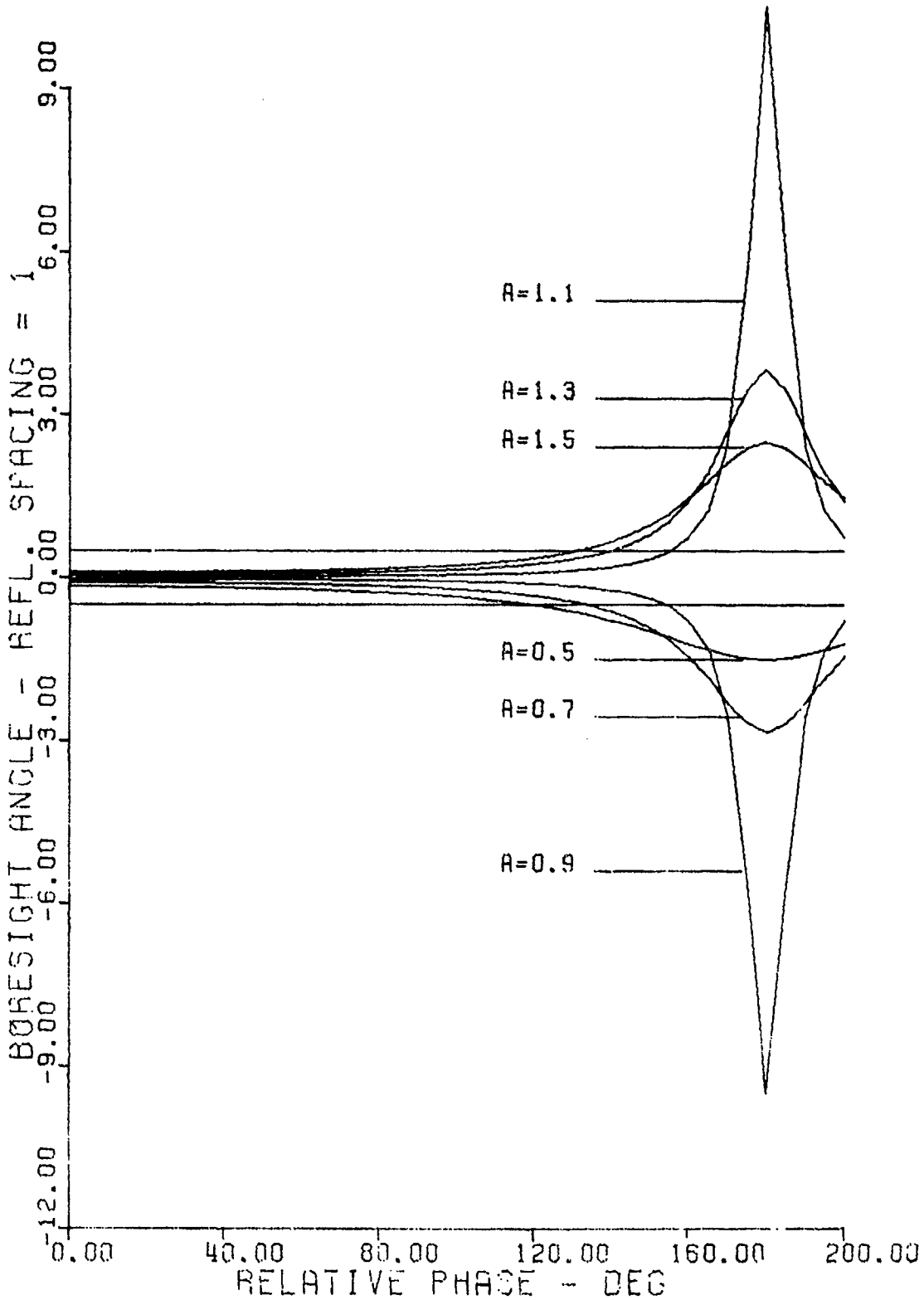

FIG. 2-3--BORESIGHT POSITION FOR TWO REFLECTORS

means of changing this phase would permit independent sampling of several values of target position. The phase is a function of the difference in propagation paths from the reflectors, thus viewing the target from a different aspect angle would change the relative phase. This could be achieved by tracking (or illuminating) the target from several locations, and might be termed space diversity. The separations would be chosen sufficiently large to yield independent samples. The phase also depends upon the radar wavelength. If the target is illuminated by frequencies over a sufficiently large bandwidth, independent balance points result. This technique is called frequency diversity. Finally, if the phase of the return from the reflectors is sensitive to the polarization of the incident illumination, polarization diversity might yield the desired samples. It should be noted that each diversity technique can also yield a relative amplitude change which might be beneficial. However, with the possible exception of polarization diversity, the amplitude sensitivity to the parameter changes is probably too small to be useful. Diversity techniques will be discussed in more detail in the following chapters.

III. SUMMARY OF PRIOR GLINT INVESTIGATIONS

A. Early History

Target scintillation effects were first observed in the form of target fading during early search radar experiments. This scintillation, which was basically amplitude noise, effectively reduced the maximum detection range of the search radar equipment.

Scintillation was soon observed in the testing of experimental tracking radars. Throughout most of the World War II years, the effects of target noise on tracking performance were thought to be easily explained as a direct result of amplitude scintillation introducing an additional modualtion component at the scanning or lobing frequency. Such modulation interfered with the desired tracking modulation produced by the conical-scan or lobe-switching mechanism. This theory was supported by the dramatic effects of propeller modulation on radar tracking noise [2]. Since this additional modulation due to amplitude scintillation affected the angle tracking loop via the scanning frequency, and because amplitude scintillation demonstrates a decreasing power density with increasing frequency, it was logical to attempt to reduce the effect by increasing the lobing or scanning rate. In fact, it was assumed that if a tracking mechanism could be devised which would derive tracking information from all lobes simultaneously (i.e., an infinite scanning rate), it would be possible to

eliminate the problem completely. It was this motivation which led the U. S. Naval Research Laboratory (NRL) to the development of a high-speed lobing radar (1943) and a simultaneous-lobing (monopulse) radar (1944). These units, however, upon testing did not yield the results which were expected. Rather, they showed that, at least at the short ranges tested, amplitude scintillation made a relatively small contribution to the total noise [2,3]. This suggested that another mechanism might be responsible for part of the observed tracking noise.

The advent of more accurate guidance systems produced a need for more accurate tracking equipment than that previously required. This need, together with the rather suprising NRL results, was responsible for several theoretical programs to study the phenomena in detail. The work began about 1947 and was done mainly by NRL, Hughes Aircraft Company, MIT, and several governmental and private concerns in Great Britain. Most of these organizations also initiated empirical studies of the target scintillation problem. While it seems that these efforts were originally reported between 1947 and the mid-fifties in classified documents the majority of the basic results had appeared in unclassified form in the professional journals by the late fifties. Additionally, some of the original documents are now declassified.

The initial theoretical work at NRL and elsewhere soon revealed that there was indeed another mechanism by which target scintillation could cause tracking errors. This effect -- glint -- was determined to originate in the changing relative phases of the received voltages

from various parts of a complex target. These time-varying phase angles, in the phasor summation performed by the antenna aperture, resulted in a time variation in the apparent angle-of-arrival of the radar return. As early as 1951, Brockner [4] published a paper discussing the relative relationship of the various forms of tracking noise, i.e. amplitude noise, glint noise, servo noise, and receiver noise. He concluded that at relatively short ranges, the glint noise was the predominant term.

While there was basic agreement as to the origin of glint, there evolved two schools of thought as to the appropriate modelling technique and interpretation of results. These might be loosely classified as the statistical approach and the deterministic technique.

Statistical methods

Statistical techniques were first developed by Delano (at Hughes, 1950) and later published in a paper which has served as the basis for many subsequent glint analyses [5]. Using as a model a set of isotropic secondary radiation sources located near the tracking axis and having statistically independent amplitudes and phases, he obtained an expression for the probability density of the fluctuation of the output of an open-loop tracker. He assumed that gross changes in aspect were sufficiently slow to guarantee stationarity of the assumed statistics of the model, and that the number of random scatterers was large enough to produce a Rayleigh distribution of the echo amplitudes. (Kerr [6] has determined that as few as five or six sources having independent phases and constant amplitudes is sufficient for Rayleigh

statistics.)

Muchmore, (also at Hughes, 1952) extended Delano's work to include the spectra of the reflected signals [7]. Using the statistical model and several different types of target motion, he derived expressions for the spectra of the amplitude scintillation and glint-induced fluctuations of the open-loop error signal. In a 1952 Hughes Technical Memo [8], Muchmore presented a review of the available experimental data on both amplitude and angular scintillation. This data consisted mainly of cross-section measurements and scintillation spectra for various aircraft, as obtained by Hughes and NRL. Because most of the data was obtained under widely varying conditions, he attempted to correlate the various results using the statistical model. Within the restrictions imposed by some of his assumptions and mathematics, he was successful in showing that at least the spread of the data obtained on various targets and by various experimenters could be made to agree.

Deterministic Methods

Concurrently with the work using the statistical approach to target modelling, other investigators were developing deterministic techniques. At the University of Texas, Feagin and Watson [9,10] used a multipoint target to obtain the balance point (the point the radar would track if its servos were infinitely fast) for both a conical-scan radar and for a monopulse radar which used amplitude in one tracking plane and phase in the other. At Ohio State, Peters and Weimer [11,12] used the coherent summation of contributions from a similar model and derived general expressions for the balance point of various

types of radars. Defining the pointing error as the difference between the actual balance position of an ideal tracker and the balance position which would exist if the signals from all the point scatterers arrived in phase, they established bounds for this quantity in terms of the ratio of the total amplitudes received under these two conditions. The Ohio State group also made extensive measurements of balance point and cross-section for various geometrical shapes.

Lewis, [13], further developed the technique of Peters and Weimer to show that conical-scan and phase monopulse radars (ideally) track the phase center of the target. This result was determined from a mathematical development for the balance point, as measured from some reference point on the target, in terms of the total field phase at the radar. The balance point was seen to vary directly as the derivative of the phase with respect to change of aspect angle.

While Lewis did not state it as such, the derivative of phase with aspect angle is actually the slope of the phase front, or line of constant phase. The concept of visualizing angular scintillation as distortion of the echo phase front was reported by Howard of NRL in late 1959. This concept has probably contributed more to the understanding of glint than any other work. In his report [14], Howard showed that the slope of the echo signal phase front is identical to the angular error for both dual- and multi-point targets. He further reasoned that since the distortion is a property of the backscattered wave, glint affects all angular-locating devices, even search radar.

Analog Simulation

Because it was evident that much of the discrepancy between various experimental measurements was due to the difficulty of controlling the experimental variables, particularly of an aircraft in flight, considerable effort was devoted to the development of laboratory glint simulators. MIT devised a simulator for the case of a two-point-source target and an interferometer-type tracker [15]. By 1956, NRL had constructed a closed-loop simulator capable of generating tracking data for various multiple-reflector rigid body targets having a variety of random target motions [2]. This simulator was particularly useful in subsequent studies of the effects of servo bandwidth, target noise bandwidth, and AGC characteristics on closed-loop tracking performance. However, it was partially limited in that it had no provision for non-random relative motion of different parts of the target, as might be caused, for example, by flexing of control surfaces.

AGC Studies

Because the effect of target glint is to introduce a component of target noise into the tracking loop, several theoretical, simulation, and experimental investigations were undertaken to determine the effect of automatic gain control time-constant on this noise [2,7,16, 17]. It was generally agreed that a slow AGC reduced the angle fluctuations. However, Howard [17], showed that a slow AGC enhances a new noise component, proportional to true tracking errors, which is due to amplitude noise modulation of tracking-error signals. He concluded that, because of the relative magnitudes of these two noise

components under most tracking conditions, a fast AGC would minimize over-all tracking noise.

B. Recent Contributions

The first literature of this decade appeared in the form of a debate between the major advocates of the two differing approaches to glint modelling. Commenting on the 1960 unclassified version of Muchmore's scintillation spectra work [7], Peters and Weimer questioned the validity of the assumption of using a random distribution of scatterers as an aircraft model [18]. They stated that if the range of aspects is restricted, or if the time of observation is held to the order of one second (a typical servo response time), the amplitude of the echo is not likely to be Rayleigh distributed. Because Delano reasoned that the Rayleigh statistics of observed data (which was obtained over wide aspects) indicated that five or six scatterers with equal amplitudes and random phases was an appropriate model, the absence of Rayleigh statistics (in an actual tracking situation) might invalidate such a model. Peters and Weimer further noted that their studies of cross-section patterns of two different aircraft indicated that the depth of successive minima and the magnitude of successive maxima tend to repeat. Such a repetition would not exist if there were more than two effective scatterers. They concluded their criticism of the indiscriminate application of Delano's model by attempting to demonstrate discrepancies which arise when the model is used in the analysis of the two-point target and linear scatterer cases. In essence, they showed that, using Delano's results, there was no pointing error for

the case of equal scattering amplitudes, except at null points, where the amplitude of the return is zero. Because error was known to exist, it was argued that this descrepancy illustrated the inadequacy of the statistical model.

In the same issue of the IRE Transactions, Muchmore replied to the comments of Peters and Weimer [19]. He refuted their descrepancy argument by pointing out that, for the two source target, the region of the nulls is exactly the region where the glint error occurs. (This is in agreement with the findings of Howard [14]). Because in practice the probability of all scatterer amplitudes being exactly the same is essentially zero, he stated that the case of similar, but not identical, amplitudes is more instructive. In this case, the nulls do not go completely to zero, thus the return can be detected and glint observed. With regard to the question of the number of scattering centers effective over small aspect angles, Muchmore's reply was more qualitative. He simply pointed out that the assumption of many random scatterers was the most reasonable.

The debate was continued in a subsequent issue of the Transactions, with communications from Delano, Peters and Weimer, and Siegel (of the University of Michigan) [20,21,22,23]. No new information was revealed by these discussions, with one possible exception. Delano noted that aircraft model measurements by Radiation, Inc. indicated that echo amplitudes were Rayleigh distributed over as little as 5° of aspect angle. The importance of this fact was, of course, challenged by Peters and Weimer, who pointed out that, because of typical aircraft velocities

and tracking servo response times, 0.5° was a more appropriate observation interval. Their contention that the Rayleigh distribution may not hold over such a small angular increment is supported by Katzin [24], whose presentation of measurements on a B45 aircraft show that Rayleigh-distributed envelopes are observed only if the aspect angle changes by more than four degrees over the period analyzed. In an Australian study, Moll [25] also observed a departure from the Rayleigh distribution during portions of experimental runs.

There have been several glint-oriented papers published in the open Russian literature. Ostrovityanov [26] observed that the results of several American investigators had indicated a possibility that the angular error could become infinite. Because this is not a practical result, he outlined a mathematical development which seems to indicate that Meade's result for the boresight angle [1] should be instead for the tangent of that angle. (This is a plausible result, for the infinite argument which arises in the case of two equal-amplitude, oppositely-phased sources would then lead to a boresight angle of 90°, in agreement with the phase-front concept of Howard [14]). He also presented a detailed statistical development in which he refined the probability density expressions of Delano to account for certain physical discrepancies. Gubonin [27] extended Delano's results to include the probability density function for glint when there is one sinusoidal, deterministic reflector included among the random, independent reflectors. For this case, the density function is more narrow than that for random reflectors alone, i.e., it is less probable that the apparent target

position lies outside the extent of the target. It was the existence of such a dominant deterministic reflector which Moll believed responsible for the observed departure from Rayleigh statistics [25].

In 1967, the Battelle Memorial Institute began the task of performing a complete study and analysis of the glint literature (both classified and unclassified) as applied to air defence missile system design. Their report, an excellent analysis of all glint investigations, includes an unclassified description of a "universal glint model" [28], which was apparently developed as a continuation of the work of Peters, et. al., at Ohio State.

The Battelle approach was a deterministic one, but it was unique in that it did not require isotropic sources. Instead, it was based upon the coherent summation of the fields due to "scattering complexes," or extended-target reflectors, which may represent, for example, aircraft control surfaces or jet engine intakes. Assuming such complexes to be non-interacting, the non-isotopic amplitude and phase patterns of each complex are measured on a coherent, static cross-section pattern range, and the total target field obtained by the summation of the appropriate contributions from the complexes. For cases where complexes are interacting, due to coupling or multiple reflections, these complexes are lumped together and considered as a single complex. Using the summation expression for the total field, Battelle obtained the direction of the normal to the phase front by taking the gradient of the phase term. The spatial derivatives of the amplitude and phase components of the individual complexes, which result from the gradient

operation, are obtained from the measured cross-section plots. Relative motion between complexes is included by adjusting the individual phase terms to include differential Doppler.

In discussing the model, Battelle reached one conclusion which differed from a generally-accepted hypothesis concerning the correlation between glint errors and echo-amplitude minima. Howard [17] and others had postulated that there was a negative correlation between these quantities, i.e. glint error was maximum at regions of local minima. This correlation was based upon an extension of the two-point-source case. The Battelle model indicated that a field minima from any complex would result in large glint error. Such a component minima would not, in general, correspond to a general amplitude null.

The most recent contribution to the glint literature was from Dunn and Howard of NRL [29]. Their objective was to show that glint for a complex target corresponds to a deviation of the Poynting vector from the radial direction, and thus a corresponding deviation in the direction of the power flow. To demonstrate this, they assumed a target model consisting of a collinear, non-uniform array of electrically short dipoles. Because the spatial patterns of the electric and magnetic fields from such an element are well known, it was mathematically feasible to determine the total E and H fields resulting from the coherent summation of the individual element fields at a general observation point. The analysis using these total fields showed that there was indeed a component of the time-averaged Poynting vector orthogonal to the radial direction. This proved that the power flow is not necessarily

radial, and, at a given observation point, may be in such a direction as to indicate the target position to be outside the actual target span. Because of this, even the simple search radar is susceptible to glint. This was illustrated by observing the change in the measured pattern of a horn antenna, as the relative phase between a closely-spaced pair of illuminating horns was varied. The authors discussed the glint averaging effect of a finite antenna aperture, and developed equations for relationships between Doppler and angular scintillation. They also discussed the effects of various diversity techniques; these comments will be further reported in the next section.

C. Application of Diversity

As early as 1956, Peters and Weimer [11] suggested two diversity techniques which might be used to reduce pointing errors. Both of these seem to be based on the concept that maximum error occurs at amplitude minima. The first suggestion was to servo-control the radar frequency to maintain the amplitude of the return within certain limits. The other idea was to accept and clamp the error signal to the servo only when the amplitude is greater than a certain minimum value.

Birkemeier and Wallace [30] investigated the case of pulse-to-pulse frequency modulation for possible angle tracking accuracy improvement. They used a statistical target model consisting of elements uniformly distributed along a strip and having independent random phase angles. Their motivation in performing the study was that the glint-inducing phase interference effects from the target could be made to occur more rapidly by progressively varying the radar carrier frequency.

Ray [32] analyzed the improvement in radar range and angle detection with frequency agility. He stated that the amount of frequency shift necessary for decorrelation of the returns from a target is a function of the range dimensions of the target complex. He analyzed both the case where the target range dimension is much less than the range resolution of the radar, and the case where this dimension approaches or exceeds the range resolution. In both cases, a significant improvement in performance was predicted. While his discussion of angle detection was restricted to the angular-locating accuracy of a search-type beam, much of his analysis should be applicable to automatic tracking radars.

The most pertinent discussion of diversity (as applied to improved radar tracking) to appear in the open literature was contained in the recent paper of Dunn and Howard [29]. The authors first commented on space diversity, as achieved by locating several radar receivers at positions widely separated with respect to the phase-front distortion pattern. Each receiver then observes independent samples of angular scintillation. The average of the various error-signal outputs thus exhibits a reduction of target noise power. The authors point out that the averaging provided by an antenna when the phase-front distortion region spans a large portion of the antenna aperture is also a form of space diversity. Frequency diversity is indicated as another technique for averaging target scintillation, either instantaneously or within a short period of time. The object is to provide sufficient separation between frequencies such that the scintillation at each frequency is uncorrelated with that at the other frequencies. An example presented shows that,

for two reflectors displaced by 10 yards in range, a frequency change of 18 MHz causes a full cycle of change in the received relative phase. The authors note that space-diversity effectiveness is determined by the angle subtended at the target, while frequency-diversity effectiveness is determined by the range distribution of the target. It may therefore be possible to combine effectively the two techniques. In the case of polarization diversity, the effectiveness is dependent upon the polarization characteristics of each scattering element. It was also noted that some of the deeper signal fades may be averaged by diversity techniques.

D. Elevation Error Studies

There exists another problem in radar tracking which has an effect quite similar to that of target glint. This problem is the multipath phenomenon, which produces elevation errors when a radar is tracking a target at a low elevation angle above the earth. Because the radar receives a return from the target image in the (partially) conducting earth's surface, in addition to the direct return from the target, and because these returns are from slightly different angles, the effect is quite similar to the glint caused by the two-reflector target. There have been many analytical and theoretical studies of this glint-related problem. Much work has been done in England by the RRE and others [33, 34] and the effect is discussed in several texts and reports (e.g. [6,35]).

E. Comments

The preceding summary of investigations is not intended to be an

exhaustive survey of all glint studies. However, it is felt the material covers the major contributions, as reported in the open literature, in sufficient detail to indicate the direction of the glint research efforts.

Several conclusions might be reached concerning prior glint studies. It appears that the various investigators have lacked unity of purpose in the design and techniques of their analytical and experimental efforts. This is no doubt due to the extended period of time during which the studies were conducted, and the varying research goals of the various facilities doing the research. However, in some cases it may be that the research was performed to substantiate the need for a particular radar design or tracking technique; in such cases the common research goal of increased understanding of a problem may have suffered.

The lack of unity of purpose of the various researchers is most evident in the reports of experimental series. The parameter studies have ranged from true glint (property of the propagating wave front) to tracking noise, as measured by both open-loop and closed-loop receiver output voltages and with and without amplitude scintillation effects removed. In addition, the data may be referenced to a fixed point on the target or to the radar "center of gravity," and may or may not include the effects of boresight errors. In many cases, it is not possible to ascertain which of these forms of the glint parameter was measured. Such vast differences make it extremely difficult to compare the various results. For this reason, considerable planning should go into the development of any future measurement programs to insure that the effect being measured is glint alone, and that the results depend

as little as possible upon the radar used in the measurements. In fact, it might be more efficient to postpone extensive test programs until more analytical model computations have been performed. An experimental effort could then be devoted to verification of these computations by measurements at a few carefully selected sample points.

With regard to the debate of statistical vs deterministic modelling techniques, it is probable that a better model is one which incorporates features from both types. Peters and Weimer argued that the requirement for six or more scatterers to be active over all aspect angles is too stringent. This seems to be a valid point. Additionally, the statistical model demands stationary statistics. However, Delano's contention concerning the impracticability of knowing the exact amplitude and phase contributions from all scattering points on a moving target also seems valid. Howard has noted that random roll, pitch, and yaw of an aircraft target in flight can only be described statistically. Thus, although it seems that Delano's statistical model may not be valid for real targets (because of the number-of-scatterers and stationarity limitations), it would be most desirable to be able to include regular and random relative or rigid-body motions of the target into a deterministic model that does not require the assumption of isotropic point scatterers. The technique of coherent summation of the contributions from scattering complexes, as introduced by Battelle, provides a basis for such a model. Because the contributions of the various complexes are measured quantities, the computed return-field configuration is realistic. The statistical nature of the field when the target has relative or rigid-body motion

might then be determined analytically be appropriately modifying the phase terms of the individual contributions. In this way, no statistical stationarity is required, and the basic non-isotropic nature of the scatterers is preserved.

The remainder of this study will be devoted to the development and implementation of an analytical glint model which will be based upon the Battelle concept of coherent summation of the contributions from non-isotropic scattering complexes. The method of obtaining the glint information from the resultant total field, however, will be considerably more straightforward than the Battelle gradient approach, and one which is easily implemented on a digital computer.

IV. DEVELOPMENT OF A GLINT MODEL

It was noted near the end of Chapter III that the Battelle concept of a target model composed of independent, nonisotropic scattering complexes seems to be a very realistic one. However, the mathematical processing of the measured scattering complex data, as developed by Battelle, involves the gradient of the phase term. It thus requires not only the measured amplitude and phase patterns of the complexes, but the slope of these patterns in orthogonal directions at each point in space as well. The resulting expression for the direction of the normal to the phase front is rather complex. Moreover, the actual amplitude and phase of the total field is not a direct result of the process of evaluating this expression. It is reasonable to presume that a deterministic model which would characterize the amplitude and phase of the reflected wave, in addition to the normal to the phase front, might prove very useful in formulating a signal processing scheme to reduce glint error. This can be achieved by forming the coherent sum of the contributions from the scattering complexes (with the phases modified for motion, if required) and then using simple geometrical relationships to determine the glint error. Information concerning dynamic effects, such as the spectra of amplitude and angle scintillations during a particular type of target or tracker maneuver, can be determined by an appropriate point-by-point analysis.

It should be evident that an exact representation of the glint signature at various aspect angles for a single target will have little resemblance to the exact values at the same angles for another target, even if the two are quite similar. The precise structure of the back-scattered interference pattern is too dependent upon target surface configuration to permit such a simple extrapolation of results. Indeed, because of the extremely fine lobe structure of the cross-section pattern for a large, complex target, the amount of data and the number of calculations necessary to form a complete sphere of information even for a single such target may be prohibitive. Also, the radar wavelength at microwave frequencies is very small compared to typical distances between scattering complexes. An actual target in flight probably has flexing motion between complexes amounting to appreciable portions of a wavelength. Thus the task of determining the exact coordinates of the complexes with respect to the overall airframe of a particular target cannot be accomplished.

It might seem that the limitations just discussed would negate any utility of a deterministic model. However, it is emphasized that the motivation in the development of the model to be described is to permit the exact computation of representative field parameters over representative aspect sectors for representative classes of targets. Then a determination of the dynamic behavior of these parameters along a realistic series of sample points within each sector can be made. Such a procedure will permit the analytical evaluation of various compensation and smoothing schemes in a set of realistic field

environments.

Several basic assumptions are necessary before beginning the development of the model. It is presumed that the technique of representing a radar target by an array of scattering complexes is valid. This assumption demands that the scattering pattern of each complex be independent of other complexes, and that insignificant error be introduced by the physical dissection of the target into scattering complexes, e.g. edge effects at lines of dissection. Moreover, it is necessary that, at ranges of interest for the complete target, the fields of the individual complexes have a far-field amplitude and phase variation with range. (The validity of this assumption will be investigated in a following section.) The discussion will be oriented toward the problem of a monostatic tracker in a homing situation; however, the techniques can be applied to any tracking radar, although a bistatic configuration would be more involved.

A. Obtaining Amplitude and Phase Patterns for the Scattering Complexes

For maximum versatility of the model in studying the effects of diversity on glint behavior, it is desirable that the amplitude and phase data for individual scattering complexes be recorded with frequency and polarization as variable parameters. (A discussion of space diversity will be delayed until a later section.) A possible scattering range implementation for obtaining the data is depicted schematically in Fig. 4-1. This configuration permits the recording

of the amplitude and phase of orthogonal components of the reflected signal, as a function of the aspect angle of the scattering complex and the transmitted polarization and frequency.

The transmitter comprises a backward wave oscillator (BWO) which is frequency-stepped by an analog voltage from a frequency programmer. For each frequency increment, a polarization programmer alternately connects the BWO to horizontally and vertically polarized feeds on the transmitting antenna by means of a SPDT diode switch (SW).

Horizontally and vertically polarized feeds on the receiving antenna provide simultaneous signals to separate phase-and-amplitude receivers. (A single receiver could be used on a time-shared basis.) A sample of the BWO output provides the required phase reference for the receivers.

The target positioner has two degrees of freedom about some defined coordinate origin on the scattering complex (azimuth and elevation angle variations) and is controlled by a positioner programmer. This programmer, together with the frequency and polarization programmers, provide digitally-coded outputs identifying the aspect angle, frequency, and polarization parameters. This data is recorded on magnetic tape, along with the digitized amplitude and phase outputs of the horizontal and vertical receivers. Synchronism of the various parameter changes is maintained by a clock.

Several comments regarding the range implementation just discussed are in order. It is envisioned that the coherent static measurements would be made on a large, ground-level radar range such as the RAT SCAT

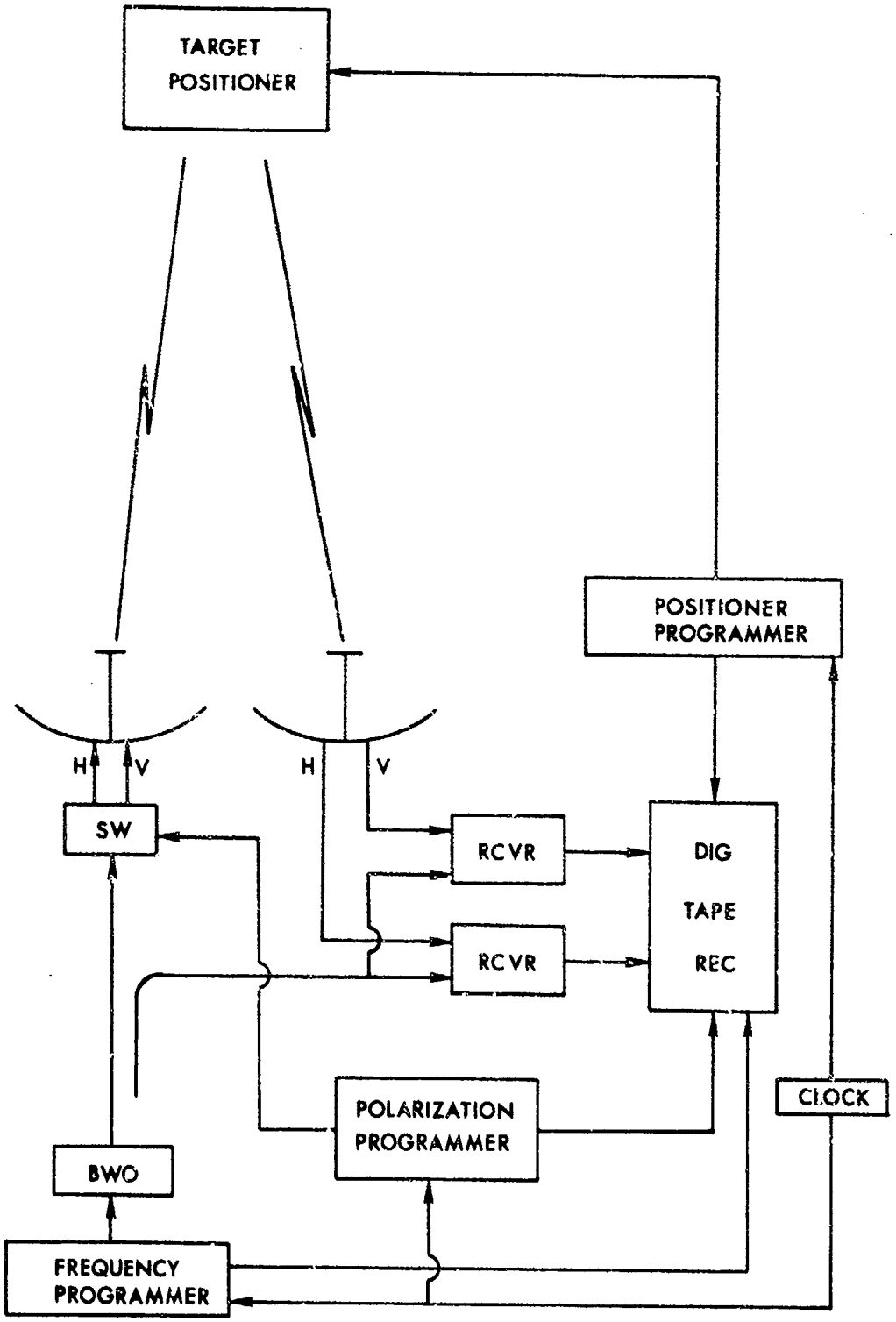

Fig. 4-1.--Scattering range implementation.

facility in New Mexico [36]. Because such a range utilizes the multipath effect in achieving target illumination and receiving the radar return, it actually has a finite bandwidth associated with a particular combination of antenna and target heights. Since the proposed range tests involve measurements over a band of frequencies, a careful study should be made to verify that this band is within the operating bandwidth of the range.

Because the validity of this model depends upon the summation of appropriate field contributions from the various complexes, the registration accuracy with which each complex is mounted on the positioner pylon will be of extreme importance. Also, care should be taken to be sure that the physical size of the complex is within the limits imposed by the range length and antenna diameter. If the data is to be essentially independent of the type of antenna used in the measurements, uniform illumination across the aperture is desired. Caster [37] states that if a complex target subtends less than 1/8 beamwidth, this condition will be achieved. Thus, using the approximate relationship for beamwidth of a uniformly illuminated aperture, $\theta_B = \lambda/D$, a 1 meter dish operating at 10 GHz would permit a maximum target dimension of 3.75 meters at a range of 1 km.

Transmitting alternate orthogonal linear polarizations, as opposed to continuous circular polarization, is preferred because, with this measurement technique, the phase of the received signal is not lost, as in the case of a conventional range receiver using a bolometer (integrating) detector. The rotation frequency of the linear electric

rotation of the two degrees of freedom for the scattering range positioner. Assume the range to the positioner to be constant for all scattering measurements and let frequency be a fixed parameter. Then, for a specified receiving polarization, the amplitude and phase data are a function of the coordinates θ^i and ϕ^i, as measured in the system centered at 0_i. Now let a spherical coordinate system, with origin 0, be associated with some point on the target. The aspect point P, at coordinates (r,θ,ϕ), and thus all field values determined from the model, will be referenced to this origin. Finally, let the location of each origin 0_i, relative to 0, be specified by the coordinates (d_i,θ_i,ϕ_i), and let all coordinate axes have the same relative orientation. This geometry is shown in Fig. 4-2.

Propagation path determination

Because the technique of coherent summation uses the amplitude and phase contribution from each complex at the field point P, it is necessary to know the spatial attenuation and phase retardation over the propagating path from each complex. These effects can be easily determined if the distance from P to each secondary origin is known. To derive an expression for this distance, consider the geometry shown in Fig. 4-3, where the secondary origin is denoted by 0". From the law of cosines,

$$D^2 = r^2 + d^2 - 2rd \cos \alpha \qquad (4\text{-}1)$$

or

$$D^{-1} = [r^2 + d^2 - 2rd \cos \alpha]^{(-1/2)} .$$

$$= (1/r)[1 + (d/r)^2 - 2(d/r) \cos \alpha]^{(-1/2)} \qquad (4\text{-}2)$$

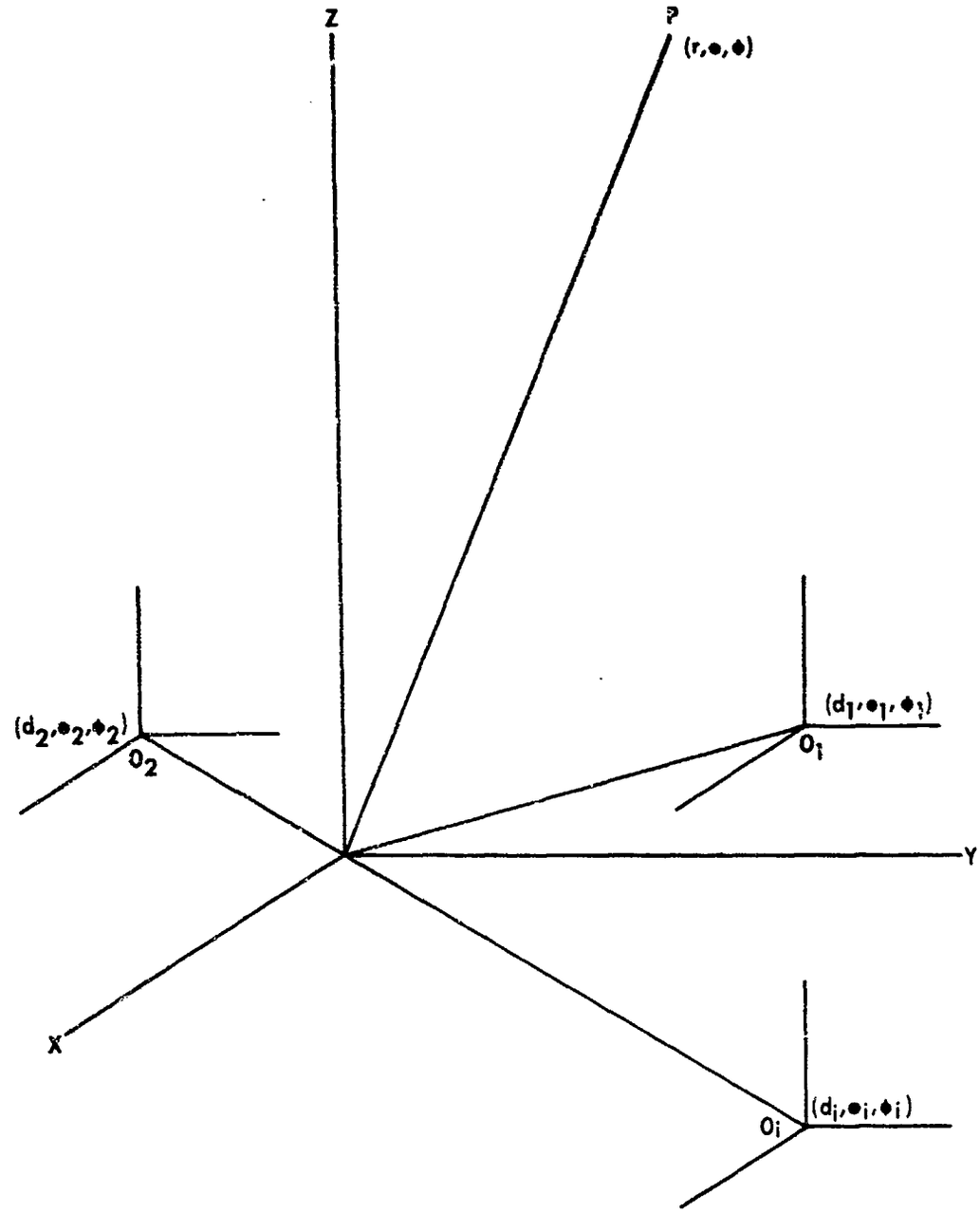

Fig. 4-2.--Coordinate specifications for target, scattering complexes, and field point P.

Letting $x = \cos \alpha$ and $G = d/r$,

$$D^{-1} = (1/r)[1 + G^2 - 2Gx]^{(-1/2)}. \tag{4-3}$$

This can be expanded in a binomial series, provided

$$(G^2 - 2Gx)^2 < 1. \tag{4-4}$$

To express the convergence condition in terms of physical parameters, note that, from (4-3),

$$D^2 = r^2 + r^2(G^2 - 2Gx)$$

or

$$G^2 - 2Gx = (D/r)^2 - 1. \tag{4-5}$$

Thus (4-4) is equivalent to

$$[(D/r)^2 - 1]^2 < 1$$

or

$$(D/r)^4 - 2(D/r)^2 < 0$$

or

$$(D/r) < \sqrt{2}\ . \tag{4-6}$$

Inequality (4-6) gives the convergence condition in terms of the distances from the primary and secondary origins to the field point P. The quantity (D/r) is positive, and for a given r and d, has a maximum value when O" and P are diametrically opposed, or

$$D_{max} = r + d. \tag{4-7}$$

Substituting this maximum value in (4-6), the maximum displacement of

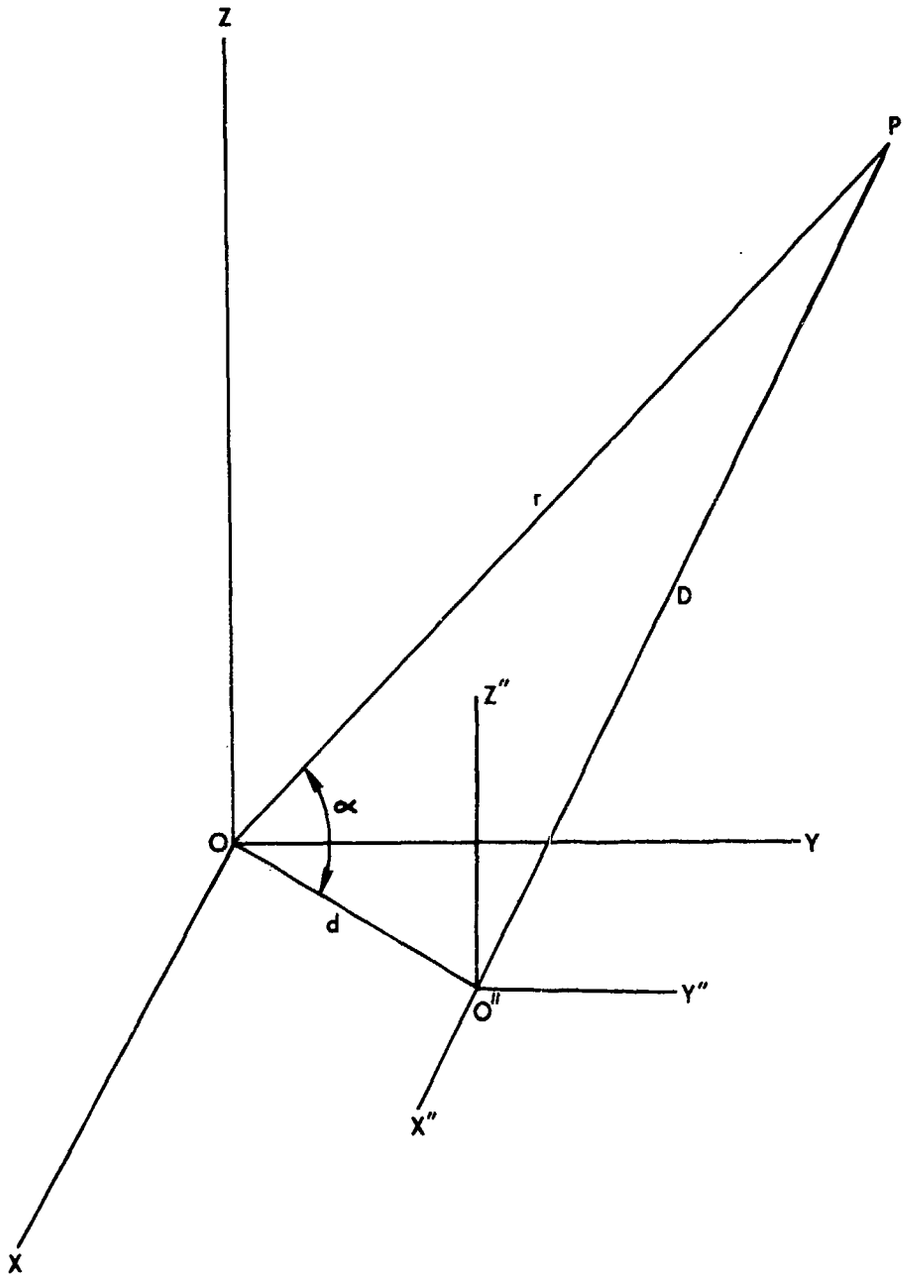

Fig. 4-3.--Geometry for deriving the path length D and for determining the coordinates of P relative to the secondary origin 0''.

the secondary origin from the primary origin becomes

$$d_{max} = 0.414r. \tag{4-8}$$

This condition is easily satisfied in practice because the range is usually much greater than the maximum target dimension. Returning to (4-3), the binomial series expansion is

$$D^{-1} = (1/r)[1-(1/2)(G^2-2Gx)+(3/8)(G^4-4G^3x^2-8G^3x^3) - (15/48)(G^6-6G^5x+12G^4x^2-8G^3x^3)- \ldots]. \tag{4-9}$$

Collecting like powers of G,

$$D^{-1} = (1/r)[1 + Gx + G^2(1/2)(3x^2 - 1) + G^3(1/2)(5x^3 - 3x) + \ldots]. \tag{4-10}$$

Replacing G by d/r, (4-10) is seen to be of the form

$$D^{-1} = (1/r) \sum_{\ell=0}^{\infty} (d/r)^{\ell} P_{\ell}(x) \tag{4-11}$$

where $P_{\ell}(x)$ is the Legendre polynomial of order ℓ and argument x.

In order to use the expression (4-11) to find the distance D, it is necessary to determine the argument $x = \cos \alpha$ in terms of the spherical coordinates of P and O". In Fig. 4-3, consider the radial lines to O" and P to be the vectors $\hat{d}$ and $\hat{r}$, respectively. Forming the scalar product of these vectors,

$$\hat{r} \cdot \hat{d} = rd \cos \alpha = xx' + yy' + zz' \tag{4-12}$$

where (x,y,z) and (x',y',z') are the rectangular coordinates of P and O", respectively. Substituting the relationships between spherical and rectangular coordinates,

$$x = r \sin\theta \cos\phi$$

$$y = r \sin\theta \sin\phi$$

$$z = r \cos\phi \qquad (4\text{-}13)$$

in (4-12) and solving for cos α yields

$$\cos\alpha = \cos\theta \cos\theta' + \sin\theta \sin\theta' \cos(\phi-\phi') \qquad (4\text{-}14)$$

where (θ,ϕ) and (θ',ϕ') are the spherical coordinates associated with P and O", respectively.

Transformation to secondary coordinates

To find the total field at P, it is necessary to know the phasor contribution of each complex C_i. Each contribution is found by examining the recorded data which represents the spatial patterns of the complex, extracting from the data the amplitude and phase values in the direction given by the angular coordinates of P relative to O_i, and modifying these values to include the effects of spatial attenuation and phase retardation over the appropriate propagation path. Because the angular coordinates of P are known only in the primary coordinate system, a coordinate transformation is required to obtain the angular coordinates of P relative to O_i.*

*The radial distance to P is usually much larger than the distances between the primary and secondary origins. This fact may permit the use of the primary angular coordinates of P in extracting the amplitude and phase values from the recorded data, thus avoiding the coordinate transformations to each secondary system. However, an examination of the fine-grain structure of the data for many complexes would be necessary to validate such an approximation.

Consider again the geometry shown in Fig. 4-3, where the secondary origin is denoted as O". Let the spherical coordinates of P with respect to O be (r,θ,ϕ) and with respect to O" be $(D,\theta",\phi")$, and let the coordinates of O" with respect to O be (d,θ',ϕ'). Let the corresponding rectangular coordinates be (x,y,z), (x",y",z"), and (x',y',z'), respectively. The known parameters are (r,θ,ϕ), (d,θ',ϕ'), and D (from (4-11)). It is desired to find the equivalent angular coordinates $(\theta",\phi")$. By translation of rectangular coordinates,

$$z" = z - z'$$
$$x" = x - x'. \tag{4-15}$$

Substituting the spherical-rectangular relationships (4-13) on the right hand sides yields

$$z" = r \cos \theta - d \cos \theta'$$
$$x" = r \sin \theta \cos \phi - d \sin \theta' \cos \phi'. \tag{4-16}$$

Again using (4-13),

$$\theta" = \arccos [z"/D]$$
$$= \arccos [(r \cos \theta - d \cos \theta')/D] \tag{4-17}$$

and

$$\phi" = \arccos [x"/ (D \sin \theta")]$$
$$= \arccos \left[\frac{r \sin \theta \cos \phi - d \sin \theta' \cos \phi'}{D \sin \theta"} \right]. \tag{4-18}$$

Equations (4-17) and (4-18) are the desired transformations.

Summation of contributions

Let the amplitude and phase contributions from complex C_i, in the direction given by the angular coordinates of P relative to O_i, be A_i and α_i, respectively. These are the values, taken from the recorded static range data, which represent the pattern of the complex in this direction. If the data are recorded according to the maximum-target-dimension criterion discussed in Section A, the amplitude and phase will have a far-field variation with range. Thus the amplitude and phase contributions of complex C_i at the field point P are

$$A_i' = \frac{R_m A_i}{D_i} \tag{4-19}$$

and

$$\alpha_i' = \alpha_i - 2k(D_i - R_m) \tag{4-20}$$

where $k = 2\pi/\lambda$ is the wave number, D_i is the distance from O_i to P, and R_m is the range at which the static measurements are made (constant for all complexes). The factor of two in the propagation path term arises because of the assumed monostatic configuration.

Let the total number of complexes be N, and let $\bar{E}_i = A_i'/\underline{\alpha_i'}$ be the phasor representation of the contribution of C_i at P. Then the total received signal at P is

$$\bar{E} = A/\underline{\alpha} = \sum_{i=1}^{N} \bar{E}_i. \tag{4-21}$$

In terms of known quantities, (4-21) becomes

$$\bar{E} = \sum_{i=1}^{N} A_i' \angle \alpha_i'$$

$$= \sum_{i=1}^{N} \frac{R_m A_i}{D_i} \angle \alpha_i - 2k(D_i - R_m) \quad . \tag{4-22}$$

The procedure for using (4-22) to find the total field $\bar{E}$ at a given point P thus involves the use of (4-11) to find the distance to each complex C_i, the use of transformations (4-17) and (4-18) to find the angular coordinates of P with respect to each origin O_i, and the use of these coordinates to determine the contributions A_i and α_i from the recorded data.

Provisions for motion

Providing for a turning movement of the target requires two modifications of the above procedure. First, because the target is turning, the aspect angle is changing with time. This change can be accounted for by making modifications of the angular coordinates of P which reflect the change in aspect angle. A derivation of the coordinate changes for the case of constant roll, pitch, and yaw rates is given in Appendix A. Second, the turning motion results in a Doppler shift in the radar frequency of the return from each complex. On an instantaneous basis, such a frequency change is equivalent to a phase change. Thus the Doppler effect can be included by an appropriate modification of the phase angle α_i of each complex. A discussion of this modification for the case of constant turning rates is included in Appendix A.

If there exists relative motion between a complex and the overall airframe, as in the case of vibratory motion of a control surface, the

phase contribution from that complex must be modified. The appropriate change consists of the addition of a phase term which represents the particular phase modulation due to the motion.

C. Determination of the Glint Error

For this analysis, the glint error will be defined as the angular deviation of the instantaneous apparent radar center from the origin O. Referring to Fig. 4-4, the position of the apparent radar center, C, may be expressed in linear units at the target along line OC, as measured in the plane JKLM, which is normal to OP and contains O. The plane OPQ is defined as the elevation plane, while the transverse plane is that which is orthogonal to the elevation plane and intersects it along the line OP. The glint error will be determined separately in these two planes and then the results combined to find the total error.

The phase front may be defined as the range change increment, in linear units, required to reach a position having some reference phase α_o. The phase, α, is related to range. r, by

$$\alpha = -kr. \tag{4-23}$$

If the reference phase is taken to be $\alpha_o = 0$, then the phase front, as measured from the range coordinate where α is determined, is simply

$$F = -\alpha/k. \tag{4-24}$$

Because the range of values for the phase angle is

$$0 \leq \alpha < 2\pi$$

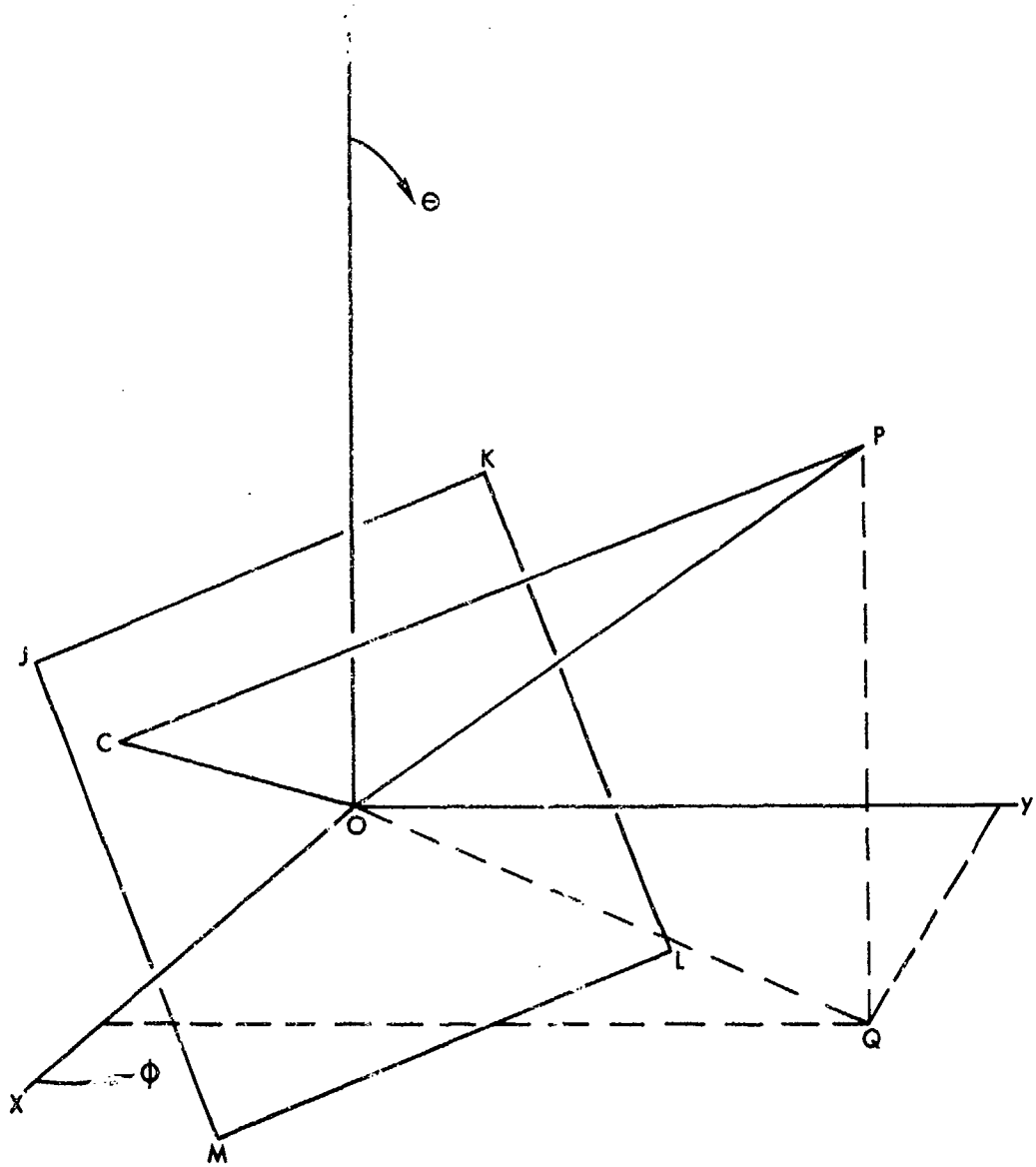

Fig. 4-4.--Geometry of the apparent radar center.

the phase front is a number which satisfies

$$0 \leq F < \lambda. \tag{4-25}$$

It is assumed that the phase front is a well-behaved function of aspect angle in the vicinity of P. This will be said to be true if a region the size of a typical airborne radar aperture (less than one meter) spans no more than one full cycle of the distorted wave front. For the case of the two-reflector target, Dunn and Howard [29] showed that this requires a range greater than

$$R_{min} = d\Delta/\lambda \tag{4-26}$$

where d is the reflector spacing and Δ is the aperture diameter. It is assumed that this relationship is also reasonably valid for more general target configurations, and moreover, that the phase front is approximately a linear function of aspect angle over the region around P. Stated another way, it is assumed that the range is large enough for the phase front over the region of interest to be approximately planar.

To determine the glint error, consider the geometry depicted in Fig. 4-5, where OC'P lies in either the elevation or the transverse plane, and where C' is the projection of the apparent radar center C in this plane. The range R is assumed to be much larger than Δ (the diameter of the region of interest), and thus the contributions A_i and α_i may be considered constant over the solid angle subtended by Δ at each origin O_i. F_1 and F_2 are the values of the phase front at the

two extremes of Δ. The linear glint error OC' is the parameter to be determined.

By definition of the apparent target center, the line PC' is normal to the phase front. The slope of the phase front is

$$m_1 = (F_1 - F_2)/\Delta \tag{4-27}$$

while the slope of PC' with respect to OP is

$$m_2 = OC'/R. \tag{4-28}$$

By similar triangles, these slopes are identical, therefore

$$\frac{OC'}{R} = \frac{F_2 - F_1}{\Delta}$$

or

$$OC' = R(F_2 - F_1)/\Delta. \tag{4-29}$$

Substituting from (4-24) for the phase front in terms of the total field phases at the extremes of the sampling region, α_1'' and α_2'',

$$OC' = \frac{R(\alpha_1'' - \alpha_2'')}{k\Delta} . \tag{4-30}$$

However, in determining these total field phases, the phase contribution from each complex, α_i', must be obtained in a slightly different manner than that indicated by (4-20). The illumination path from P to the complex is still D_i, but the path for the radar return from the complex is now the distance from O_i to the extreme of the sampling region where the field is to be determined. Denoting this distance by D_i',

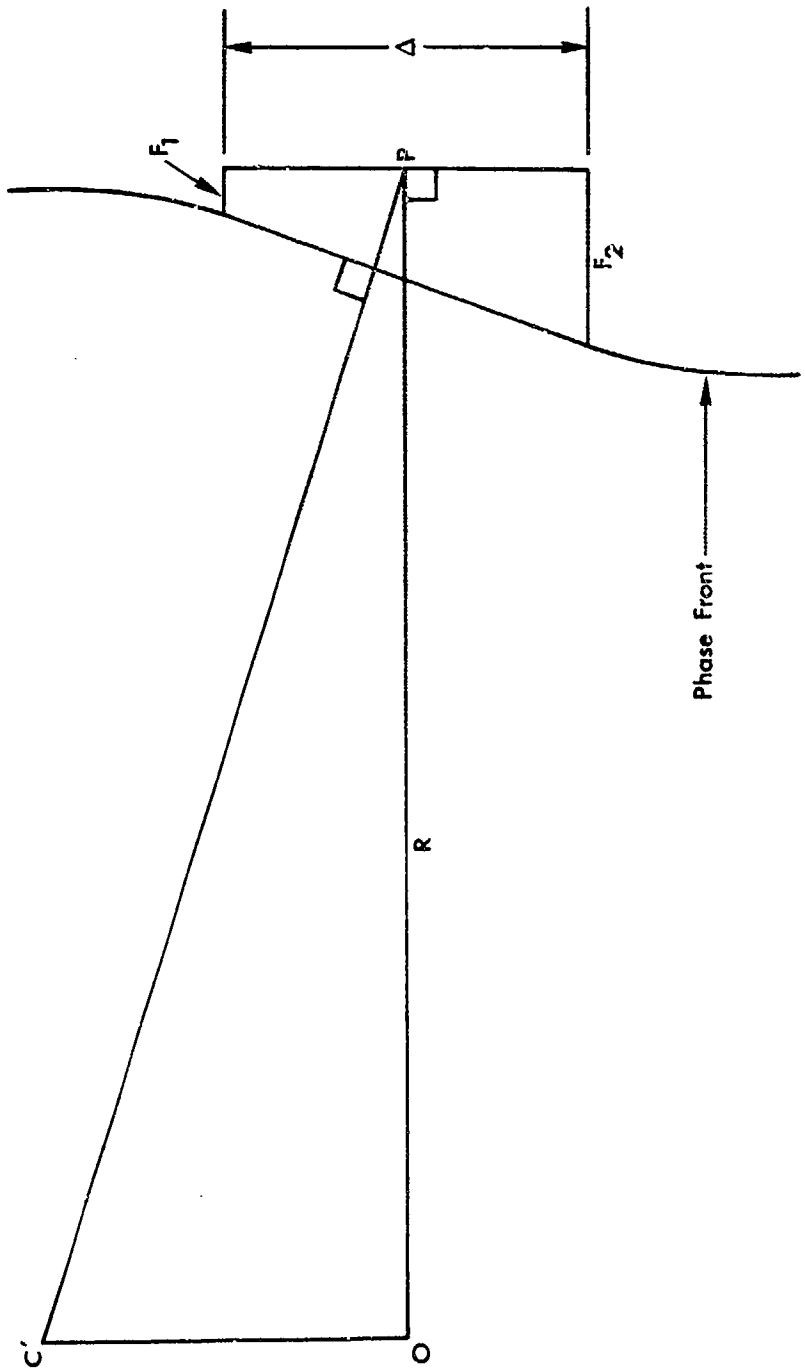

Fig. 5-5.--Geometry for the determination of glint.

the propagation path over which spatial attenuation and phase retardation takes place becomes $(D_i + D_i' - 2R_m)$. Substitution of this value in place of $2(D_i - R_m)$ in equations (4-19) and (4-20) gives

$$A_i' = \frac{R_m A_i}{D_i + D_i'} \tag{4-31}$$

and

$$\alpha_i' = \alpha_i - k(D_i + D_i' - 2R_m). \tag{4-32}$$

(The substitution in (4-19) is trivial because the small difference in values has negligible amplitude effect.) These contributions can then be summed to find the total field phase at each region extremity, and the results used to find the linear glint error from (4-30).

The total linear glint error in the plane normal to OP is found simply by forming the square root of the sum of the squares of the components in the elevation and transverse planes. To express the error in angular units, let A be the angular deviation corresponding to a linear error OC. Then

$$A = \arctan (OC/R). \tag{4-33}$$

If the value of Δ is kept quite small, the angular glint error determined by this technique is very close to the direction of the actual normal to the phase front. On the other hand, if Δ is made approximately the diameter of an actual tracking antenna (but within the limitations of (4-26)), a determination of the general effect of aperture averaging of the distorted wave front can be made. A computer

implementation to study samples of this effect and others will be described in the next chapter.

V. IMPLEMENTATION OF THE MODEL

As an extension of the development of the glint model described in the previous chapter, a series of FORTRAN IV computer programs were written to illustrate the determination of target glint from the backscattered wavefront. The known results of several configurations of isotropic scatterers, observed in a far-field situation, were used to establish the validity of the computer techniques. An effort was made to keep the programs sufficiently general to permit their use in describing the effect of such parameters as tracking aperture size, target motion, and diversity techniques. The entry of the amplitude and phase data for the scattering complexes was implemented through a separate subroutine to facilitate use of the programs with measured static range patterns, should they become available. Detailed flow diagrams and listings of the various programs and subroutines which evolved are presented in Appendix B.

A. Program Philosophy

Fig. 5-1 is a summary flow diagram which illustrates the basic computer implementation. The parameters which are read into the program at execution time include radar wavelength, aperture diameter, coordinates and identifying codes for the various scattering complexes, target motion data, and the sampling time increment. The space trajectory over which glint or other field parameters are to be

determined is established by a subroutine called TRAJ. Any desired trajectory is thus easily incorporated simply by preparing a subroutine which describes the desired series of observation points, in spherical coordinates, as a function of time. The field parameters are then computed at each of these sampling points.

The first operation in the computation of the field parameters is the appropriate modification of the coordinates obtained from TRAJ to account for any change of aspect angle due to target motion. The modified angular coordinates of the observation point are then transformed into equivalent coordinates with respect to each scattering complex, and these values used to select the appropriate amplitude and phase values from the scattering complex data. This selection is provided by a subroutine named AMPPHI, which may be written to provide either values for a desired group of theoretical scatterers, or values from actual recorded data from scattering complexes. The resulting phase values are then adjusted to include any Doppler effects due to target motion.

Having obtained the appropriate amplitude and phase values for each complex, the next computation involves the determination of the distances from the observation point, P, to each complex, and the distances from each complex to the extremes of the aperture. These propagation paths are then used to find the field contributions of each complex at each extreme of the aperture, and the contributions summed to obtain the total field values.

The glint in each tracking plane is determined from the total

field phase at the aperture extremes as indicated in equation (4-30). The time, glint error in each plane, total returned amplitude and phase at P, and the amplitude contribution at P due to each complex are written into magnetic disk storage for future processing and analysis. The program then transfers control to repeat the computations at the next sample point along the trajectory.

B. Synthesis of Scattering Complex Patterns

In order to illustrate the computer implementation of the glint model, it is desirable to generate some form of nonisotropic amplitude and phase patterns to represent those which might be obtained from actual scattering complexes. Because measured data for the complexes will probably display considerable amplitude and phase sensitivity to changes in aspect angle, any synthesizing technique which might be used should produce patterns with a corresponding fine-grain lobe structure.

One data synthesis approach which might be utilized is to adapt the basic techniques developed in Chapter IV to obtain the total field amplitude and phase patterns from various three-dimensional arrays of spherical reflectors. If the electrical spacings between the various reflectors in a given array are sufficiently large, the resulting amplitude and phase patterns will display the desired fine-grain lobe structure. An AMPPHI subroutine implementing this technique was written and tested with reasonable success. However, the generation of the data for each point on each pattern required the phasor

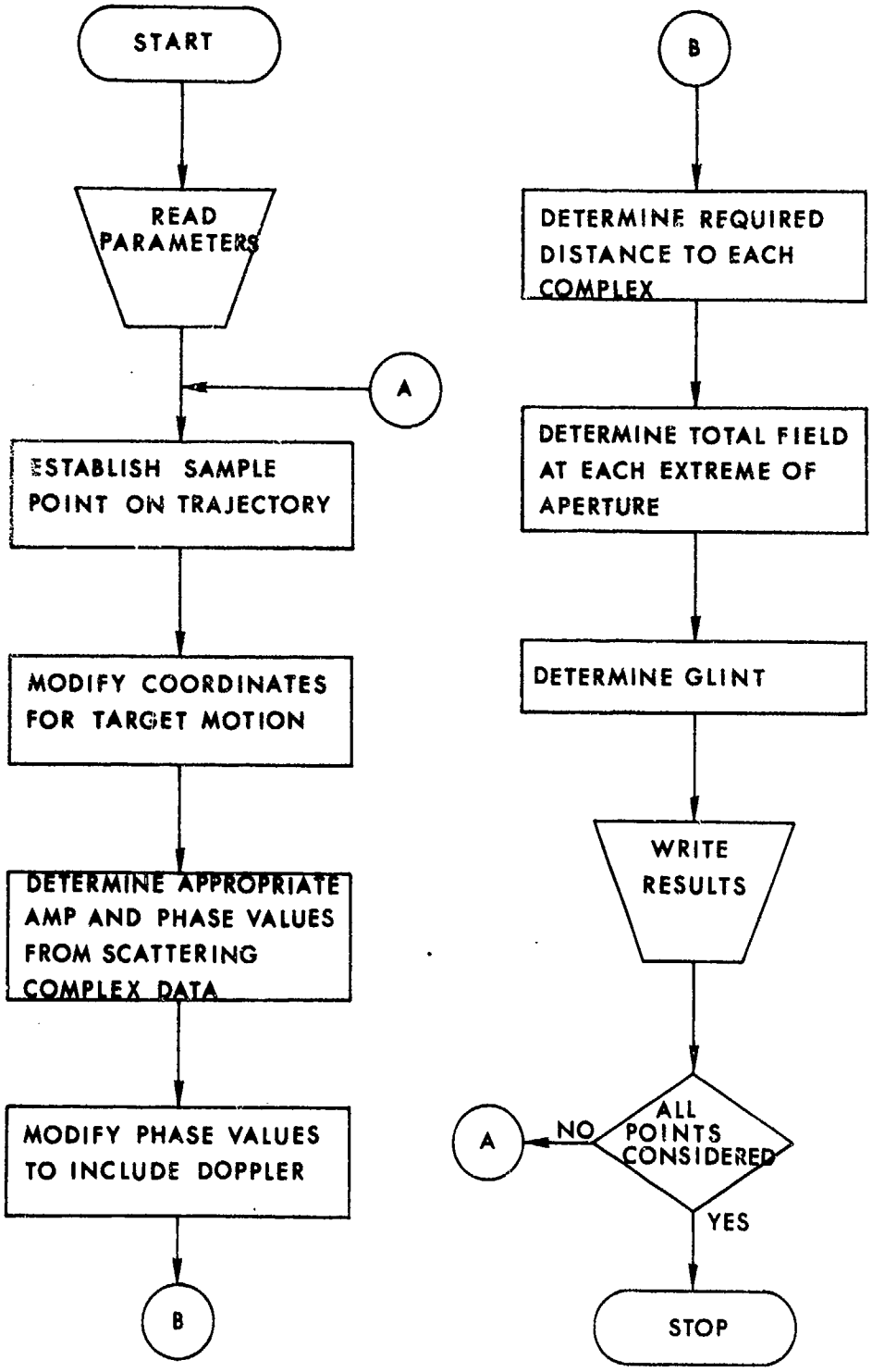

Fig. 5-1.--Summary flow diagram of computer implementation.

summation of the contributions from many different spheres. Because many different data points were required to describe adequately each pattern, it became apparent that the computation time for this synthesis technique was quite large. For this reason, a more direct analytical approach was needed.

Another pattern-generation technique which could be used is to describe the desired function of aspect angle by an algebraic equation. An equation of the form

$$f(\phi) = K \cos(n\phi), \tag{5-1}$$

where K is a constant and n is an integer, generates a polar lobe pattern. As n becomes large, the number of lobes also increases. The product of two functions of this form can be used to generate a large variety of polar patterns. Expressed as a logarithmic (power) amplitude function, such a product is

$$A = 10 \log_{10} [K \cos(n_1\phi) \cos(n_2\phi)]^2 \text{ dB}. \tag{5-2}$$

Here K is some maximum amplitude, n_1 is some small integer, and n_2 is a large integer. Thus the latter cosine function provides the desired degree of fine-grain lobe structure, while the former results in a slowly-varying amplitude envelope. Fig. 5-2 is a plot of equation (5-2) with K = 10, n_1 = 1 and n_2 = 90. A phase pattern can be generated in a similar manner by use of a function of the form

$$\alpha \simeq 180 \cos(n_3 \phi) \text{ deg} \qquad (5\text{-}3)$$

where the integer n_3 is chosen to provide the desired rapidity of phase change with aspect angle.

Because of the relative simplicity of this second technique of pattern synthesis, it was used in most of the computer studies. A further simplification was to restrict trajectories used with a synthesized target to elevation angles near $\theta = 90°$, i.e. near the azimuth plane. Table 5-1 summarizes the amplitude and phase generating functions for four synthesized scattering complexes which were used in the studies. The additional sine functions involving θ were included in the amplitude equations to provide a degree of variation in the elevation plane. Table 5-2 lists the spherical coordinates of each of these four complexes, relative to a primary origin, which were used for many of the computer data runs. This arrangement was assigned the designation configuration No. 10.

C. Illustrations of Phase Front Behavior

To provide insight into the nature of phase front distortion, it is instructive to examine the phase front patterns for several target configurations. These can be obtained by describing a trajectory which varies over the desired region of aspect angles while maintaining a constant range, converting the computed total field phase at each sample point to the equivalent phase front by use of (4-24), and plotting the result.

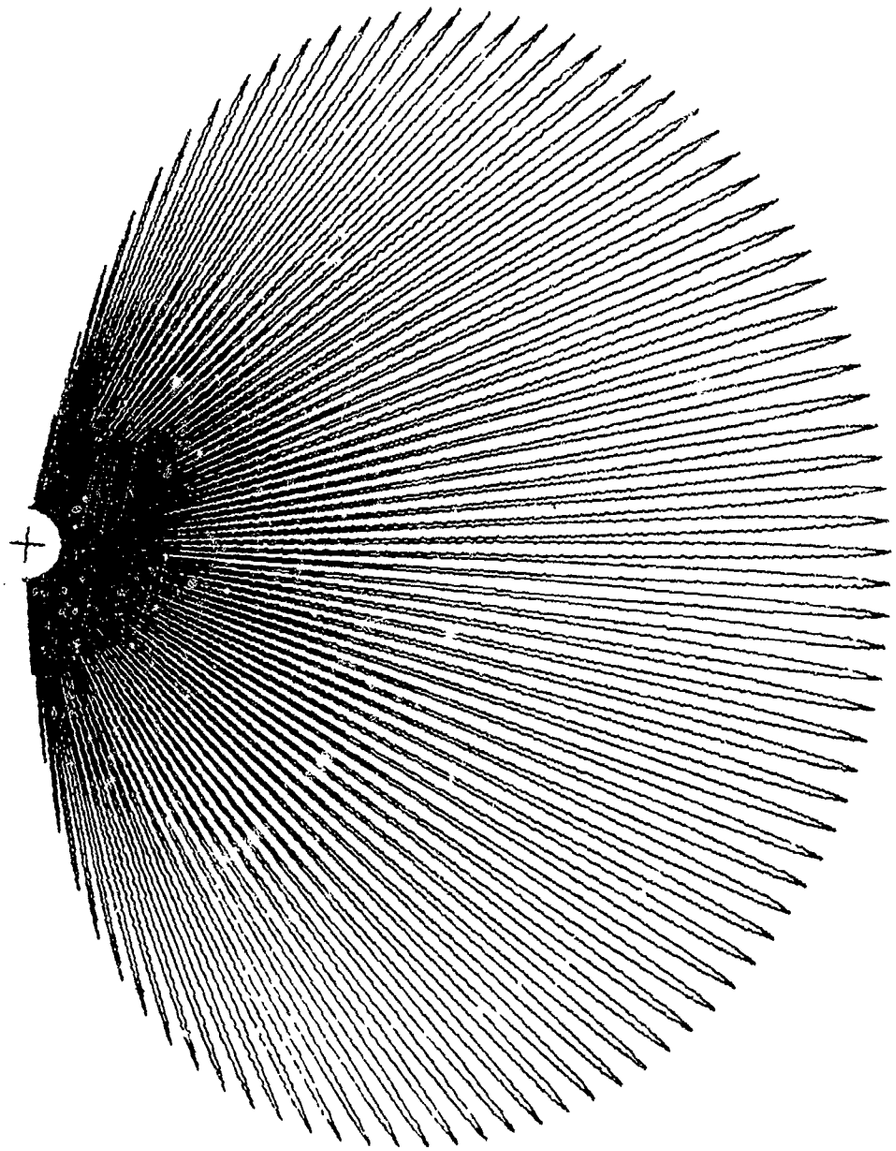

FIG. 5-2--SYNTHESIZED AMPLITUDE PATTERN
FOR A SCATTERING COMPLEX

TABLE 5-1

AMPLITUDE AND PHASE GENERATING FUNCTIONS FOR SYNTHESIZED SCATTERING COMPLEXES 20, 21, 22, 23

COMPLEX	GENERATING FUNCTIONS
20	$A = 10 \log_{10} [\sin(\theta) \sin(\phi) \cos(360\,\phi)]^2$
	$\alpha = 180 \cos(720\,\phi)$
21	$A = 10 \log_{10} [0.9 \sin(\theta) \sin(\phi) \cos(72\,\phi)]^2$
	$\alpha = 180 \cos(360\,\phi)$
22	$A = 10 \log_{10} [\sin(\theta) \cos(\phi) \cos(360\,\phi)]^2$
&	$(-\pi/2 < d < \pi/2)$
23	$A = 0 \qquad (\phi > \pi/2)$
	$\alpha = 180 \cos(720\,\phi)$

TABLE 5-2

SPHERICAL COORDINATES FOR SCATTERING COMPLEXES

IN TARGET CONFIGURATION NO. 10

Complex	d(m)	ϕ'(deg)	θ'(deg)
20	20	180	90
21	5	180	90
22	10	90	90
23	10	-90	90

Fig. 5-3 is a plot of two different phase front patterns for two isotropic reflectors. Note that the ordinate is plotted full-scale in units of inches. The abcissa is the azimuth angle, ϕ, as measured from the line joining the reflectors. In the upper plot, the amplitude ratio between the reflectors is 0.9, while the lower pattern was obtained for a ratio of 1.5. In both cases the spacing was one wavelength at 10 GHz, and the range was 1 Km. The apparent direction to the midpoint of the reflectors from any given observation point is given by the normal to the phase front at that point. From the figure, it is seen that the maximum slope of the phase front is much larger for the amplitude ratio nearest to unity (A=0.9), which results in a larger glint error. Also, the magnitude of the ratio as it compares to unity governs the algebraic sign of the error, i.e. to which side of the mid-point of the reflectors the apparent target center lies. Both of these observations are compatible with the results of Meade, as depicted in Fig. 2-3.

A full-scale phase front plot for the synthesized complex target which is described in Tables 5-1 and 5-2 is presented in Fig. 5-4. The azimuth angle is measured from the positive x-axis (ϕ=0), and the observations are made in the θ=90° plane at a range of 1 Km. The radar frequency is 10 GHz. Note that the larger size of the target configuration produces a much more rapid variation of the phase front with aspect angle than that shown in Fig. 5-3.

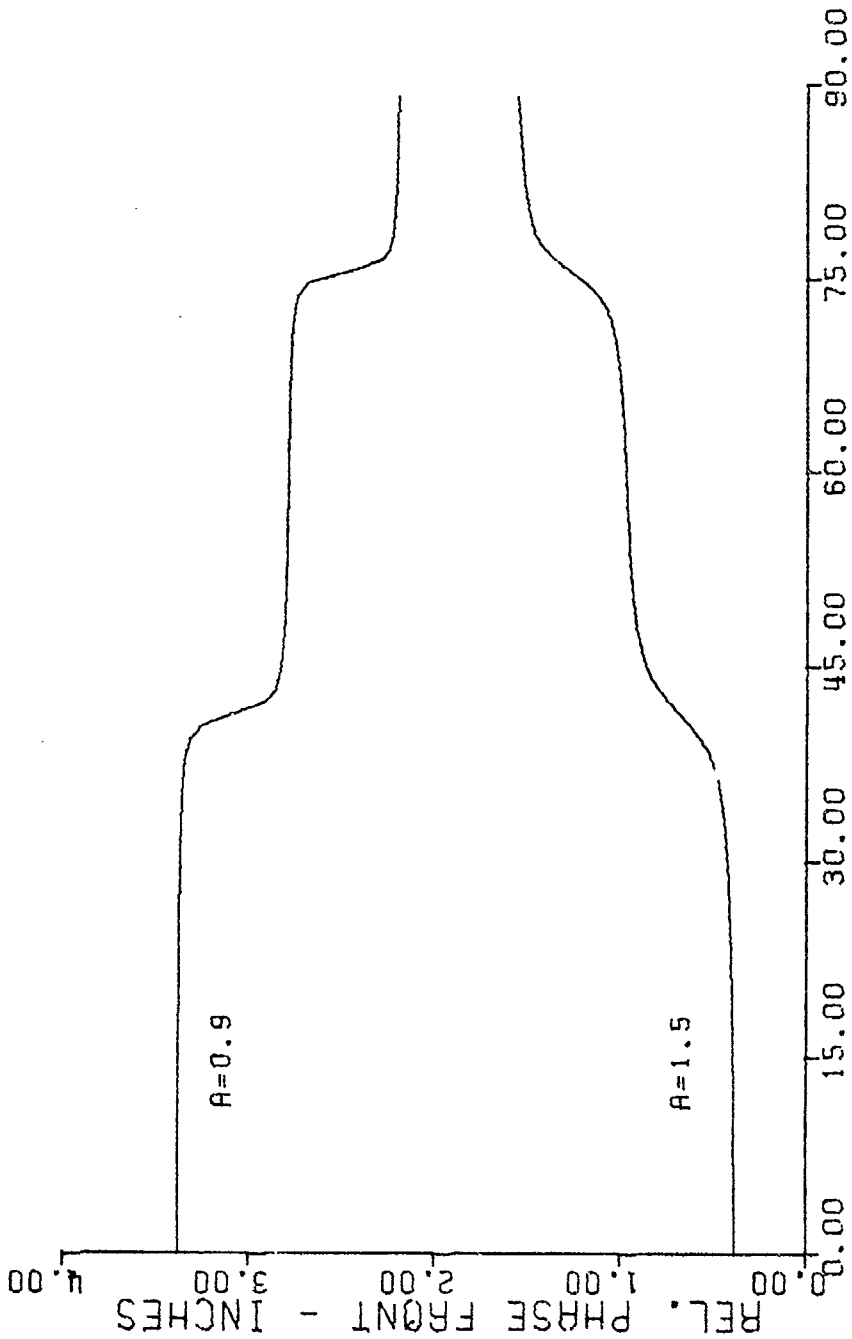

FIG. 5-3--PHASE FRONTS FOR TWO REFLECTORS SPACED ONE WAVELENGTH APART

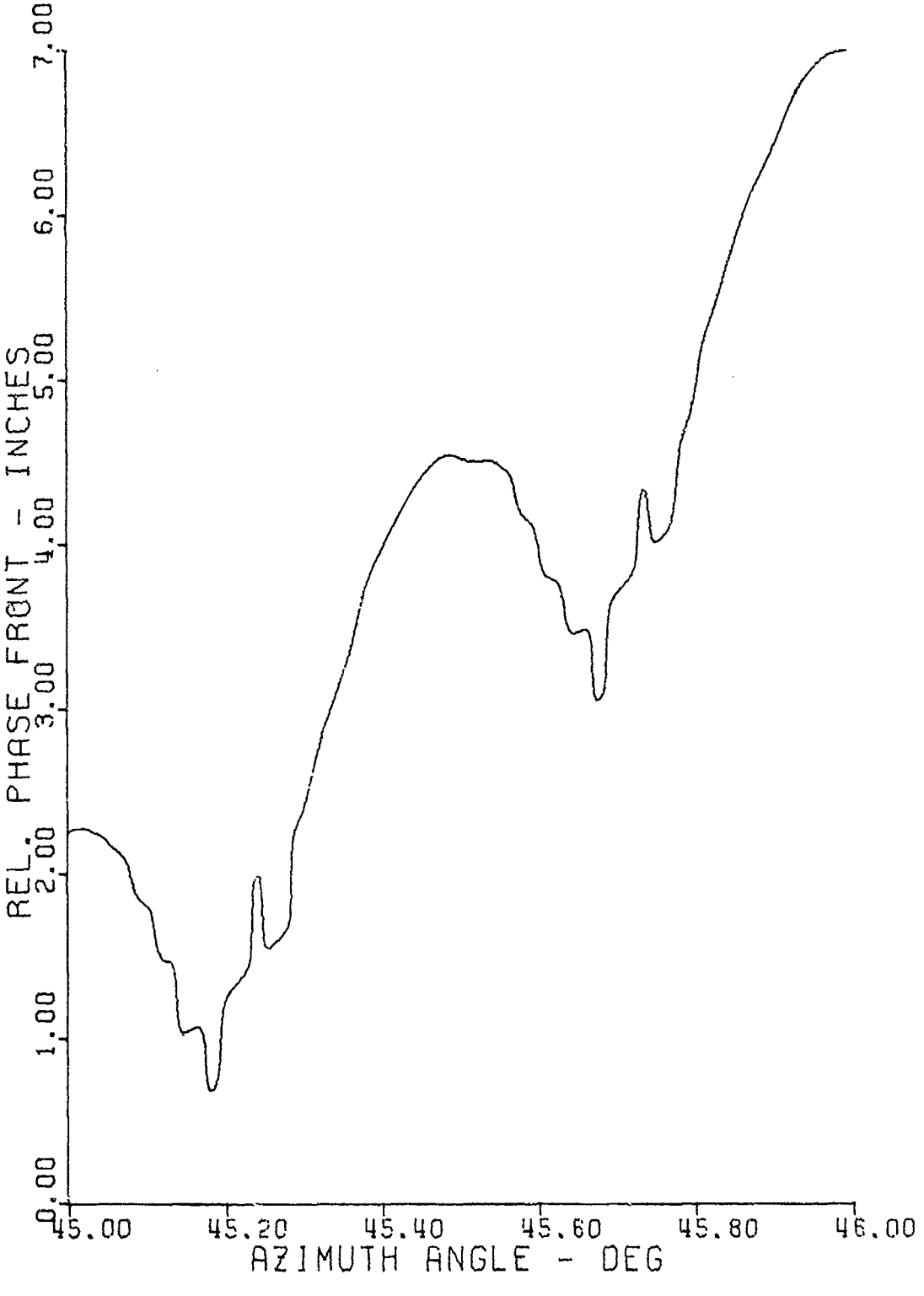

FIG. 5-4--PHASE FRONT IN THE AZIMUTH PLANE FOR SYNTHESIZED TARGET CONFIGURATION NO. 10

D. Glint Error for Sample Configurations

Comparison with results of Mead

A glint error determination was made for the two-reflector target used in the example problem in Chapter 2. The trajectory consisted of a single sample point at a range of 1000 m along the perpendicular to a line joining the two reflectors. An AMPPHI subroutine was written which incremented the phase for one of the reflectors in 5 degree steps and also varied the amplitude ratio, A, between the reflectors. The reflectors were spaced one wavelength at the 10 GHz radar frequency, and the glint error for each combination of relative phase and amplitude was normalized to this spacing. Fig. 5-5 is a family of curves depicting the results for various values of amplitude ratio. The figure compares quite favorably with Fig. 2-3; in fact, the computer-generated plots appear to be overlays.

Range dependence of glint

If linear glint is independent of range, an angular boresight-tracking-error value from a radar measurement could be converted to a measurement independent of range by multiplying the value by the range to the target. Such a range dependence for two isotropic reflectors, R_1 and R_2, can be illustrated by consideration of Fig. 5-6. The origin is designated by 0, and the apparent target center by C. A series of observation points lie along the radial line OP'. The arcs centered on 0 and C represent the phase fronts which would result from a single reflector at 0 or C, respectively. Note that this construction yields a phase-front-difference between the pairs

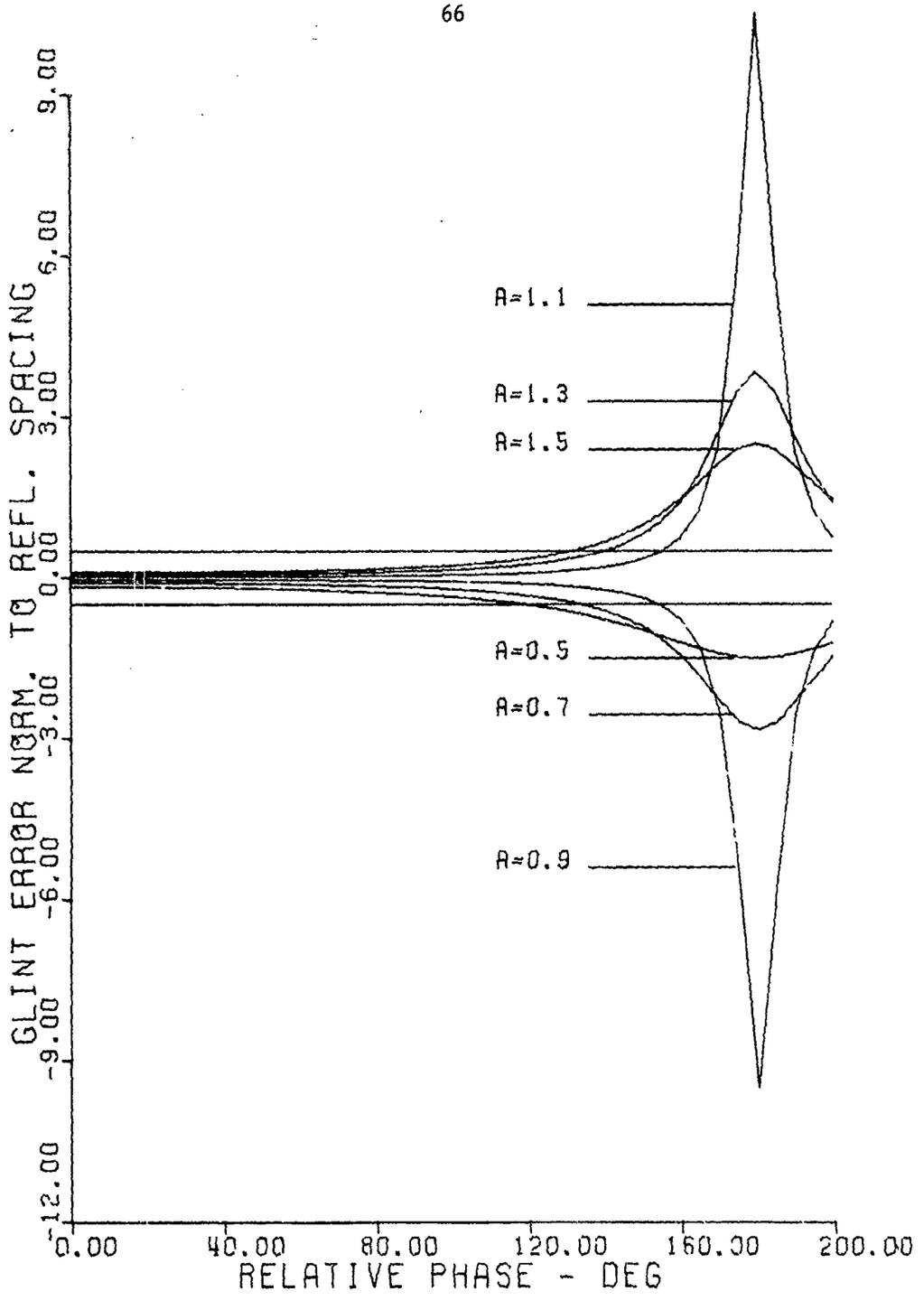

FIG. 5-5--GLINT ERROR FOR TWO REFLECTORS

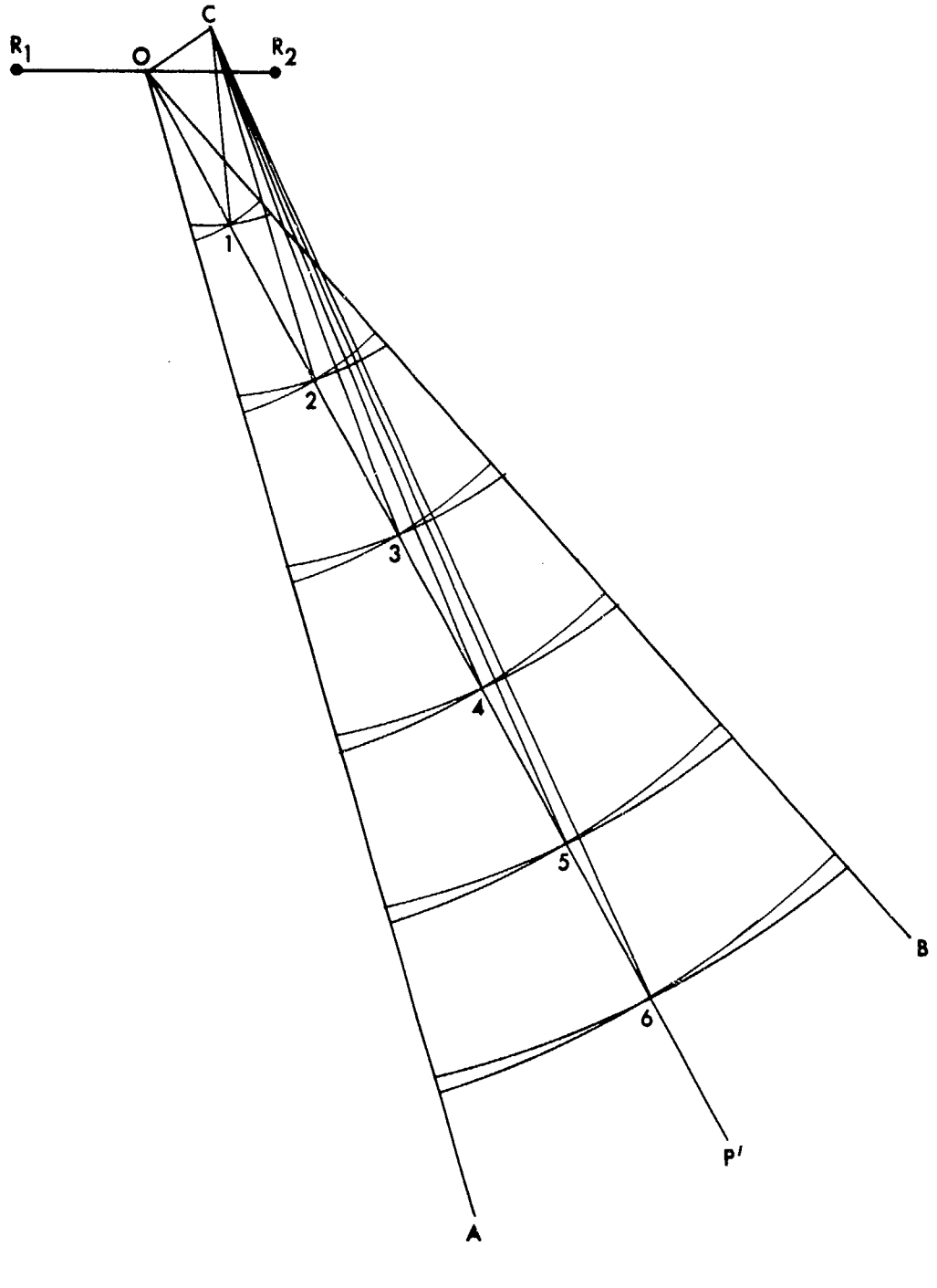

Fig. 5-6--Geometrical illustration of range dependence of glint for two isotropic reflectors.

of arcs which is constant with range along the radial lines OA and OB. This result is compatible with the concept of phase retardation of a propagating wave. Note also that the angular glint decreases with range. From a physical viewpoint, this means that at a sufficiently large range, the target configuration appears as a single point which produces amplitude scintillation but induces no appreciable angular glint. Fig. 5-7 shows the linear and angular glint dependence for two isotropic reflectors spaced two meters apart at 10 GHz.

For the case of a target configuration more complex than that just described, it appears that the range dependence can no longer be easily described. The different combinations of the various target elements produce lobing patterns which have effective centers away from the origin. Thus changing range changes the relative contributions from the various scattering centers, with a resulting change in the linear glint error. To illustrate this effect, the two isotropic reflectors used in generating Fig. 5-7 were replaced by two identical nonisotropic reflectors having amplitude patterns similar to Fig. 5-2. The resulting glint behavior with range is shown in Fig. 5-8. Note that the angular glint continues to show a decreasing trend with increasing range, in accordance with the physical reasoning discussed earlier.

Analysis of glint waveforms for a synthesized target

A plot of linear glint error vs time for configuration No. 10 is shown in Fig. 5-9. The component of error in the transverse tracking plane was computed and plotted at 0.025 second increments

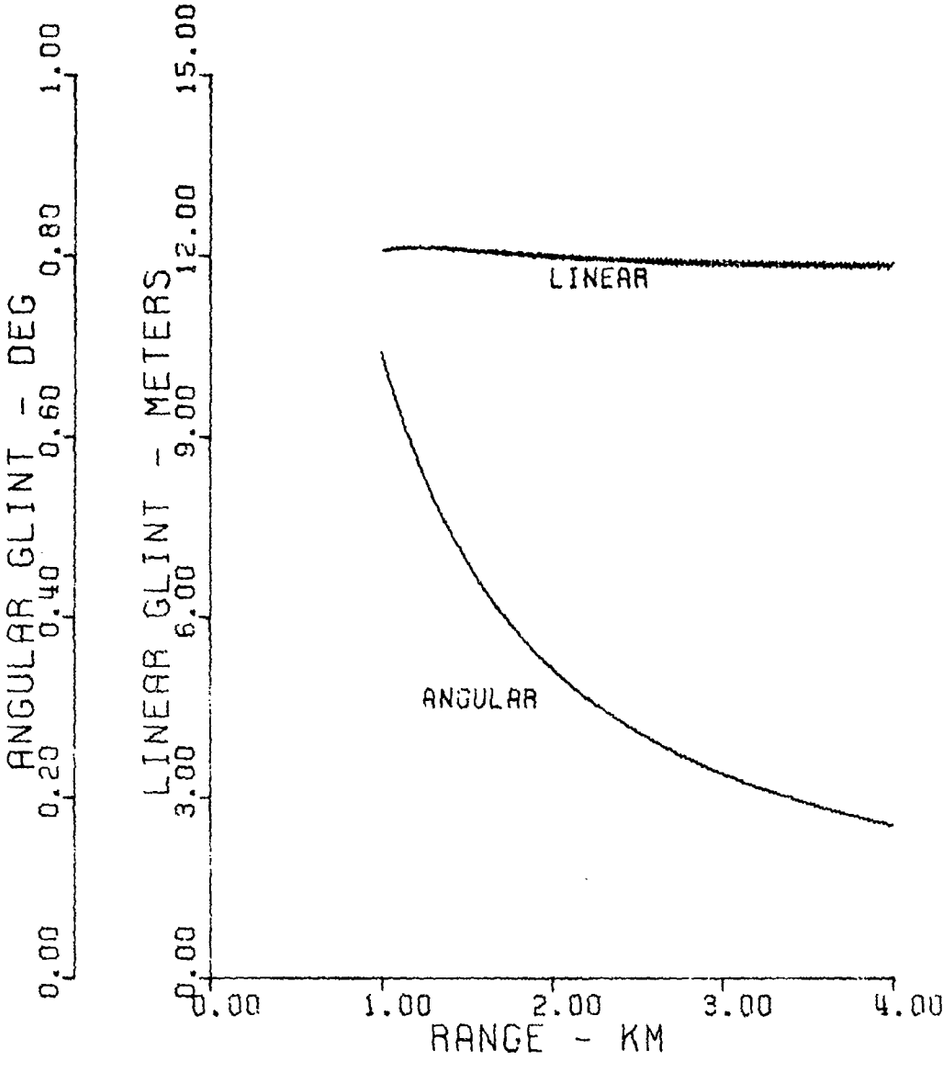

FIG. 5-7--RANGE DEPENDENCE OF GLINT FOR TWO ISOTROPIC REFLECTORS, TWO METERS APART

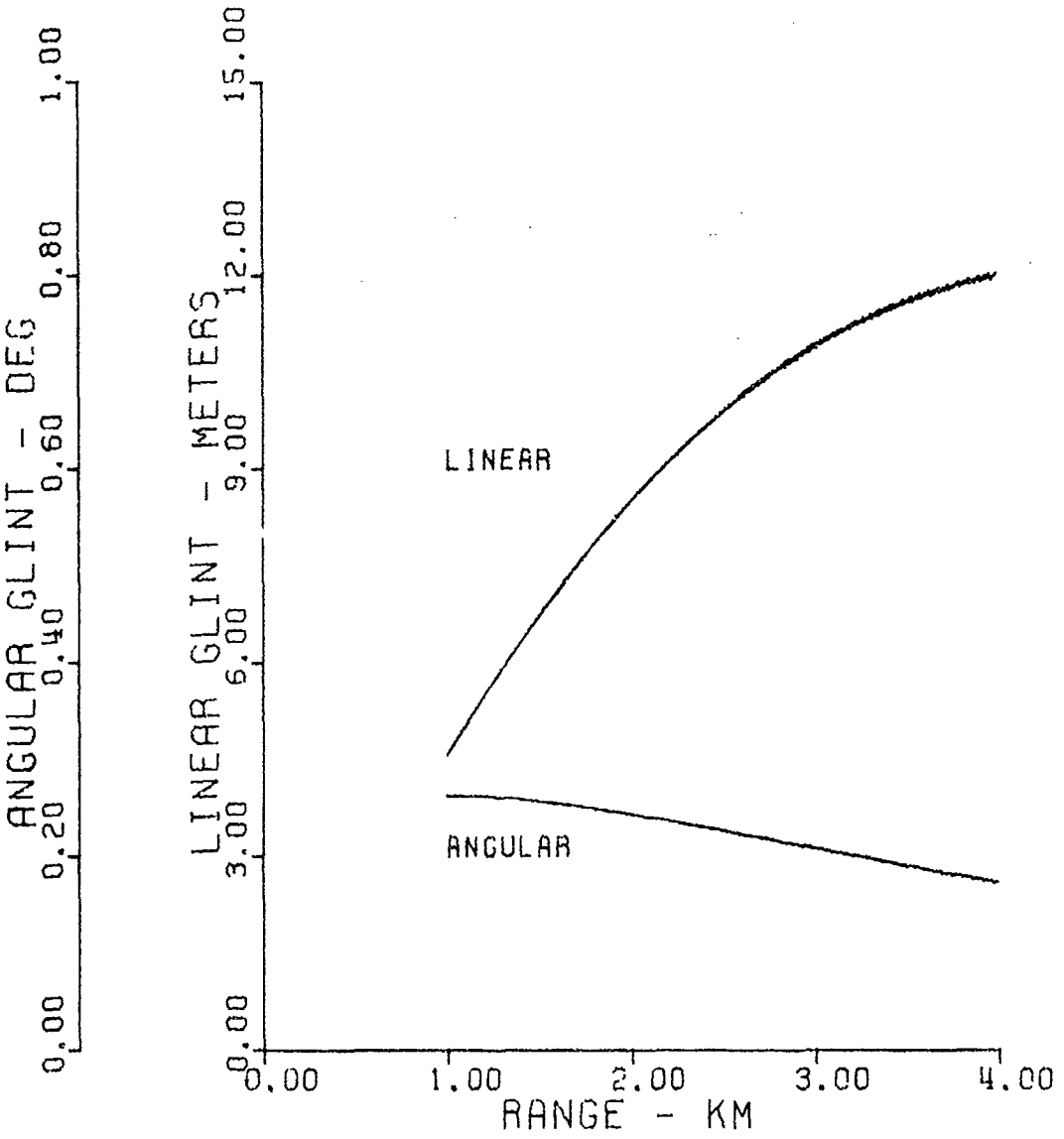

FIG. 5-8--RANGE DEPENDENCE OF GLINT FOR TWO NON-ISOTROPIC REFLECTORS, TWO METERS APART

along the trajectory listed in Appendix B as trajectory No. 11. This trajectory provides a series of sample points having a maximum range of 4.65 Km, a minimum range of 900 m, and aspect angles which vary about nominal values of θ=90°, ϕ=45°. The projected target extent from this aspect is approximately 20 meters. The root-mean-squared (RMS) value of this waveform is 11.9 meters, as measured from the origin.

Fig. 5-10 presents a probability distribution for the glint waveform of Fig. 5-9. This plot was generated by a program which divided the total range of glint error shown on the abscissa into one meter intervals and scanned the 1001 data points of Fig. 5-9 to determine the number of values falling within each interval. Each of these numbers was then normalized to the total number of data points and plotted vs the abscissa value corresponding to the midpoint of the appropriate interval.

The spectral density for the waveform of Fig. 5-9 is shown in Fig. 5-11. No attempt was made to calibrate the spectral determinations in terms of meters/$\sqrt{\text{Hz}}$, therefore the ordinate values can be used only as a relative indication of the frequency content of the glint waveform. The published experimental curves of Howard and others [2,3,8,24,29] indicate little spectral energy above about 15 Hz. This value was increased to 20 Hz as a maximum expected frequency component, and Shannon's sampling theorem used to establish the sampling increment of 0.025 seconds. The 25 seconds of available data established the lowest resolvable frequency at 0.04 Hz. The plotted values are the

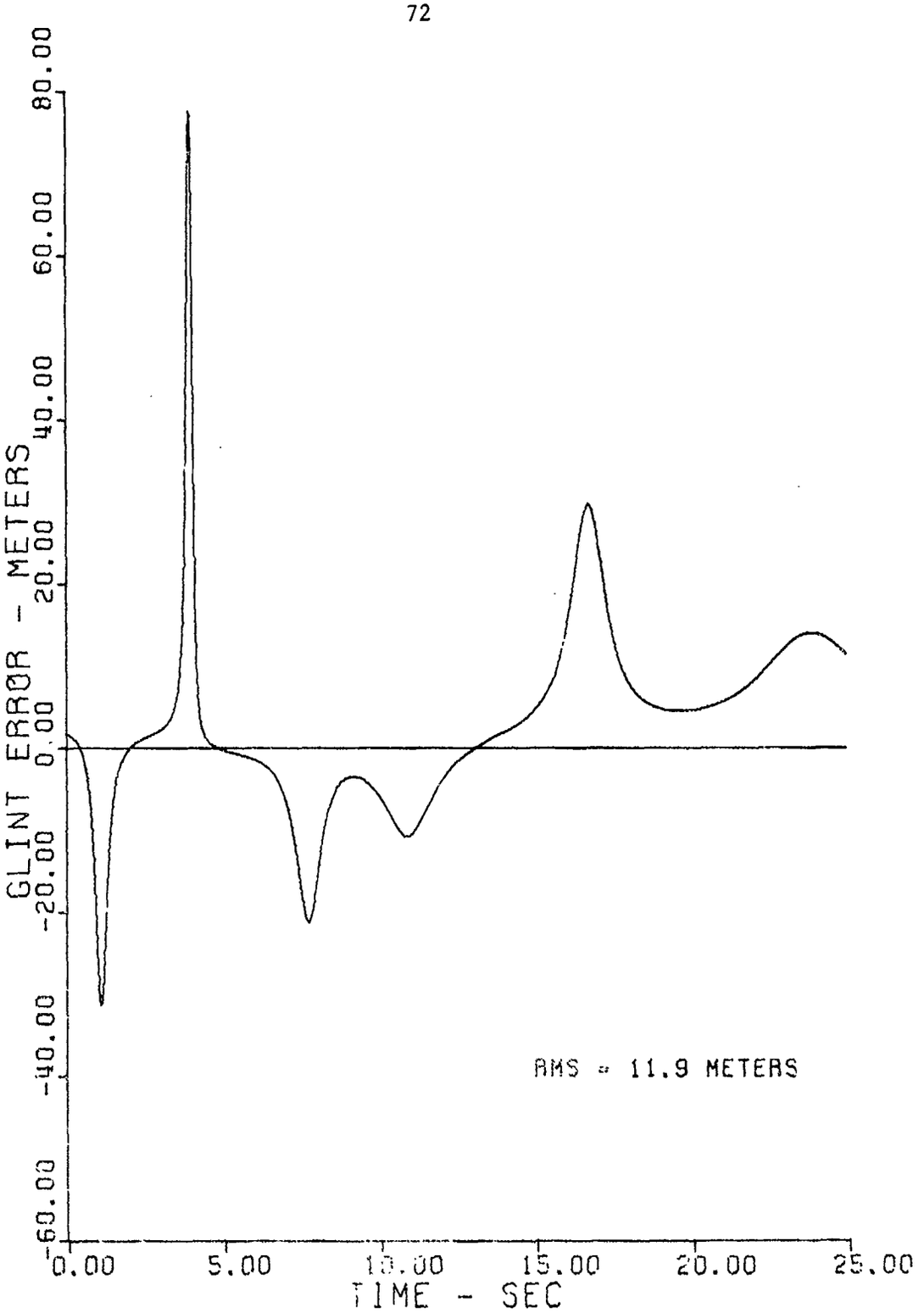

FIG. 5-9--GLINT ERROR FOR SYNTHESIZED TARGET NO. 10 ALONG TRAJECTORY NO. 11

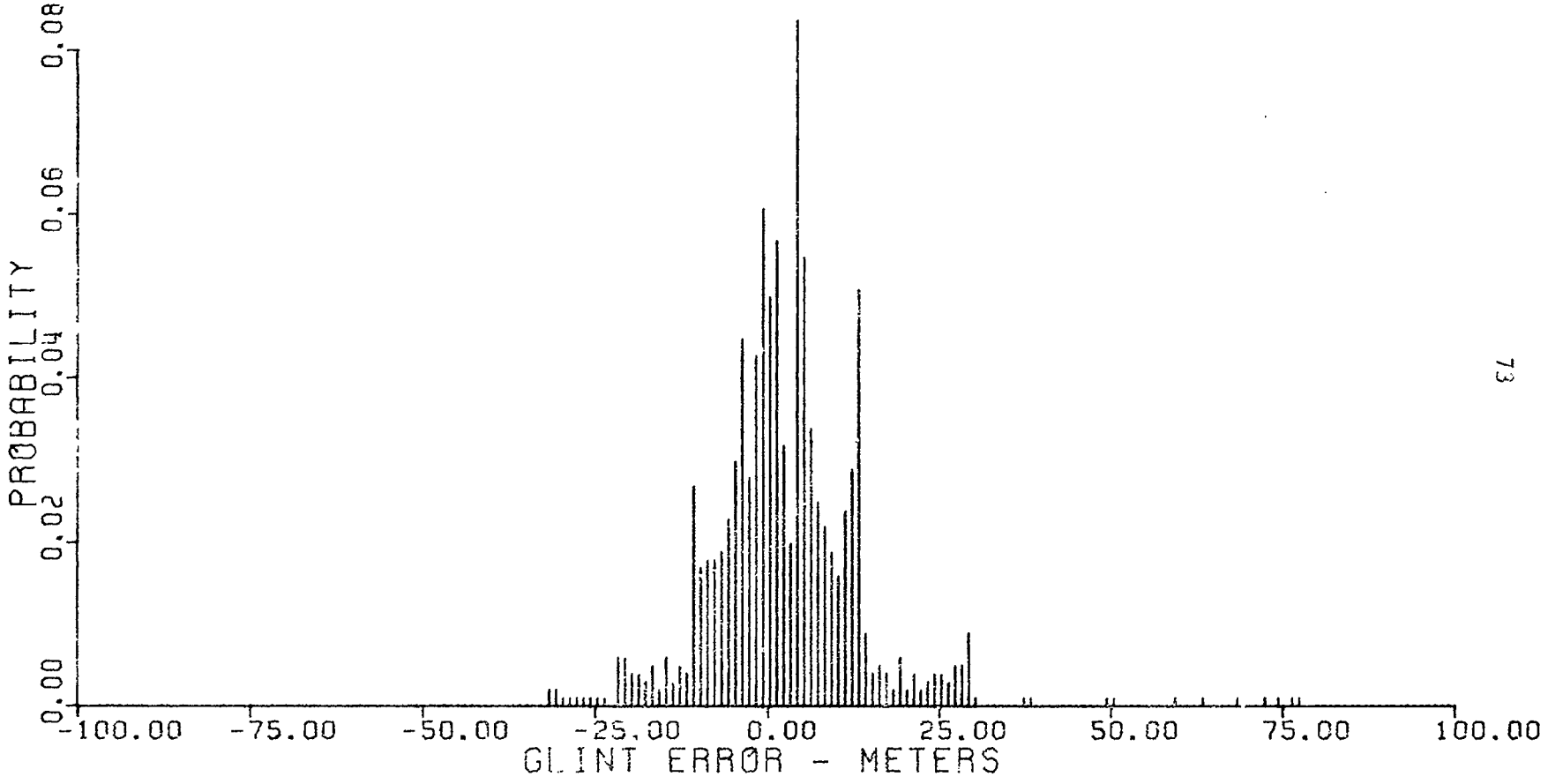

FIG. 5-10--PROBABILITY DISTRIBUTION FOR SYNTHESIZED TARGET NO.10 ALONG TRAJECTORY 11

results of a Fourier analysis at 0.04 Hz and every multiple of 0.04 Hz, up to a maximum of 7 Hz. Assuming the upper cutoff of a typical tracking servo bandpass to be 1 Hz, most of the energy in the waveform would enter the system as tracking noise.

As an illustration of the change in the glint waveform for a different aspect angle, Fig. 5-12 shows the glint error vs time along trajectory No. 15. This trajectory differs from No. 11 only in the choice of ϕ=48° as the nominal azimuth aspect angle. Fig. 5-13 and Fig. 5-14 show the probability distribution and spectral density, respectively, for Fig. 5-12. Note that although the RMS and most probable values of apparent target position have changed, most of the larger spectral components remain below 1 Hz.

Relationship between glint and field amplitude

It may be recalled from the discussion in Chapter III that several investigators indicated a negative correlation between regions of large glint error and total field amplitude. This hypothesis was tested using synthesized configuration No. 10 along two different trajectories and at several different radar frequencies. For each case, the linear correlation between the total field amplitude and the magnitude of the linear glint error was computed. The results presented in Table 5-3 show the correlation coefficients to be negative and quite large -- significant indeed for correlation between two different types of field parameters. This strong negative correlation is illustrated graphically by Fig. 5-15, in which the glint error waveform of Fig. 5-9 is superimposed with a relative plot of the corresponding total field

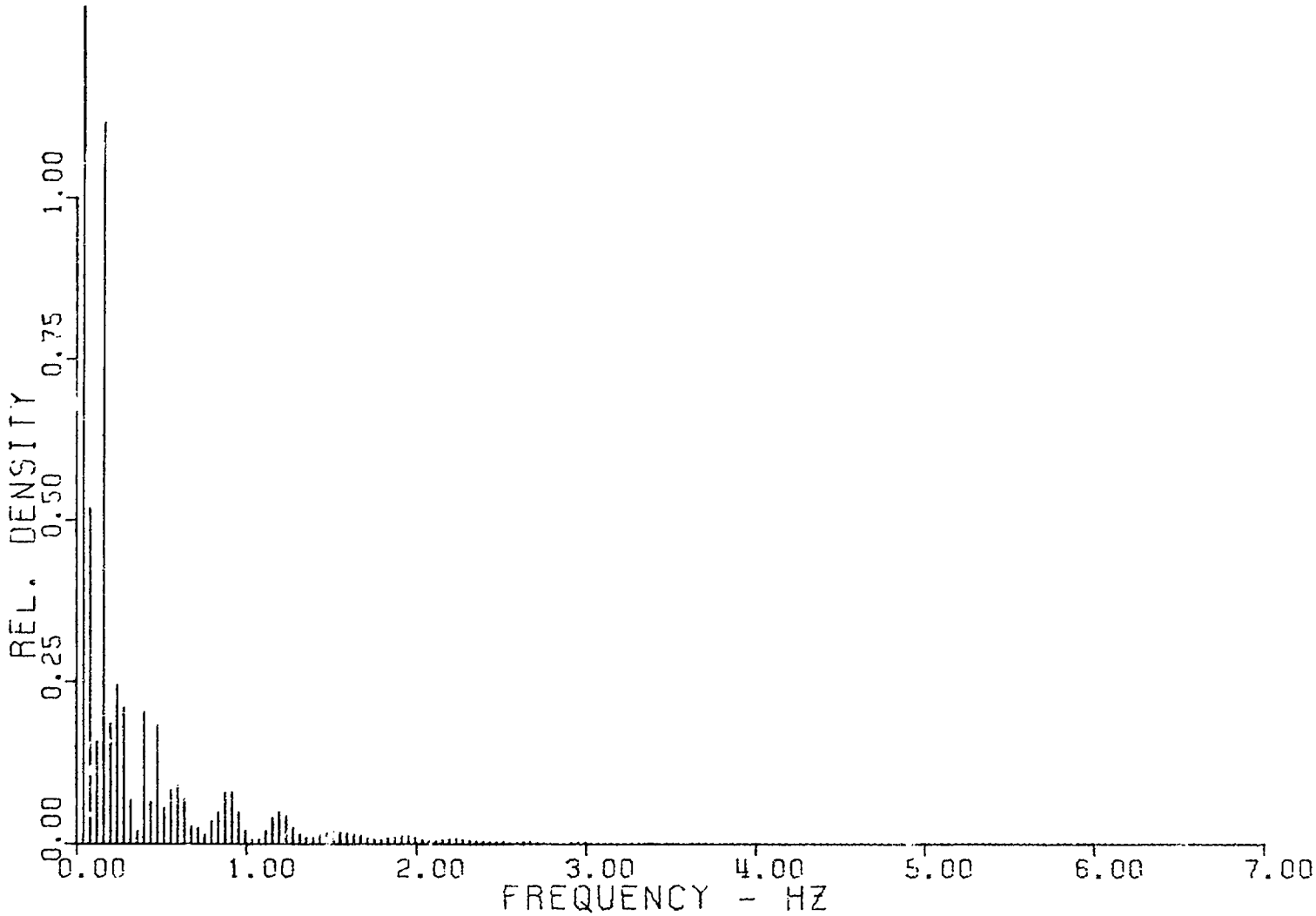

FIG. 5-11--SPECTRAL DENSITY FOR SYNTHESIZED TARGET ALONG TRAJECTORY 11

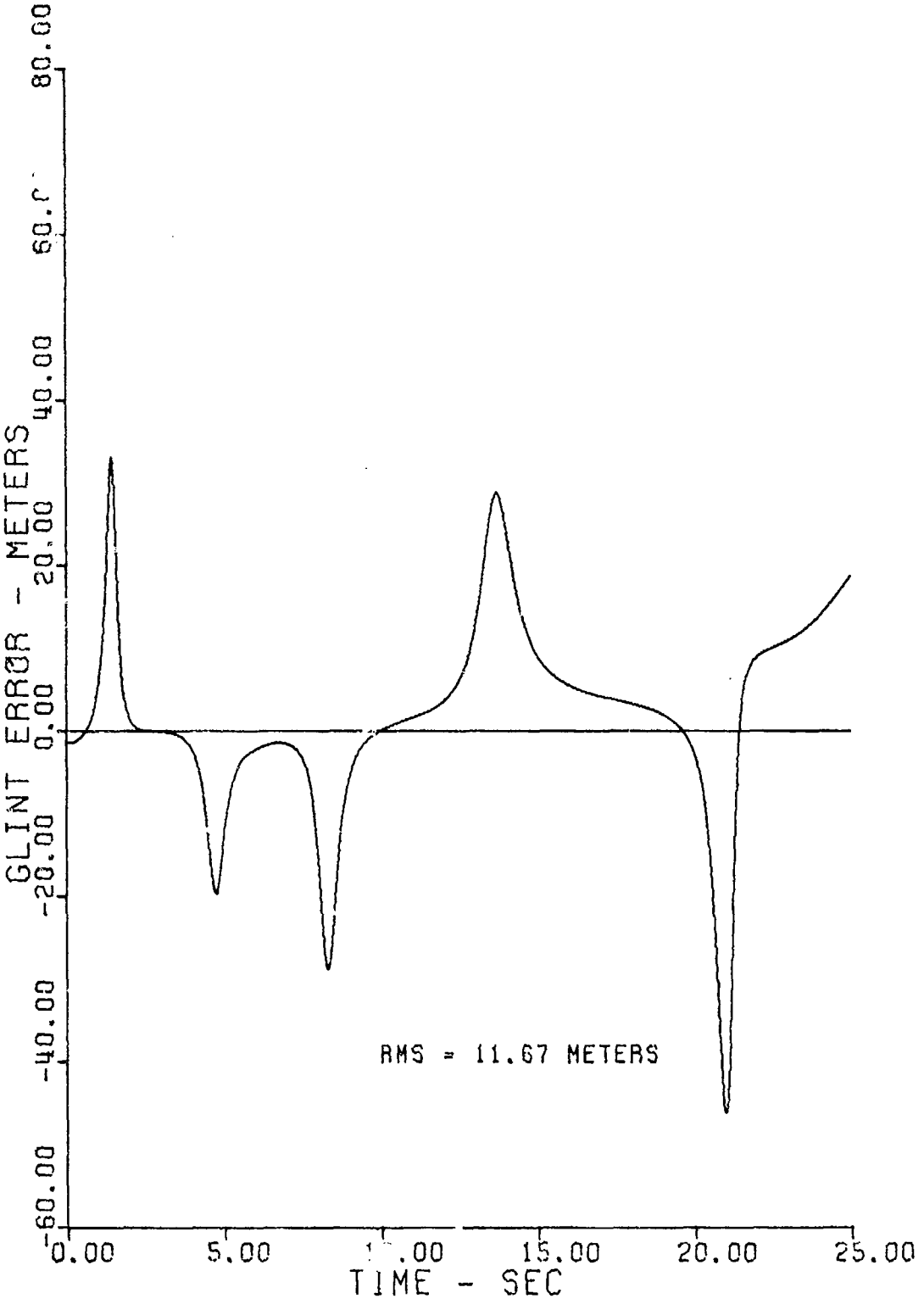

FIG. 5-12--GLINT ERROR FOR SYNTHESIZED TARGET NO. 10 ALONG TRAJECTORY NO. 15

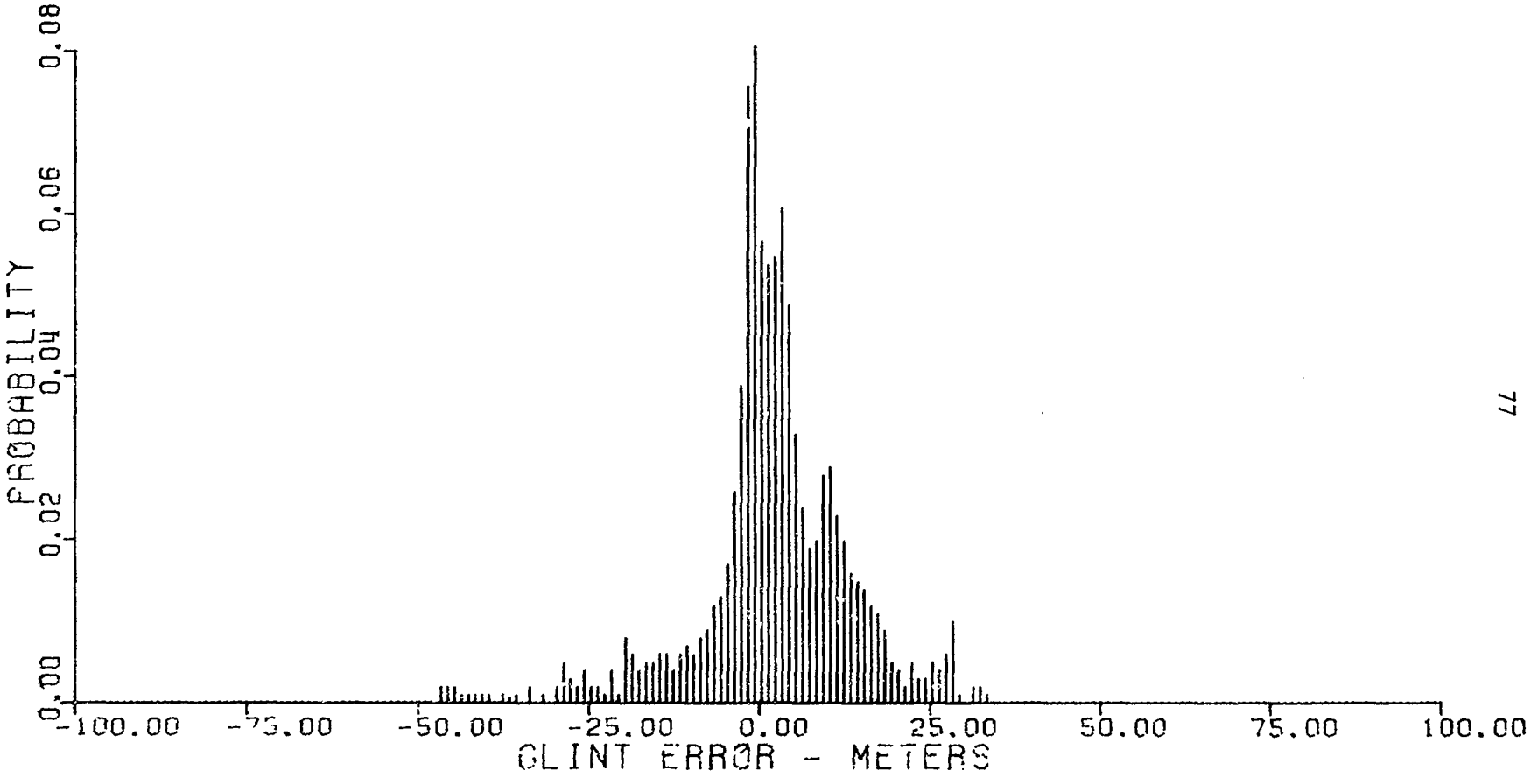

FIG. 5-13--PROBABILITY DISTRIBUTION FOR SYNTHESIZED TARGET NO.10 ALONG TRAJECTORY NO. 15

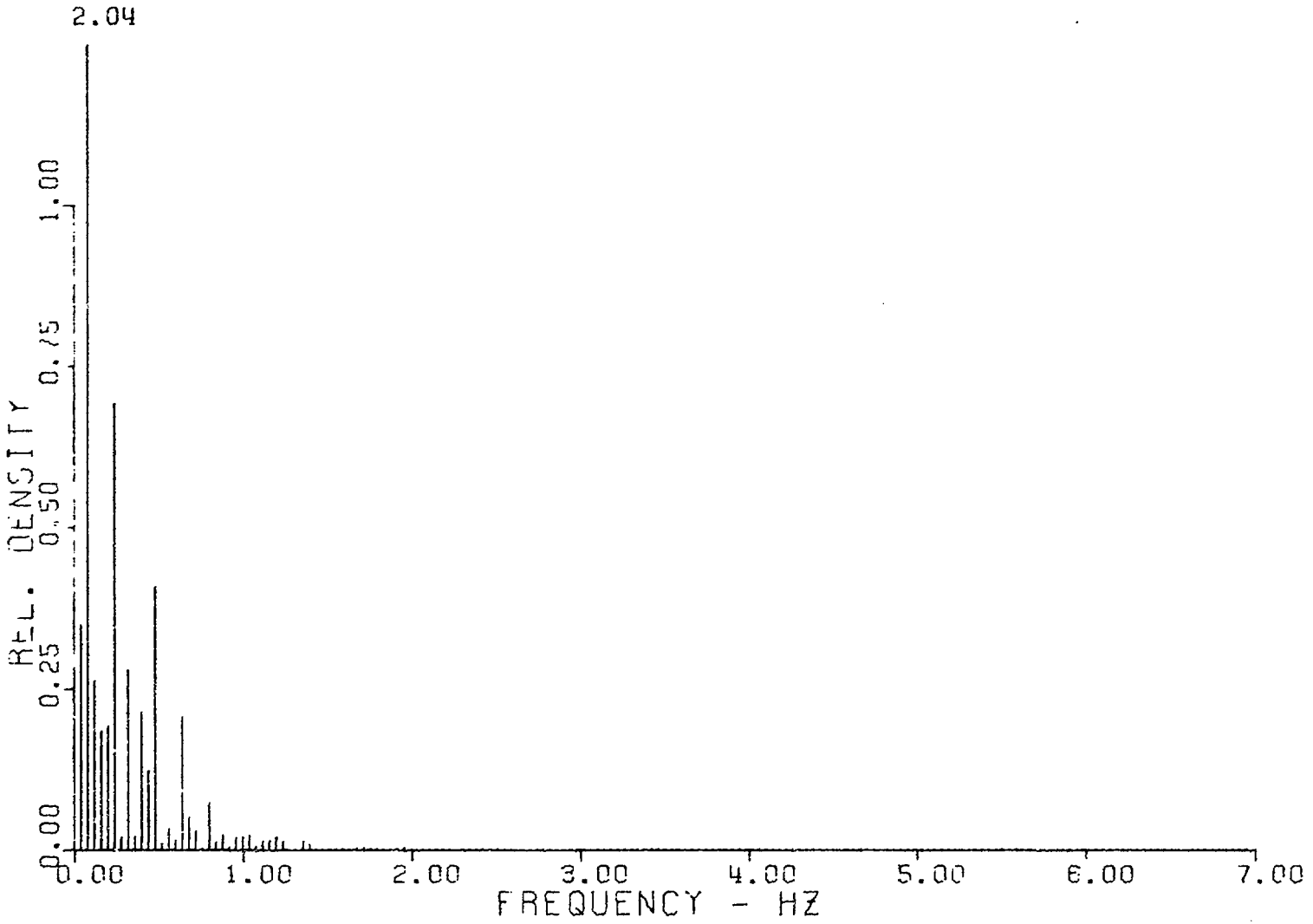

FIG. 5-14--SPECTRAL DENSITY FOR SYNTHESIZED TARGET NO. 10 ALONG TRAJECTORY 15

amplitude. Note that the regions of large positive and negative error coincide exactly with the regions of small amplitude. The linear correlation between amplitude and magnitude of glint error for this figure is -0.605.

Effect of target yaw

In order to illustrate the effect of constant angular motion of the synthesized target on glint behavior, subroutines were prepared to include the appropriate coordinate and phase modifications for the case of target yaw with an observation point in the azimuth plane. A plot of glint error vs time for a yaw rate of 0.0005 rad/sec is presented in Fig. 5-16. With the exception of the non-zero yaw rate, all parameters are identical to those producing Fig. 5-9. The linear correlation coeffecient between the sets of error values shown in these two figures is -0.14, indicating an effective decorrelation of the glint data. Probability distribution and spectral density plots for the waveform of Fig. 5-16 appear in Fig. 5-17 and Fig. 5-18, respectively. From these figures, it appears that although the waveform with target yaw is different, the characteristics of the waveform remain quite similar. The RMS error value is essentially unchanged while the probability distribution still shows significant values to $\pm$ 25 meters. The spectral content has been shifted slightly towards the lower frequencies.

Influence of scattering range angular data increment

An ultimate limitation in the usefulness of the model may be the accuracy with which scattering range pattern recorders can measure

TABLE 5-3

LINEAR CORRELATION COEFFICIENTS BETWEEN MAGNITUDE OF GLINT ERROR AND RELATIVE FIELD AMPLITUDE

FREQUENCY (GHz)	TRAJECTORY	CORRELATION COEFFICIENT
10.0	11	-0.605
10.0	15	-0.652
9.98	11	-0.599
9.96	11	-0.621
9.94	11	-0.630
9.92	11	-0.622
9.90	11	-0.438

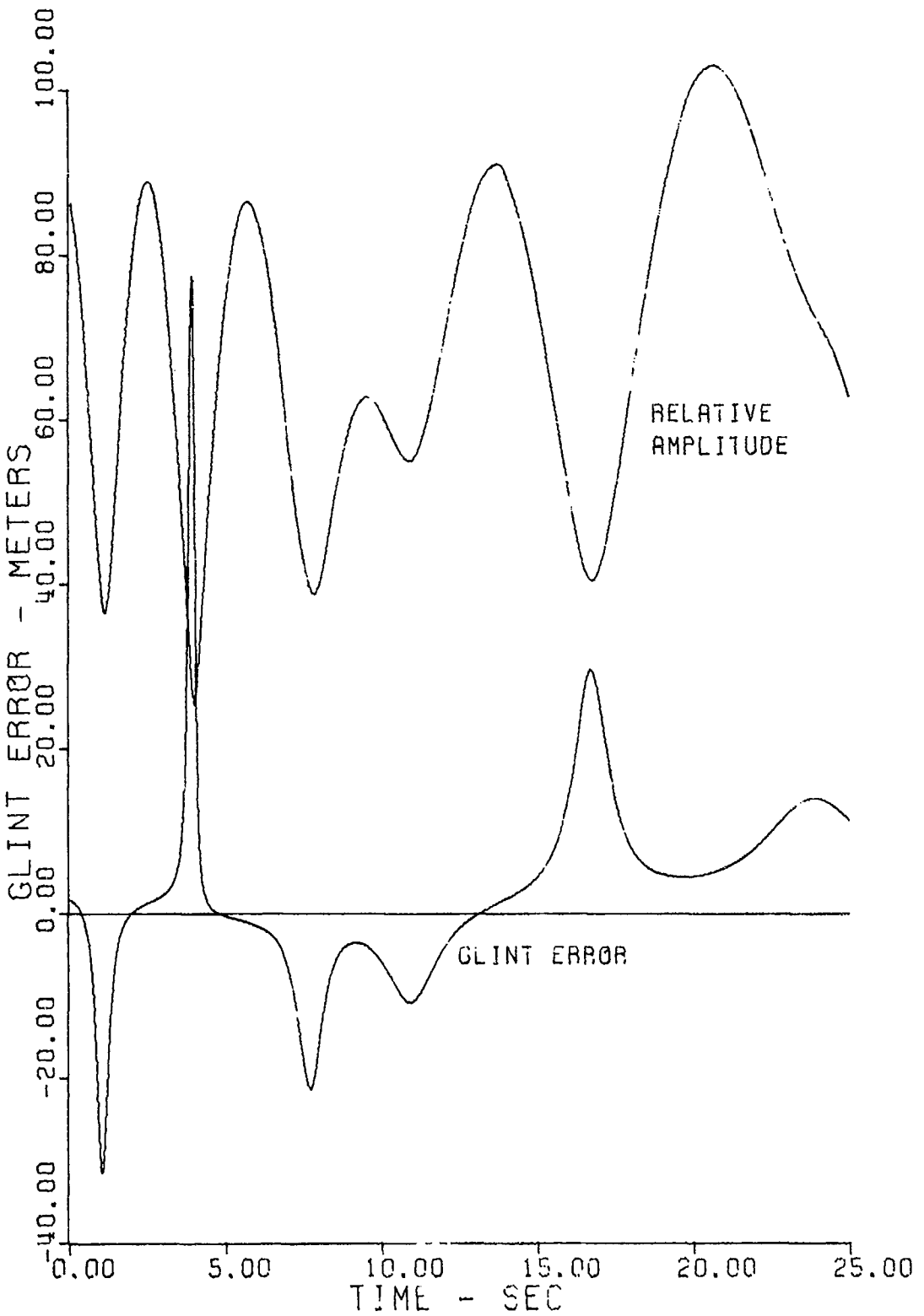

FIG. 5-15--TYPICAL RELATIONSHIP BETWEEN RELATIVE FIELD AMPLITUDE AND GLINT

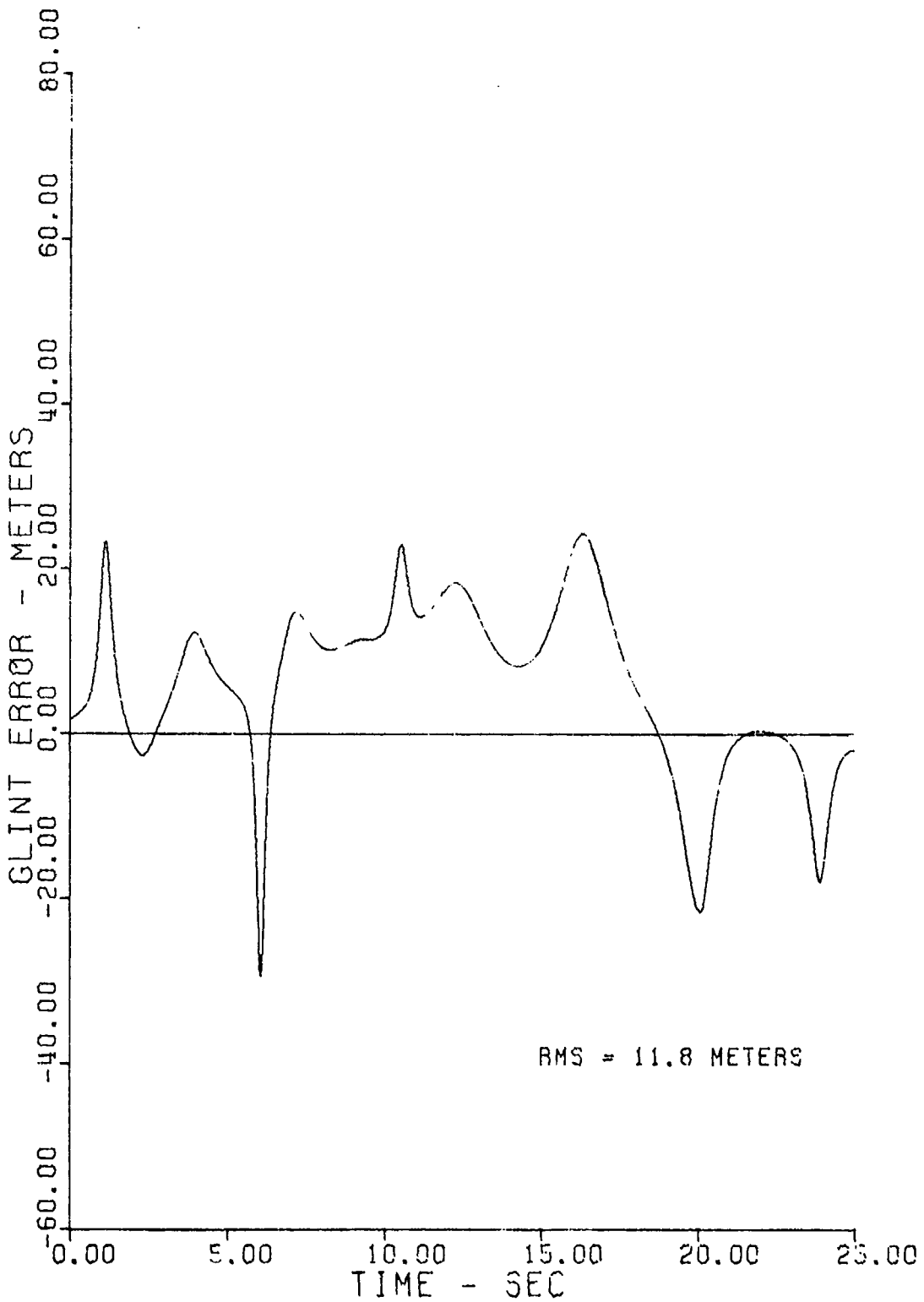

FIG. 5-16--GLINT ERROR FOR A YAW RATE OF 0.0005 RAD/SEC

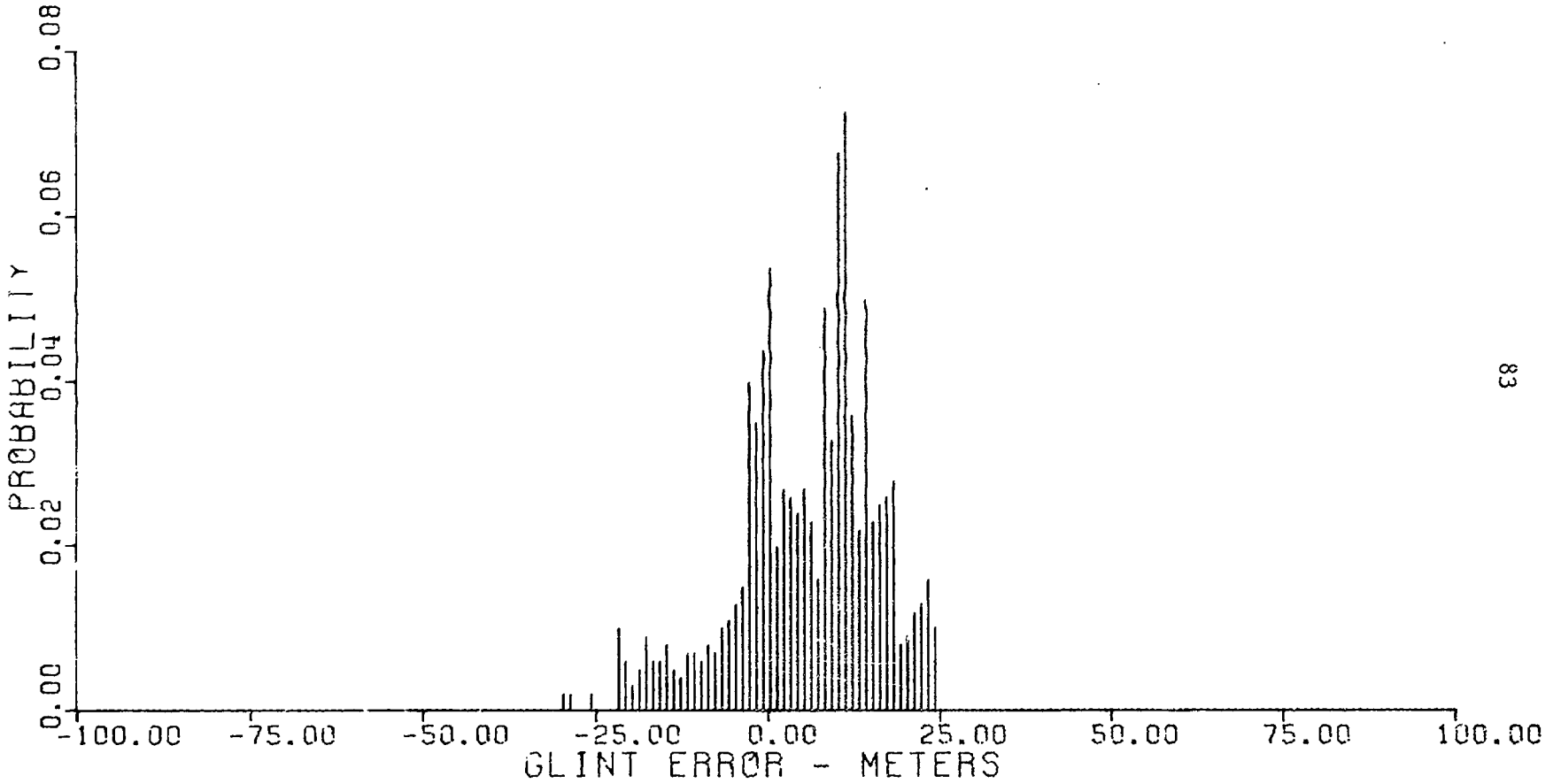

FIG. 5-17--PROBABILITY DISTRIBUTION FOR THE WAVEFORM OF FIG. 5-16

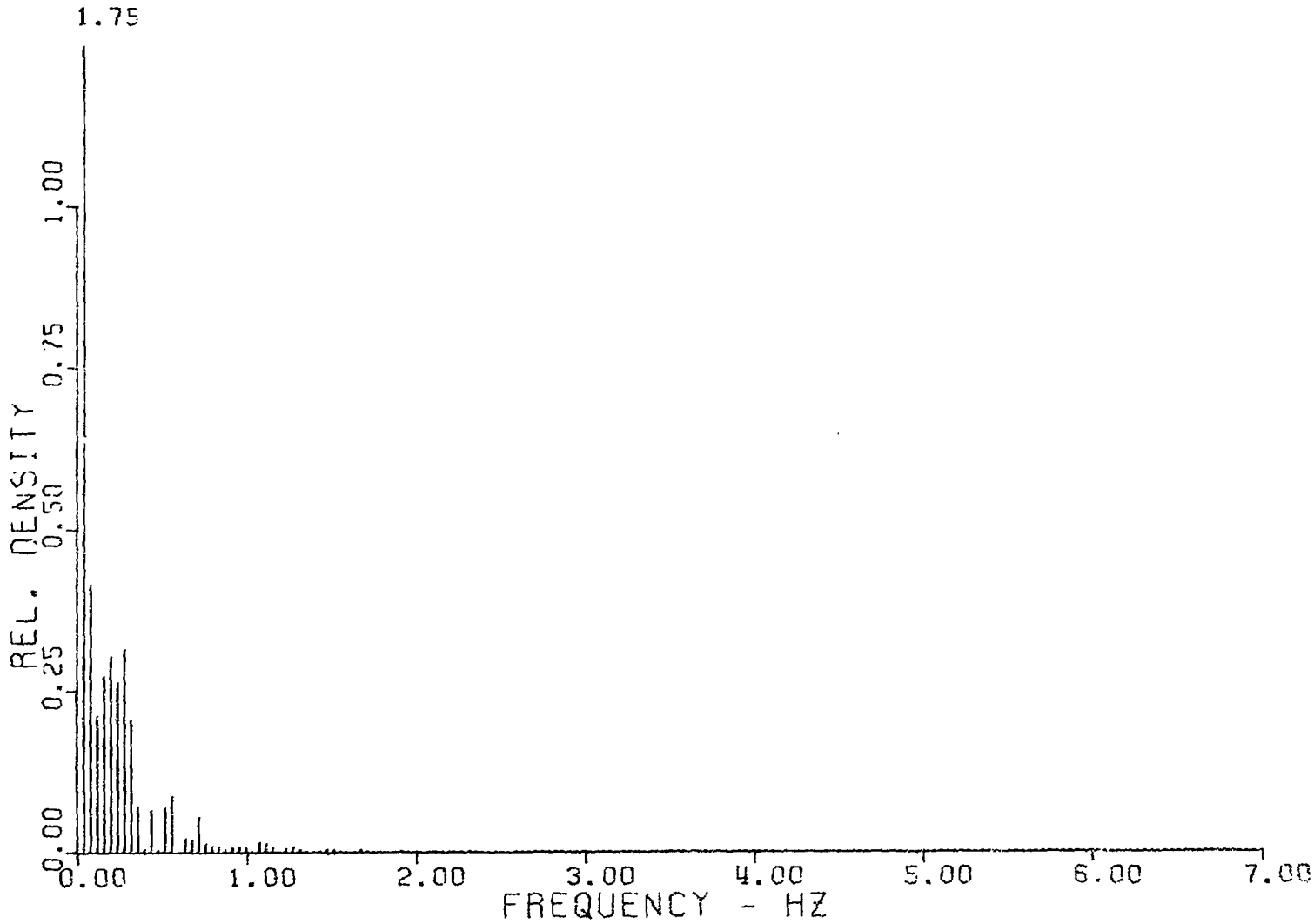

FIG. 5-18--RELATIVE SPECTRAL DENSITY FOR THE WAVEFORM OF FIG. 5-16

the angular setting of the target positioner. The required accuracy, of course, will depend upon the fine-grain lobe structure of the scattering complexes. To determine the effect of incrementing the aspect angle for a synthesized target configuration, an AMPPHI subroutine was written which not only implemented the generating functions listed in Table 5-1, but also allowed for rounding the values of the aspect angles to be used in generating the amplitude and phase data. That is, the aspect angles of each observation point in each secondary coordinate system were rounded to the nearest "R" before being used to obtain the appropriate amplitude and phase data. The result of a linear correlation between the error data of Fig. 5-9 and an identical run with R=0.25 deg was a correlation coefficient of only 0.071. This seems to indicate that, at least for complexes with lobe structures similar to those of the synthesized scattering complexes, a very accurate pattern range positioner would be required.

E. Diversity Effects

It was implied at the beginning of Chapter IV that the intended utility of the glint model developed in that chapter was primarily one of providing a means of testing and evaluating various implementation of glint compensation schemes. As an illustration of this use, this last section will demonstrate the effectiveness of two simple data processing schemes for dual frequency and dual tracker diversity techniques. The target used is that which has been designated as

synthesized configuration No. 10.

Frequency diversity

Table 5-4 presents typical correlation coefficients between sets of error data obtained over trajectory No. 11 with frequency as a parameter. A correlation of 0.5 or less was chosen as a reasonable condition for independence of the data. Ray [32] has used a similar value. Thus, judging from the values in Table 5-4, it would seem advantageous to investigate the use of the glint data obtained at two or more of these frequencies to obtain more accurate tracking information. The magnitude of RMS error before and after diversity processing will be used as a measure of accuracy improvement (or deterioration).

The first technique implemented was to simply average the two values obtained with the two frequencies at each sample point along the trajectory. The results of this operation are presented in Table 5-5, where the RMS values listed are in meters, and the values along the diagonal are the RMS values at the corresponding single frequencies. Note that in most cases, the result of averaging at two frequencies is a value less than the value at either single frequency.

Another technique of data processing which was implemented was based upon the negative correlation between glint error and total field amplitude demonstrated earlier in this chapter. The computer program selected from the pair of glint values at each sample point that value which corresponded to the frequency having the largest

TABLE 5-4

LINEAR CORRELATION COEFFICIENTS BETWEEN SETS OF GLINT ERROR DATA FOR VARIOUS RADAR FREQUENCIES

		FREQUENCY (GHz)					
		10.0	9.98	9.96	9.94	9.92	9.90
FREQUENCY (GHz)	10.0	1.0	0.138	0.404	0.186	0.326	0.163
	9.98		1.0	-0.023	0.611	-0.076	0.163
	9.96			1.0	0.025	0.457	0.156
	9.94				1.0	0.079	0.008
	9.92					1.0	0.102
	9.90						1.0

TABLE 5-5

RMS ERROR IN METERS RESULTING FROM AVERAGING THE DATA AT TWO RADAR FREQUENCIES

		FREQUENCY (GHz)					
		10.0	9.98	9.96	9.94	9.92	9.90
FREQUENCY (GHz)	10.0	11.9	8.3	8.9	8.9	9.8	12.3
	9.98		10.1	6.9	9.6	7.8	11.5
	9.96			9.6	7.6	9.5	11.3
	9.94				11.4	8.8	11.1
	9.92					12.5	11.9
	9.90						19.2

field amplitude. The resulting RMS error values are presented in Table 5-6, where the values on the diagonal are again the single-frequency RMS errors. This processing technique appears to provide improved tracking over simple averaging.

To illustrate the nature of the improvement provided by diversity, it is instructive to analyze a resulting glint waveform and compare it with the corresponding waveforms at the single frequencies. The frequency combination in Table 5-6 resulting in the lowest RMS value is 10 - 9.9 GHz. The waveform, probability distribution, and spectral density plots for f = 10 GHz have been presented in Figures 5-9, 5-10 and 5-11. The corresponding plots for f = 9.9 GHz are shown in Figures 5-19, 5-20 and 5-21. The graphs resulting from using the error-selection technique at these two frequencies appear as Figures 5-22, 5-23 and 5-24. Note that the large values of error are eliminated, with a corresponding narrowing of the probability distribution function about zero. Also, the spectral lines seem to be more concentrated near zero frequency.

As a test of a slightly more sophisticated diversity processing scheme, the error-selection technique was implemented on the basis of the amplitudes at all six of the radar frequencies previously used. This resulted in a RMS value of only 4.6 meters.

Space diversity

Perhaps the most simple form of space diversity is the phase front averaging effect provided by a finite-sized antenna aperture. All of the data presented thus far in this chapter has been generated with an

TABLE 5-6

RMS ERROR IN METERS RESULTING FROM SELECTING THE VALUE AT EACH SAMPLE POINT WHICH CORRESPONDS TO THE LARGEST TOTAL FIELD AMPLITUDE

		FREQUENCY (GHz)					
		10.0	9.98	9.96	9.94	9.92	9.90
FREQUENCY (GHz)	10.0	11.9	7.3	8.0	5.6	7.2	4.8
	9.98		10.1	7.7	7.4	6.0	5.8
	9.96			9.6	5.5	7.1	5.0
	9.94				11.4	5.7	7.5
	9.92					12.5	5.9
	9.90						19.2

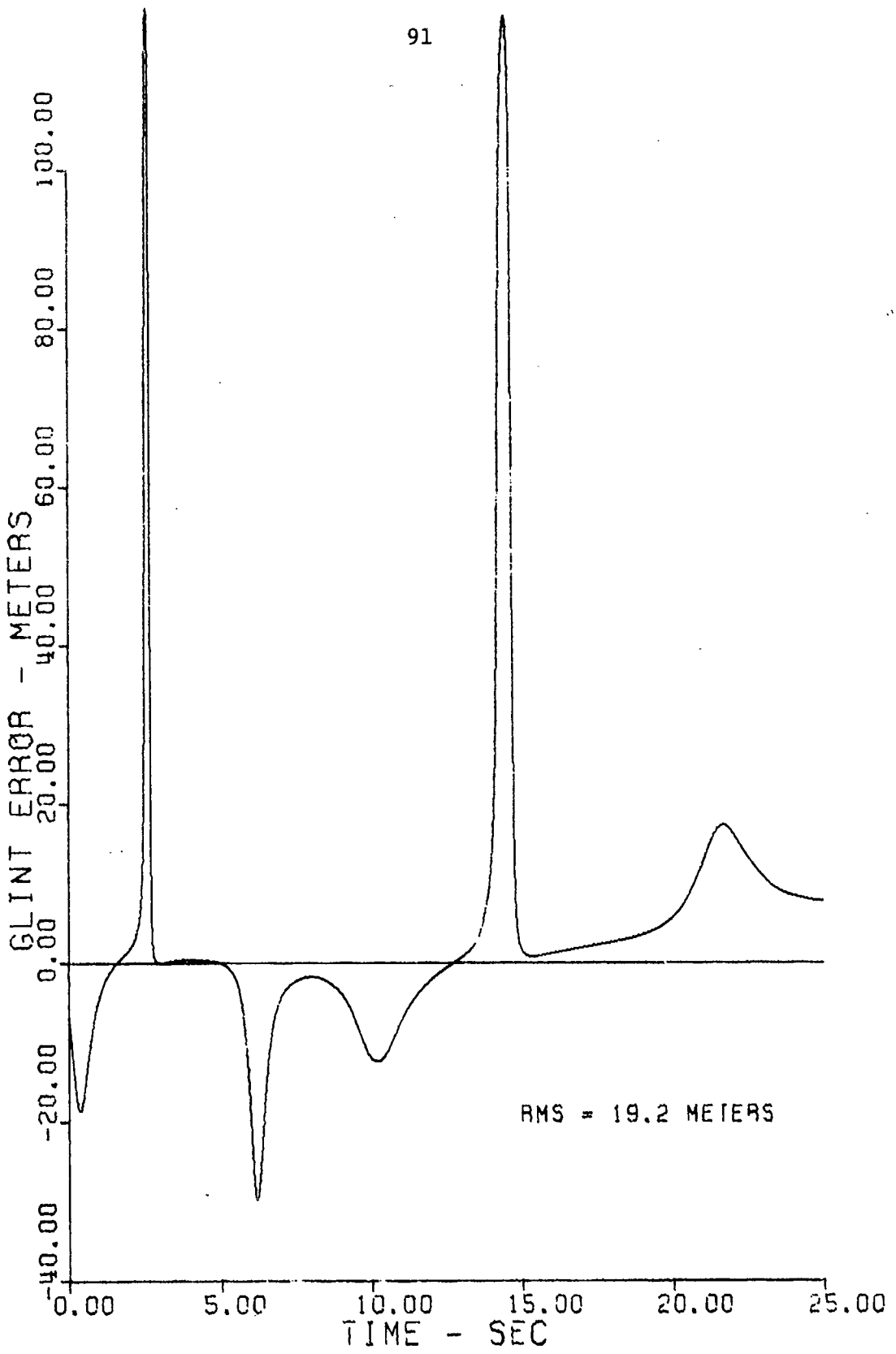

FIG. 5-19--GLINT ERROR FOR A FREQUENCY OF 9.9 GHZ

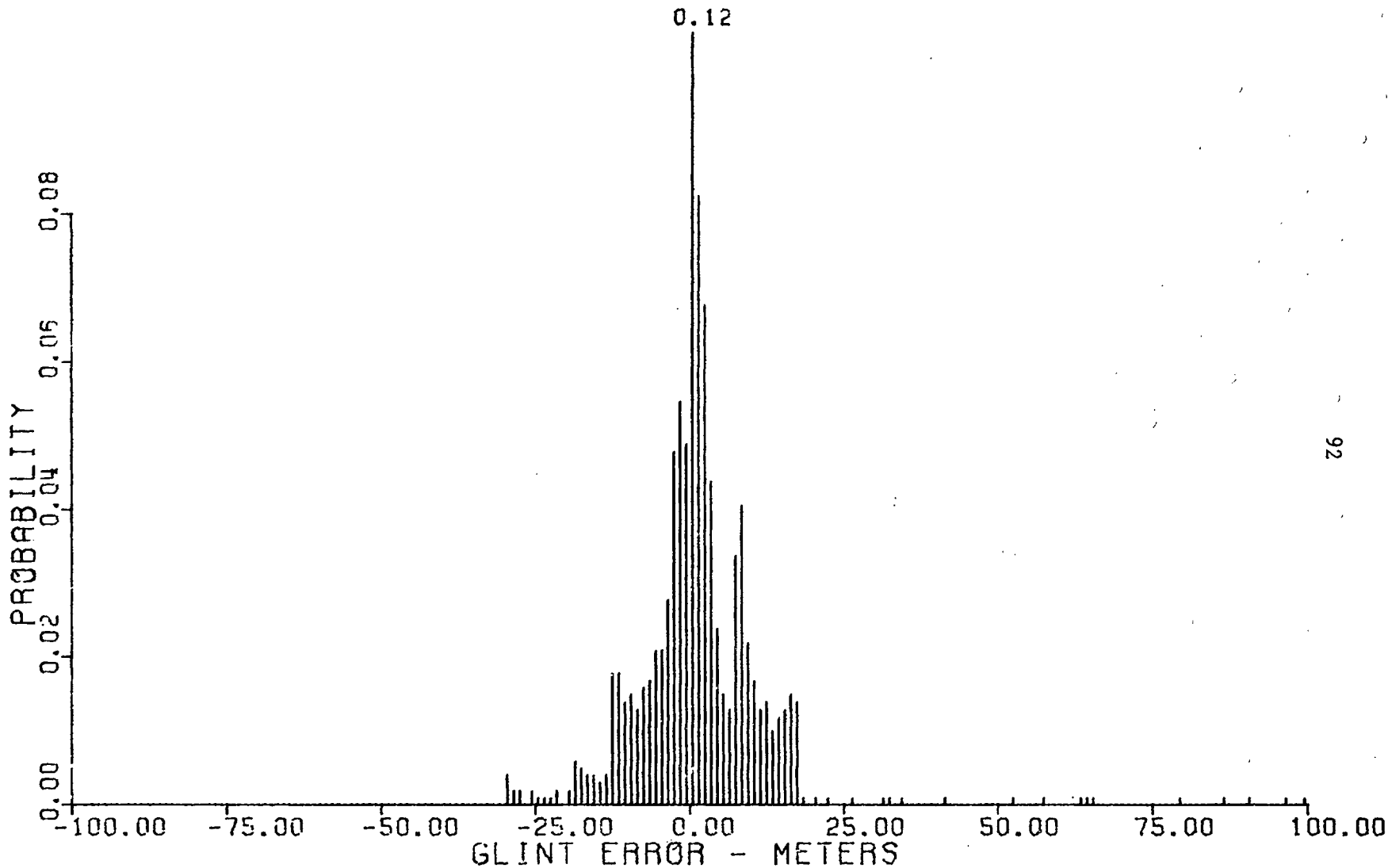

FIG. 5-20--PROBABILITY DISTRIBUTION FOR THE WAVEFORM OF FIG. 5-19

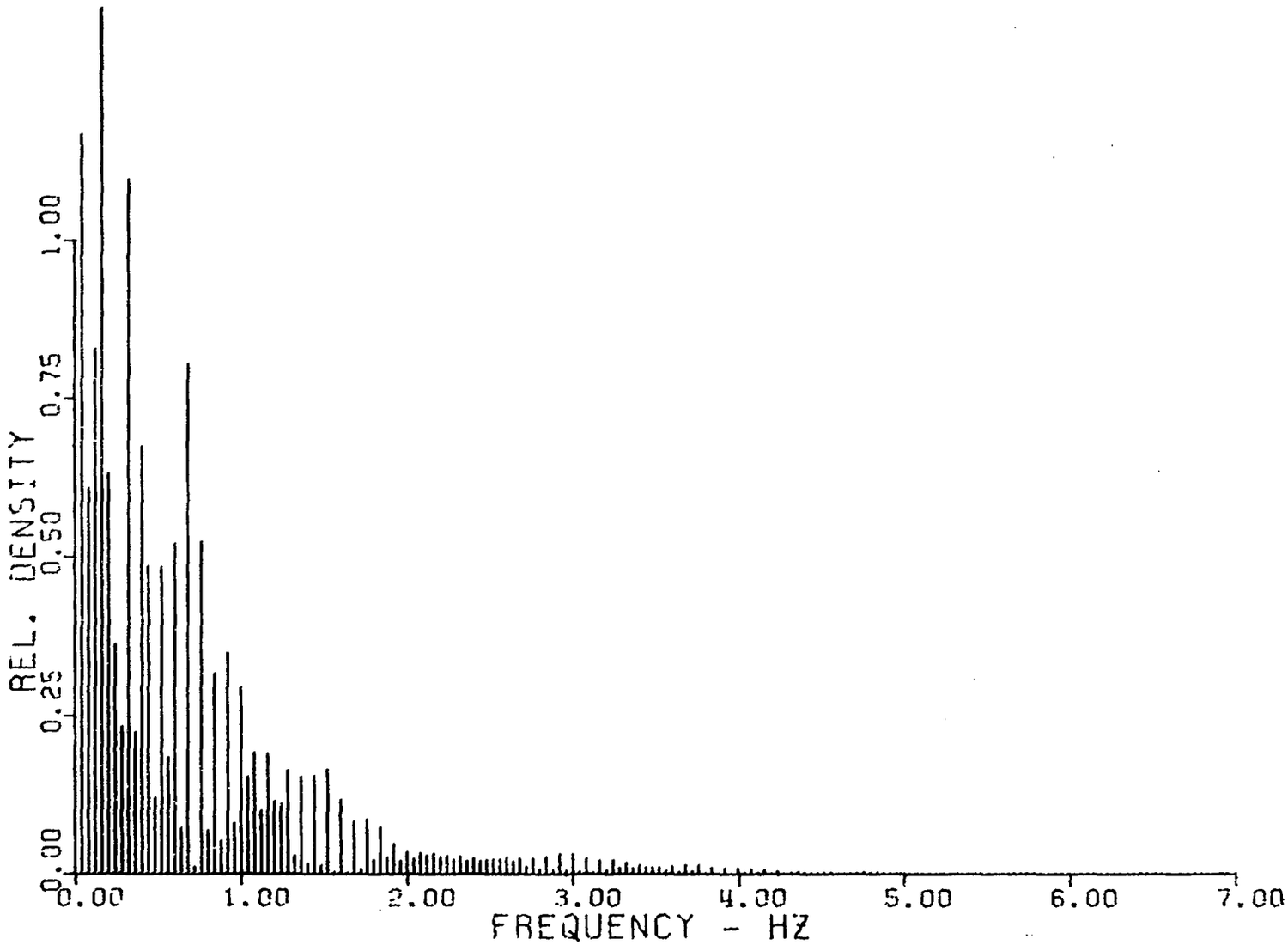

FIG. 5-21--RELATIVE SPECTRAL DENSITY FOR THE WAVEFORM OF FIG. 5-19

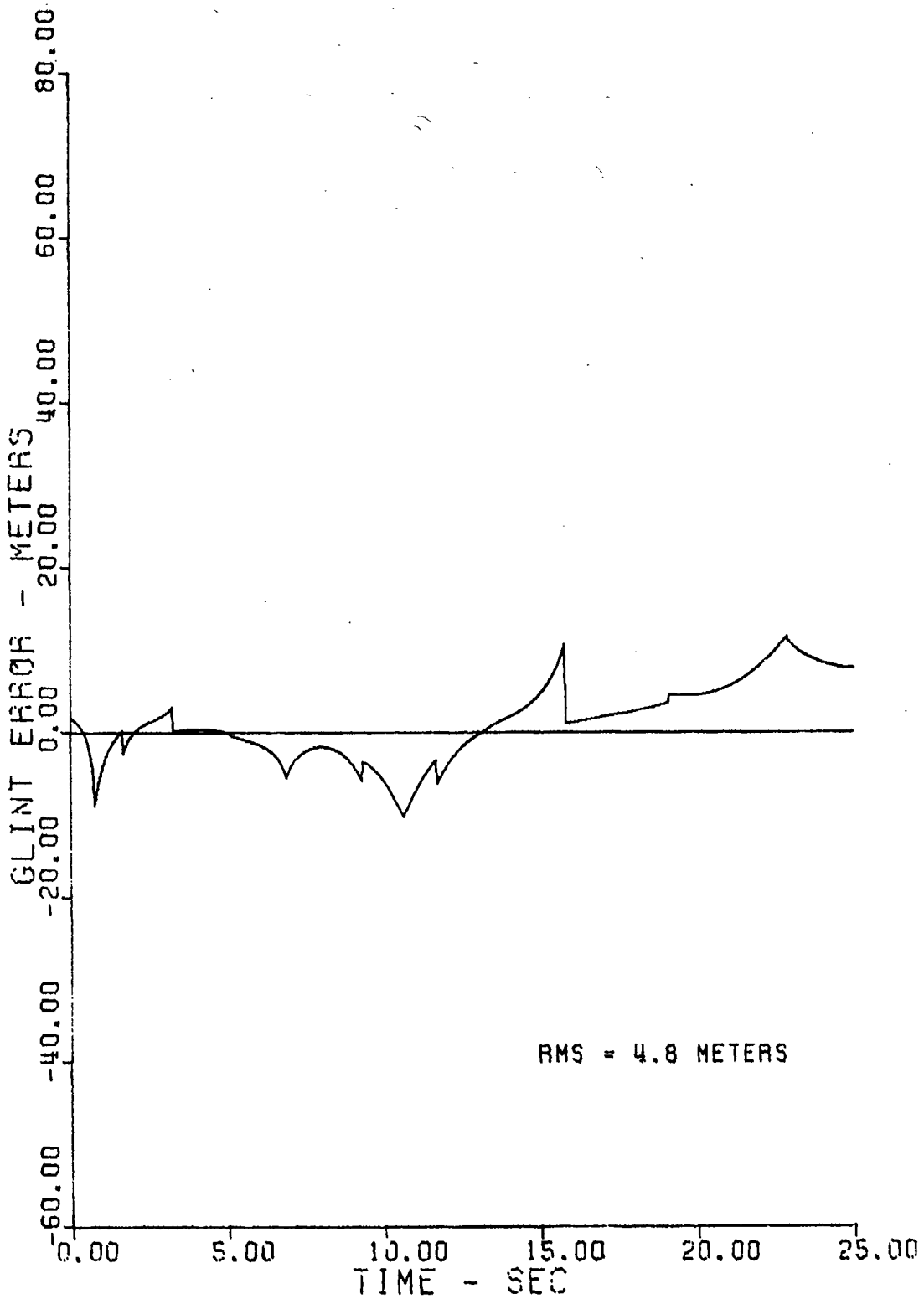

FIG. 5-22--GLINT ERROR USING ERROR-SELECTION FREQUENCY DIVERSITY

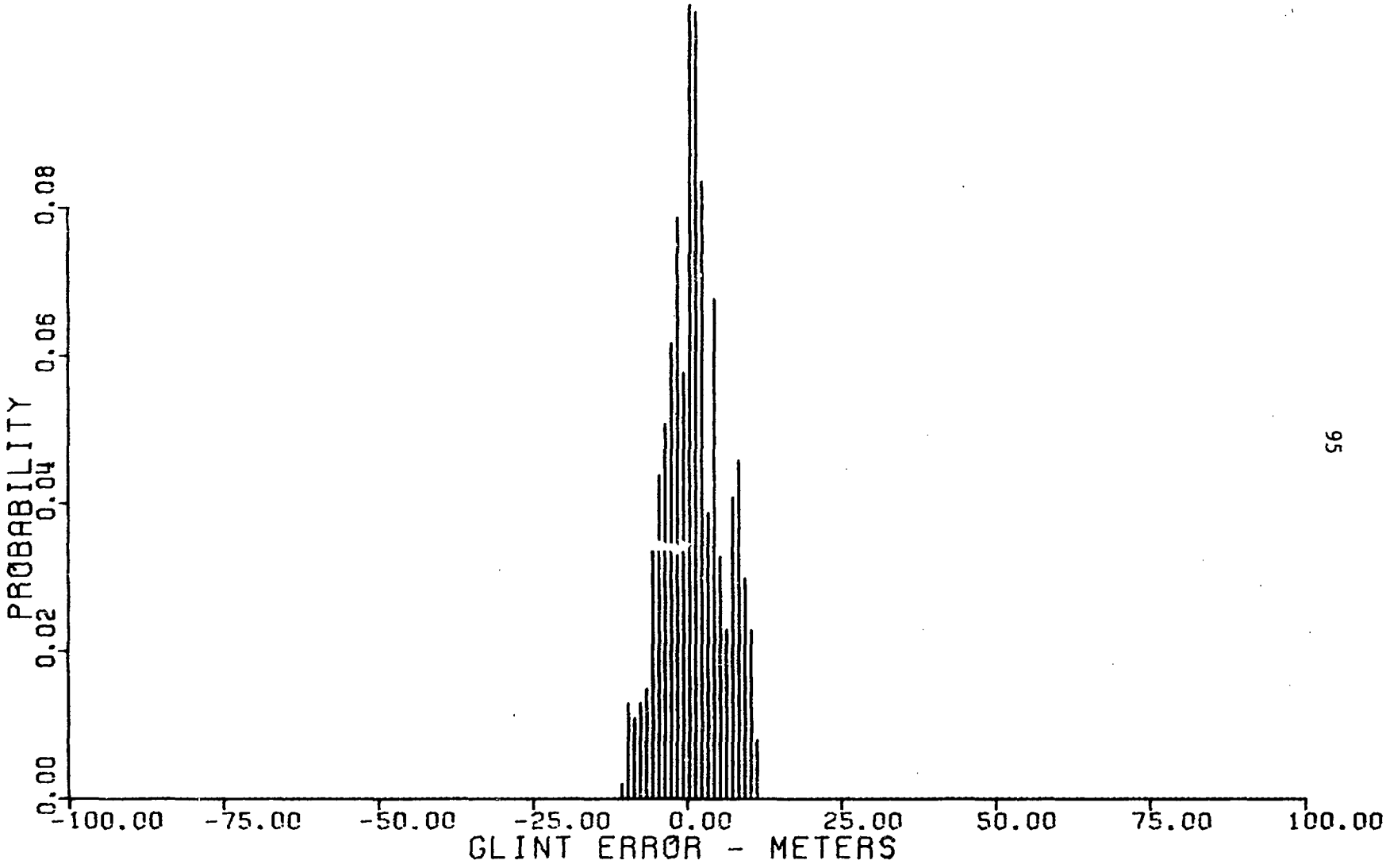

FIG. 5-23--PROBABILITY DISTRIBUTION FOR THE WAVEFORM OF FIG. 5-22

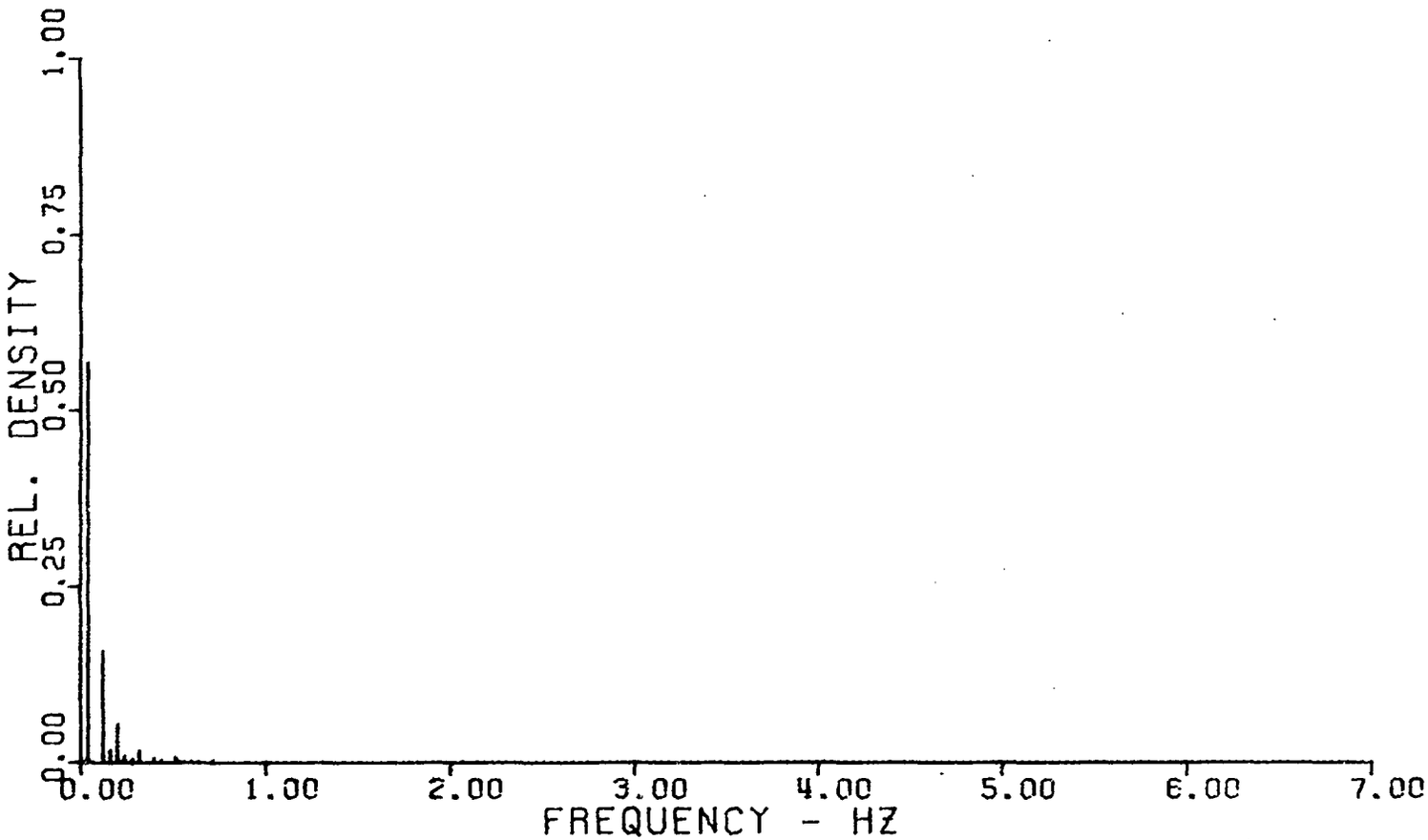

FIG. 5-24--RELATIVE SPECTRAL DENSITY FOR THE WAVEFORM OF FIG. 5-22

aperture diameter of 50 cm. To gain insight concerning the degree of aperture averaging which might be obtainable, two runs with configuration No. 10 along trajectory No. 11 and at 10 GHz were made, one with a diameter of 10 cm and the other using a diameter of 100 cm. The linear correlation coefficient between the glint errors for these two cases was 0.96. This tends to indicate that even an order of magnitude of change in aperture diameter yields little decorrelation of the data.

The more usual form of space diversity involves the use of two tracking antennas spaced some distance apart. While this technique is not practical in a homing missile application, several runs were made for configuration No. 10 at a frequency of 10 GHz and using a dual tracker to gain insight concerning the degree of decorrelation achieved by spaced antennas. Each dual tracker run was actually implemented by making two data runs of the main glint program. In each case, the TRAJ subroutine generated the normal trajectory No. 11, but for each observation point, the value of the azimuth coordinate was increased or decreased by an amount corresponding to a fixed linear distance at the value of range for the observation point. A linear correlation was then performed on the pairs of glint error values obtained for the two data runs, and RMS computations made for each data set and also on the result of using the error-selection technique based upon the received amplitude at each tracker. The results of these computations are presented in Table 5-7, where RMS_1 and RMS_2 are the RMS error values for the individual trackers, and RMD_{div} is the

corresponding value using error-selection diversity. It appears from the data that even rather small spacings can be quite effective in reducing glint error.

There is another form of space diversity which is more practical in a homing missile application. This involves the use of bistatic tracking with two or more target illuminating antennas. Because bistatic target illumination is often ground situated, the use of multiple antennas at larger spacings becomes practical. The basic program limitation to the monostatic configuration prevented investigation of this technique, but of course the model as developed could be adapted for bistatic studies.

TABLE 5-7

EFFECT OF SPACE DIVERSITY FOR VARIOUS

DUAL-TRACKER SPACINGS

SPACING (m)	CORRELATION COEFFICIENT	RMS_1	RMS_2	RMS_{Div}
1	0.383	12.0	11.8	6.1
3	0.001	12.9	11.7	5.5
6	0.045	15.5	11.7	6.4

V. CONCLUSIONS

In summary, a review of prior glint investigations reveals no analytical model which is adequate in describing glint for a complex target, and yet simple enough to permit implementation for such a realistic scattering object. The technique developed here uses the concept of coherent summation of the field contributions from various nonisotropic scattering complexes. The glint error is determined by use of a simple geometric construction together with values of total field phase in the region of the tracking aperture.

The model was implemented on the digital computer, and the results obtained for theoretical configurations of isotropic scatterers were analyzed and compared with known results from other investigations. In lieu of measured data from actual scattering complexes, nonisotropic amplitude and phase patterns were synthesized to illustrate further the modelling technique. The glint waveforms for theoretical target configurations of such synthesized complexes, as obtained over several different approach trajectories and at several different radar frequencies, were analyzed for RMS value, probability distribution, and spectral content.

Finally, the effects of using frequency and space diversity with a synthesized target were studied. The results indicate that a considerable tracking improvement can be achieved by using the easily

implemented data processing scheme of choosing the tracking-error signal which corresponds to the diversity return having the largest signal amplitude.

The data obtained and the results discussed indicate that this study could be profitably pursued both to gain valuable insight into the nature of glint, and as a tool to devise and evaluate diversity compensation schemes. It seems that this end would adequately justify the time and expense of obtaining the required amplitude and phase patterns for actual scattering complexes.

REFERENCES

1. Locke, A. S., Guidance. Princeton, N. J., D. Van Nostrand, Co., Inc. (1955).

2. Dunn, J. H., Howard, D. D., and King, A. M., "Phenomena of Scintillation Noise in Radar-Tracking Systems," Proc. IRE, 47, 855 (1959).

3. Meade, J. L., Hastings, A. E., and Gerwin, H. L., Noise in Tracking Radars. Naval Research Laboratory, Report 3759, AD 90 876 (1950).

4. Brockner, C. E., "Angular Jitter in Conventional Conical Scanning Automatic Tracking Radar Systems," Proc. IRE, 39, 51 (1951).

5. Delano, R. H., "A Theory of Target Glint or Angular Scintillation in Radar Tracking," Proc. IRE, 41, 1778 (1953).

6. Kerr, D. E., Propagation of Short Radio Waves. New York, N. Y., McGraw-Hill Book Co. (1951).

7. Muchmore, R. B., "Aircraft Scintillation Spectra," IRE Trans. AP, 8, 201 (1960).

8. Muchmore, R. B., Review of Scintillation Measurements. Hughes Aircraft Co. TM 272, AD4849 (1952).

9. Watson, R. B., and Feagin, R. B., Analysis of Angular Errors of a Track Radar System for N-Point Radar Target. Military Physics Research Lab., University of Texas (1956).

10. Feagin, R. B., Watson, R. B., and Norwood, J. M., Detailed Data Reduction Procedure for Airborne N-Point Target Backscattering. Military Physics Research Lab., University of Texas (1955).

11. Weimer, F. C., and Peters, Leon, Jr., Study of Pointing Errors in Conically Scanning and Monopulse Tracking Radars for Multi-Point Targets. Antenna Lab., Ohio State University, 601-12, AD 123 476 (1956).

12. Peters, Leon, Jr., Accuracy of Tracking Radar Systems. Antenna Lab., Ohio State University, 601-29. AD 200 027 (1957).

13. Lewis, D. E., On Tracking Radar Systems and the Target Phase Center. Antenna Lab., Ohio State University, 777-4, AD 211 187 (1958).

14. Howard, D. D., Radar Target Angular Scintillation in Tracking and Guidance Systems Based on Echo Signal Phase Front Distortion. Naval Research Laboratory, Report 5430 (1959).

15. Goldstein, M. H. Jr., and Brindey, W. E., Glint Noise and Signal Simulation for the Meteor Seeker. MIT Research Memo RM 6978-3, AD 58 119 (1952).

16. Delano, R. H., and Pfeffer, I., "The Effect of AGC on Radar Tracking Noise," Proc. IRE, 44, 801 (1956).

17. Dunn, J. H., and Howard, D. D., "The Effects of Automatic Gain Control Performance on the Tracking Accuracy of Monopulse Radar Systems," Proc. IRE, 47, 430 (1959).

18. Peters, Leon, Jr., and Weimer, F. C., "Concerning the Assumption of Random Distribution of Scatterers as a Model of an Aircraft for Tracking Radars," IRE Trans. AP, 9, 110 (1961).

19. Muchmore, R. B., "Reply to Comments by Leon Peters, Jr. and F. C. Weimer," IRE Trans. AP, 9, 112 (1961).

20. Delano, R. H., "Further Reply to Comments by Leon Peters, Jr. and F. C. Weimer," IRE Trans. AP, 9, 227 (1961).

21. Peters, Leon, Jr., and Weimer, F. C., "Reply to Comments by R. H. Delano," IRE Trans. AP, 9, 228 (1961).

22. Peters, Leon, Jr., and Weimer, F. C., "Reply to Comments by R. B. Muchmore," IRE Trans. AP, 9, 229 (1961).

23. Siegel, K. M., "Comparison Between Theoretical and Experimental Radar Cross Sections of Aircraft," IRE Trans. AP, 9, 228 (1961).

24. Povejsil, D. J., Raven, R. S., and Waterman, P., Airborne Radar. Princeton, N. J., D. Van Nostrand, Co., Inc. (1961).

25. Moll, J. W., "On the Radar Echo from Aircraft," IEEE Trans. on Aerospace and Elec. Systems, 574 (1967).

26. Ostrovityanov, R. B., "Angular Noise," Radiotekhnika i Elektronika, 4, 507 (1966).

27. Gubonin, N. S., "Fluctuation of the Phase Front of the Wave Reflected from a Complex Target," Radiotekhnika i Elektronika, 10, 717 (1965).

28. Coleman, J. T., and Someroski, F. W., A Survey and Analysis of Radar Glint As Applied to Air Defense Missile System Design. Battelle Memorial Institute, RSIC-699, AD 385 494 (1967).

29. Dunn, J. H., and Howard, D. D., "Radar Target Amplitude, Angle, and Doppler Scintillation from Analysis of the Echo Signal Propagating in Space," IEEE Trans. MTT, 16, 715 (1968).

30. Birkemeir, W. P., and Wallace, N. D., "Radar Tracking Accuracy Improvement by Means of Pulse-to-Pulse Frequency Modulation," AIEE Trans. Comm. Elec., 81, 571 (1963).

31. Gaheen, A. F., McDonough, J. T., and Tice, D. P., Frequency Diversity Radar Study: Vol I. Westinghouse Defense and Space Center, AFAL-TR-66-128, AD 480 358 (1966).

32. Ray, H. K., "Improving Radar Range and Angle Detection with Frequency Agility," Microwave J., 9, 63, (1966).

33. Senior, T. B. A., The Elevation Errors Involved in the Radar Location of a Low Flying Target. Royal Radar Establishment, Memo 1220 (1956).

34. Shaw, A. H., An Expression for the Ground Reflection Elevation Error of an Auto-Tracking Radar at Elevation Angles Comparable with the Beamwidth. Royal Radar Establishment, Memo 1457 (1961).

35. Graf, E. R., Weathers, G. D., Sims, R. J., and Fincher, C. F., A Study of Radar Tracking Error Resulting from Multipath: Analysis and Experimental Results. Auburn University Engineering Experiment Station, Tech. Rept. No. 5, AMC-14525 (1967).

36. RAT SCAT Radar Target Scatter Site. Holloman AFB, New Mexico, MDC-TR-65-26 (1965)

37. Caster, J. M., and Walier, A. A., Jr., Significance of Target Characteristics upon Precision of Monopulse Radar. Syracuse University Research Corp., DSL R-94, AD 451 663 (1964).

38. Allen, P. J., and Olin, I. D., A Four-Component Polarization Resolver for Microwaves. Naval Research Lab., Report 1086, AD 646 189 (1960).

39. Olin, I. D., A System for the Dynamic Measurement of Radar Return Polarization. Naval Research Lab., Report 1082, AD 646 188 (1960).

40. Olin, I. D., and Queen, F. D., Measurements Using a Polarization Instrumentation Radar on Navigational Buoys. Naval Research Lab., Report 5701, AD 268 727 (1961).

41. Berkowitz, R. S., Modern Radar. New York, N. Y., John Wiley and Sons, Inc. (1965).

42. Graves, C. D., Radar Polarization Power-Scattering Matrix. University of Michigan, 2144-45-T, AD 103 803 (1955).

43. Ivey, H. D., and Long, M. W., Polarization Characteristics of Radar Targets. Georgia Institute of Technology, A-158-1, AD 649 58 (1954).

APPENDIX A

COORDINATE AND PHASE MODIFICATIONS FOR UNIFORM ROLL, PITCH, AND YAW RATES

The purpose of this appendix is to develop the appropriate coordinate and phase-term modifications for the case of uniform target motion about the roll, pitch, and yaw (x,y,z,) axes. Uniform yaw will be examined first, followed by a discussion of the required adaptations to include roll and pitch.

Because yaw involves rotation of the target about the z-axis, the change in aspect angle can be included simply by modifying the azimuth (ϕ) coordinate of the aspect point P. If the elapsed time since some reference time t_o is T seconds, and the yaw rate is ω_y rad/sec, the modified azimuth coordinate of P is

$$\phi' = \phi + \omega_y T \qquad \text{(A-1)}$$

where ω_y is taken to be positive in the direction of increasing ϕ.

In addition to the effective change in position of P, the yawing motion also causes a Doppler shift in the frequency of the radar return from each complex C_i. This effect can be included by making an appropriate modification in the phase of the signal contribution from each complex before performing the phasor summation at P. To determine this modification for the complex being considered, it is first necessary to find the component of the linear velocity which is in the direction of P. This can be accomplished by considering Fig. A-1, which is a projection of the coordinate geometry in the $\theta = 90°$ plane. The tangential velocity of the scattering complex at O", relative to the primary origin O, is

$$v_T = \omega_y d. \tag{A-2}$$

The component of this velocity which is in the direction of P is

$$\begin{aligned} v_R &= v_T \cos \zeta \\ &= \omega_y d \cos (\phi - \phi' + \pi/2) \\ &= -\omega_y d \sin (\phi - \phi'). \end{aligned} \tag{A-3}$$

From the well-known Doppler formula

$$\omega' = \omega_o [1 - \frac{\hat{v} \cdot \hat{r}}{c}] , \tag{A-4}$$

where c is the speed of light in free space and $\hat{r}$ is directed from the point of observation to the moving source, it is seen that

$$\omega' = \omega_o [1 + \frac{v_R}{c}]. \tag{A-5}$$

Rearranging in terms of wavelength,

$$\lambda' = \lambda_o [1 + \frac{v_R}{c}]^{-1}. \tag{A-6}$$

Equation (A-6) given the Doppler-shifted wavelength λ' in terms of the unshifted value λ_o and the component of velocity of the complex which is towards P.

The relative unshifted spatial retardation phase is

$$\alpha = -k_o r \tag{A-7}$$

where $k_o = 2\pi/\lambda_o$ and r is the one-way path from O" to P. Similarly, the shifted phase is

$$\alpha' = -kr. \tag{A-8}$$

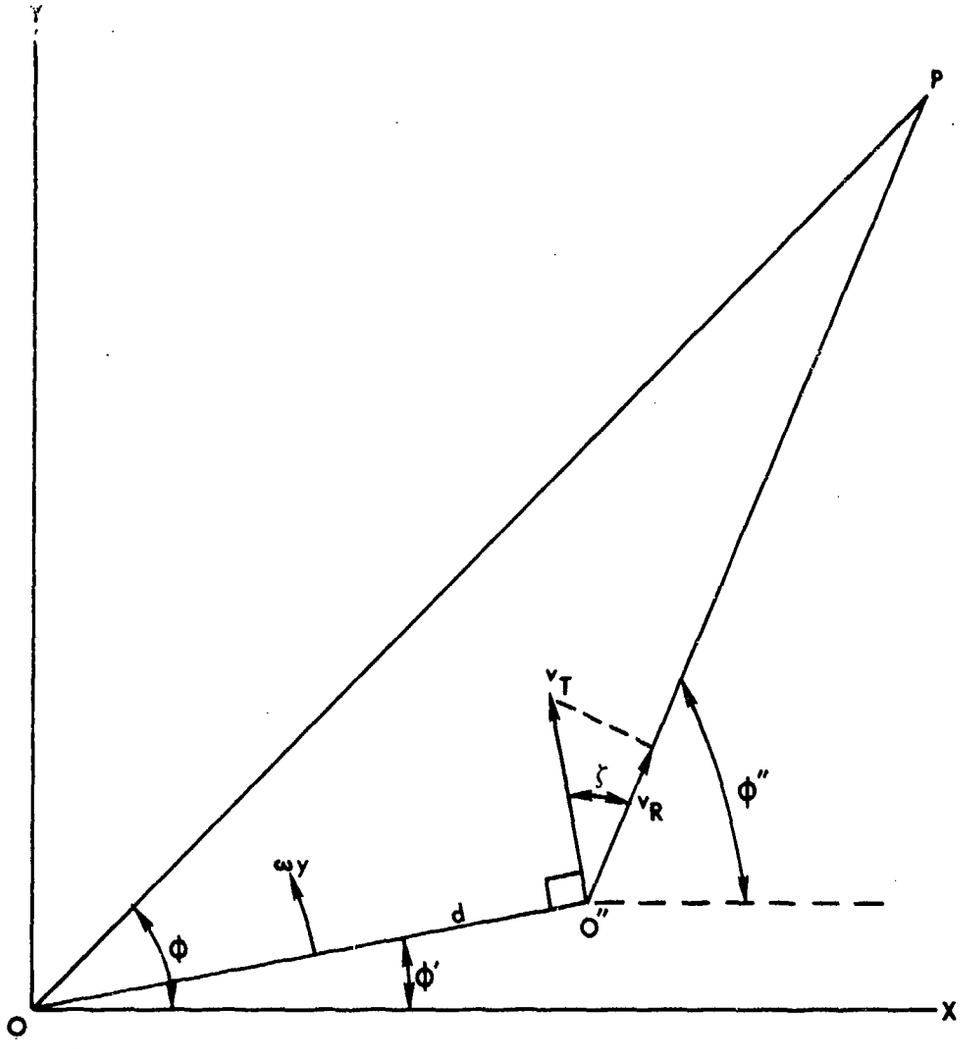

Fig. A-1.--Relative geometry for the case of uniform yaw.

Thus, the apparent change in phase due to the Doppler shift is

$$\begin{aligned}\Delta\alpha &= \alpha - \alpha' \\ &= r(k' - k_o) \\ &= \frac{2\pi r v_R}{\lambda_o c} \quad . \end{aligned} \tag{A-9}$$

This result is used in the model simply by making the substitution

$$\alpha \rightarrow \alpha + \frac{2\pi r}{\lambda_o c}\, \omega_y d \sin(\phi - \phi') \tag{A-10}$$

for the phase contribution of the complex being considered.

The proper coordinate and phase modifications for roll and pitch are more complex because rotation about these axes involves both angular coordinates. However, if a rotation of coordinates is first performed to align the z-axis with the roll or pitch axis, there is once again only an azimuth variation. For roll, the transformations are

$$\begin{aligned}\phi'' &= \arctan(-\tan\phi \sin\phi) \\ \theta'' &= \arccos(\sin\theta \cos\phi). \end{aligned} \tag{A-11}$$

After modifying the new ϕ'' for the roll rate in a manner similar to (A-1), the new coordinates of P are found from the reverse transformations

$$\begin{aligned}\phi' &= \arctan(\tan\theta'' \sin\phi'') \\ \theta' &= \arccos(-\sin\theta'' \cos\phi''). \end{aligned} \tag{A-12}$$

The analogous transformations for pitch are

$$\phi'' = \arctan (1/\tan \theta \cos \phi)$$

$$\theta'' = \arccos (\sin \theta \sin \phi) \qquad \text{(A-14)}$$

and

$$\phi' = \arctan (1/\tan \theta'' \cos \phi'')$$

$$\theta' = \arccos (-\sin \theta'' \sin \phi''). \qquad \text{(A-14)}$$

APPENDIX B

FORTRAN IV IMPLEMENTATIONS

This appendix presents flow diagrams and listings of the more important computer programs and subroutines used in the glint study. Most of the programs were originally prepared for an IBM 7040 computer, and subsequentially converted for use with an IBM System 360, Model 50.

Many different TRAJ, AMPPHI, and OUTPUT subroutines were written for use in making various data runs; the ones listed are illustrative of the general programming techniques employed. The programs which were used to analyze the data and to generate the various machine plots are not included in the listings.

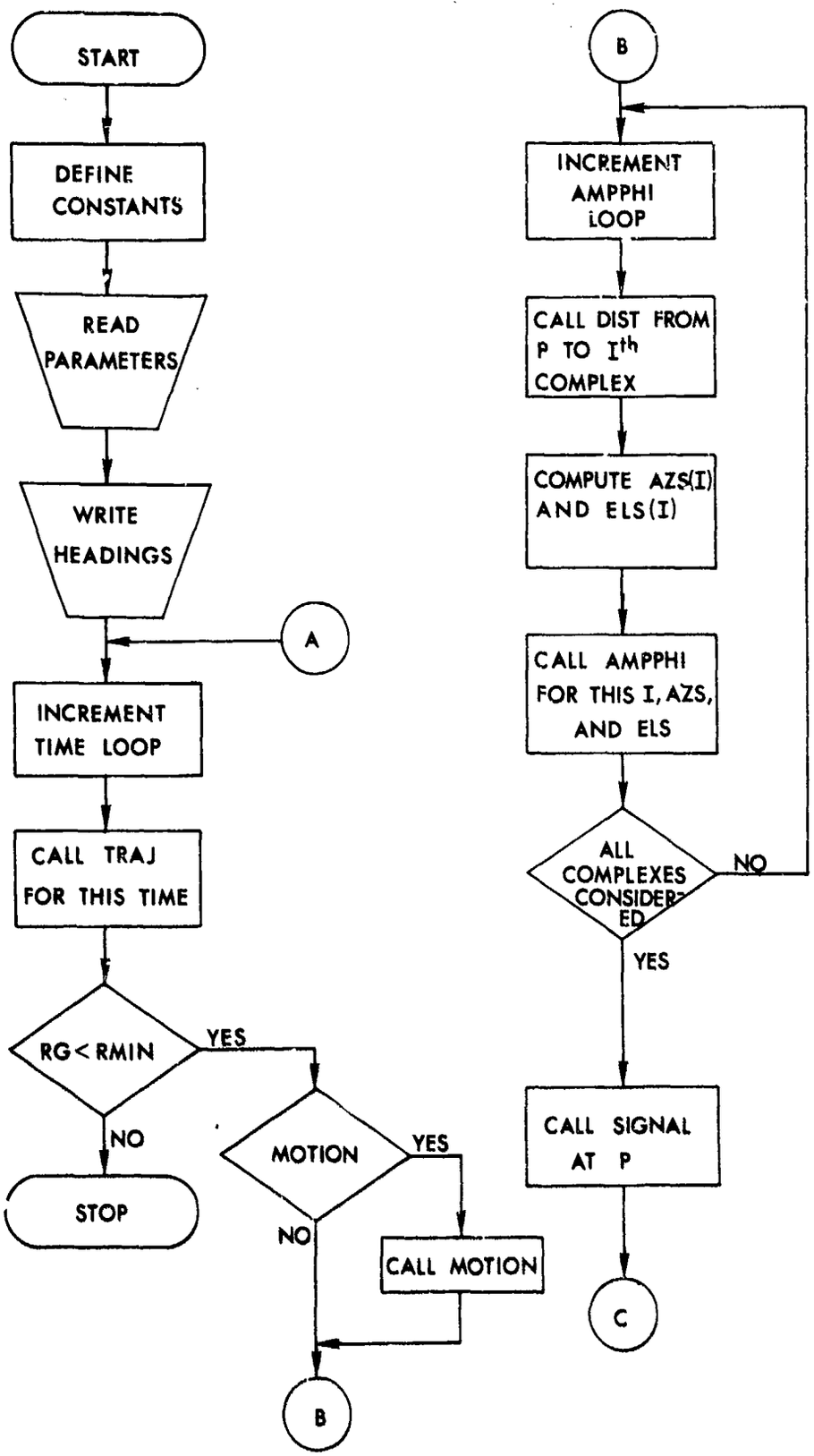

Fig. B-1.--Flowchart for main glint program.

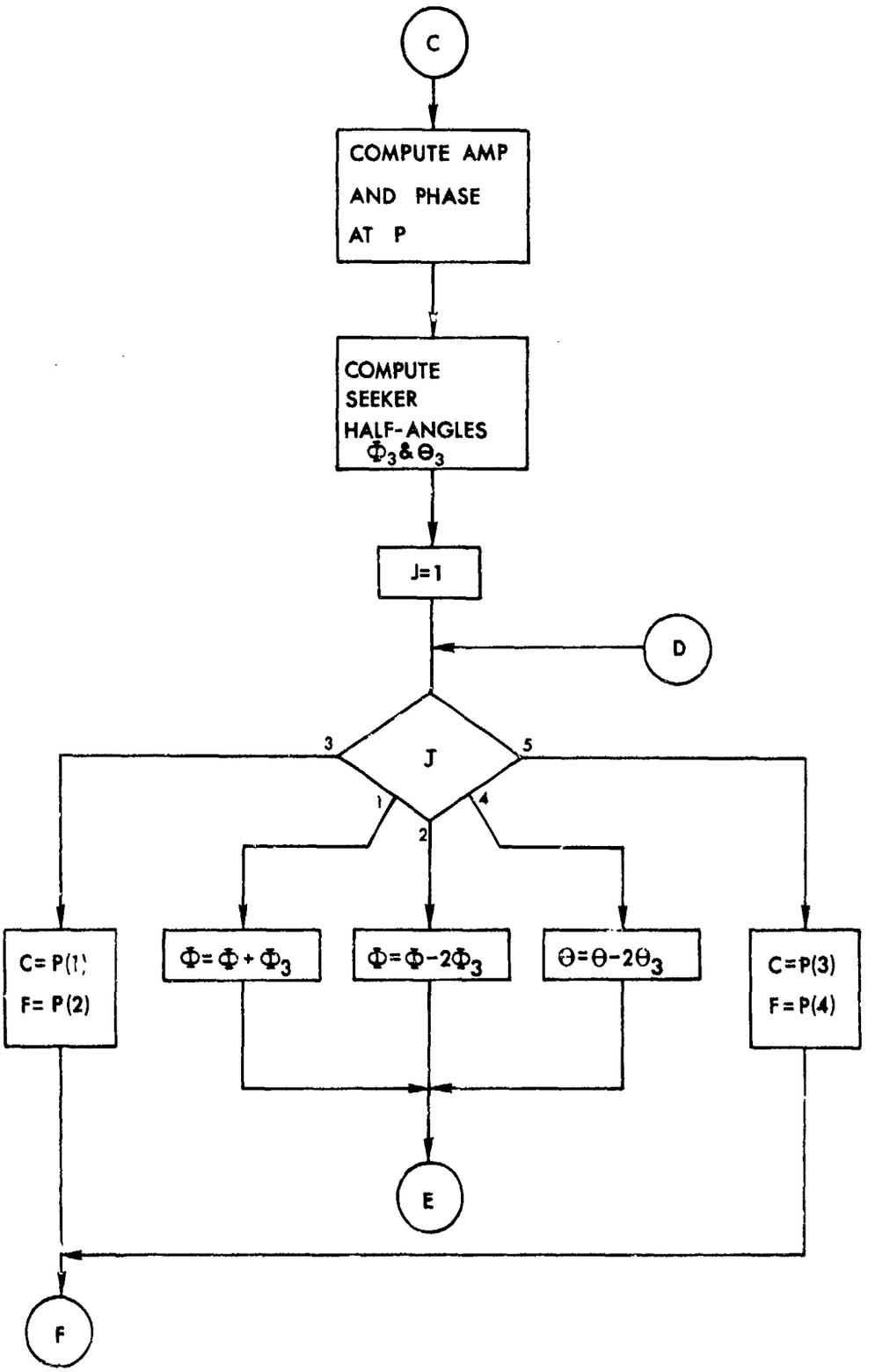

Fig. B-1.--Flowchart for main glint program, continued.

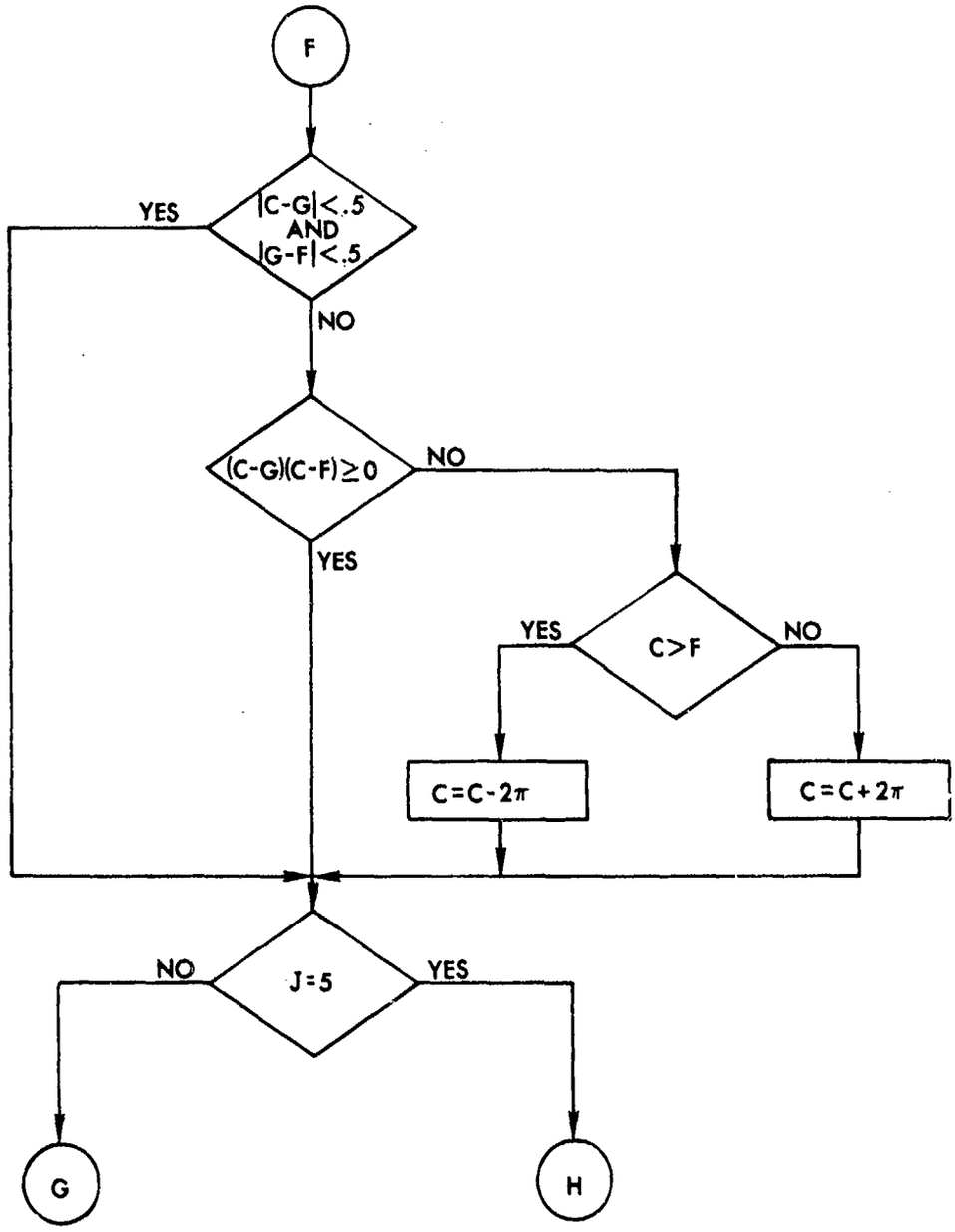

Fig. B-1.--Flowchart for main glint program, continued.

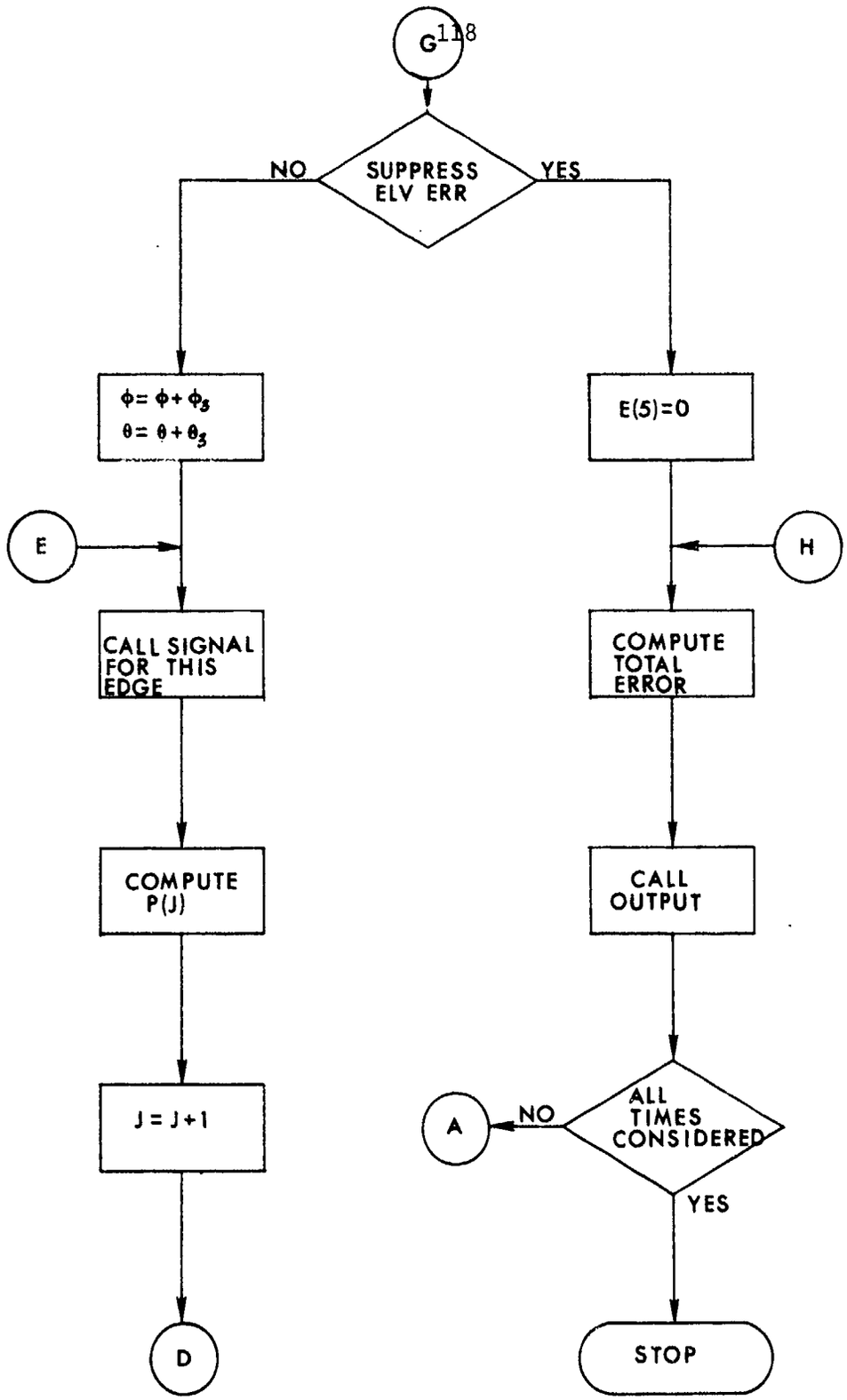

Fig. B-1.--Flowchart for main glint program, continued.

```
C     THIS PROGRAM COMPUTES GLINT ERROR ALONG A
C     PRESCRIBED TRAJECTORY.  PROVISION IS MADE
C     FOR MOTION OF THE TARGET.
C
        IMPLICIT REAL*8(D)
        COMPLEX*16 Z
        REAL LAMBDA
        REAL*8 PTH(100),P(5),E(5)
        COMMON/COM1/AZ(100),EL(100),RD(100),NO(100),
     1  ROLL,PITCH,YAW
        COMMON/COM2/AZM,ELV,RG,AMP(100),PHI(100),AMPL(100)
        COMMON/COM4/N,WAVE,CONV,RM
        COMMON/COM5/AZS(100),ELS(100)
        COMMON/COM6/ICNT,JK
        COMMON/COM7/IDCON,L,LAMBDA,RDIA
        DIMENSION COMMNT(20)
C
        PI=3.141593
        CONV=180./PI
        ICNT=0
C
C     READ WAVELENGTH, TIME INCREMENT, MINIMUM
C     RANGE, APERTURE DIAMETER, ROLL PITCH AND YAW
C     RATES, ELV ERROR SUPPRESS CODE, COORDINATES OF
C     SCATTERING COMPLEXES, AND COMMENT CARD
        READ(5,100)LAMBDA,TINC,RMIN,RDIA,ROLL,
     1  PITCH,YAW,NOELV
        READ(5,101)IDCON,N
        DO 5 NN=1,N
        READ(5,102)I,RD(I),AZ(I),EL(I)
        AZ(I)=AZ(I)/CONV
        EL(I)=EL(I)/CONV
 5      NO(NN)=I
        READ(5,103)(COMMNT(KK),KK=1,20)
C
        WAVE=(2.*PI)/LAMBDA
        DPDIA=WAVE*RDIA
        D2PI=2.*PI
        DCONV=CONV
        CALL TRAJ(L,0.,RG,ELV,AZM,CONV)
        ELV=ELV*CONV
        AZM=AZM*CONV
        WRITE(6,200)IDCON,L
        WRITE(6,COMMNT)
        CALL AMPPHI
        WRITE(6,206)JK,RM
        WRITE(6,201)RG,ELV,AZM
        WRITE(6,202)ROLL,PITCH,YAW
```

Fig. B-2.--Listing of main glint program.

```
      WRITE(6,203)LAMBDA,RDIA
C
C     INCREMENT TIME
      DO 90 K=1,1001
      T=(K-1)*TINC
C
C     CALL FIELD POINT COORDINATES FOR THIS TIME
      CALL TRAJ(L,T,RG,ELV,AZM,CONV)
      IF(RG.LT.RMIN) GO TO 97
      DRG=RG
C
C     MODIFY COORDINATES TO INCLUDE TARGET MOTION, IF
C     REQUIRED
      IF((ROLL+PITCH+YAW).GT.0.)CALL MOTION(T,AZM,
     1 ELV,ROLL,PITCH,YAW)
C
C     BEGIN FINDING AMP AND PHASE DATA FOR COMPLEXES
      DO 15 NN=1,N
      I=NO(NN)
      CALL DIST(AZM,ELV,RG,AZ(I),EL(I),RD(I),PTH(I))
      RDIST=PTH(I)
C
C     COMPUTE AZS AND ELS--THE EQUIVALENT AZM AND ELV
C     IN THE ITH COORDINATE SYSTEM
      X=RG*SIN(ELV)*COS(AZM)
     1     -RD(I)*SIN(EL(I))*COS(AZ(I))
      Y=RG*COS(ELV)-RD(I)*COS(EL(I))
      ELS(I)=ARCOS(Y/RDIST)
      AZS(I)=ARCOS(X/(RDIST*SIN(ELS(I))))
C
C     CALL AMP AND PHASE VALUES FOR ITH COMPLEX
 15   CALL AMPPHI(I,AZS(I),ELS(I),AMP(I),PHI(I))
C
C     COMPUTE TOTAL AMP AND PHASE AT THESE COORDINATES
      CALL SIGNAL(1,K,DX,DY,PTH)
      Z=DCMPLX(DX,DY)
      A=CDABS(Z)
      DG=DSIGN(DARCOS(DX/CDABS(Z)),DY)
C
C     COMPUTE HALF-ANGLES SUBTENDED BY APERTURE
      RAD=RDIA/2.
      EL3=ATAN(RAD/RG)
      AZ3=ATAN(RAD/(RG*SIN(ELV)))
C
C     BEGIN COMPUTATION OF ERROR IN THE TWO TRACKING
C     PLANES
      DO 29 J=1,5
      GO TO (21,22,23,27,30),J
```

Fig. B-2.--Listing of main glint program, continued.

```
 21     AZM=AZM+AZ3
        GO TO 28
 22     AZM=AZM-2.*AZ3
        GO TO 28
 23     DC=P(1)
        DF=P(2)
C
C     CORRECT FOR ANY PHASE CYCLE CHANGE ACROSS APERTURE
 24     IF(DABS(DC-DG).LT..50D0.AND.DABS(DG-DF).LT..50D0)
     1 GO TO 26
        IF((DC-DG)*(DG-DF).GE.0.) GO TO 26
        IF(DC.GT.DF) GO TO 25
        DC=DC+D2PI
        GO TO 26
 25     DC=DC-D2PI
C
C     COMPUTE SINGLE-PLANE ERROR
 26     E(J)=(DRG*(DC-DF))/DPDIA
        IF(J.EQ.5) GO TO 32
        IF(NOELV.EQ.0) GO TO 31
        AZM=AZM+AZ3
        ELV=ELV+EL3
        GO TO 28
 27     ELV=ELV-2.*EL3
 28     CALL SIGNAL(2,K,DX,DY,PTH)
        Z=DCMPLX(DX,DY)
 29     P(J)=DSIGN(DARCOS(DX/CDABS(Z)),DY)
 30     DC=P(3)
        DF=P(4)
        GO TO 24
 31     E(5)=0.
C
C     COMPUTE TOTAL ERROR
 32     ERROR=DCONV*DATAN2(DSQRT(E(3)**2+E(5)**2),DRG)
        G=DG
C
C     TRANSFER RESULTS TO OUTPUT DEVICES(S)
 90     CALL OUTPUT(K,T,E(3),E(5),ERROR,A,G,AMPL)
 97     CONTINUE
C
 100    FORMAT(7F10.0,I1)
 101    FORMAT(2I2)
 102    FORMAT(I2,3F10.0)
 103    FORMAT(20A4)
 200    FORMAT(1H1,34HGLINT ERROR FOR CONFIGURATION NO. ,
     1 I2,/,22H ALONG TRAJECTORY NO. ,I3)
 201    FORMAT(1HO,29HINITIAL SEEKER POSITION--RG= ,
     1 F7.1,2H M,/,26X,4HEL= ,F7.3,4H DEG,/,
```

Fig. B-2.--Listing of main glint program, continued.

```
     2 26X,4HAZ= ,F7.3,4H DEG)
202    FORMAT(1H0,21HTARGET MOTION--ROLL= ,F8.3,
     1 8H RAD/SEC,/,16X,7HPITCH= ,F7.3,8H RAD/SEC,/,
     2 16X,5HYAW= ,F9.3,8H RAD/SEC)
203    FORMAT(1H0,12HWAVELENGTH= ,2PF11.3,3H CM,/,
     1 13H SEEKER DIA= ,F11.3,3H CM//)
206    FORMAT(1H0,'AMPPHI DATA SOURCE NO. ',I3,
     1 ' AT RM = ',F7.1,' M')
       STOP
       END
```

Fig. B-2.--Listing of main glint program, continued.

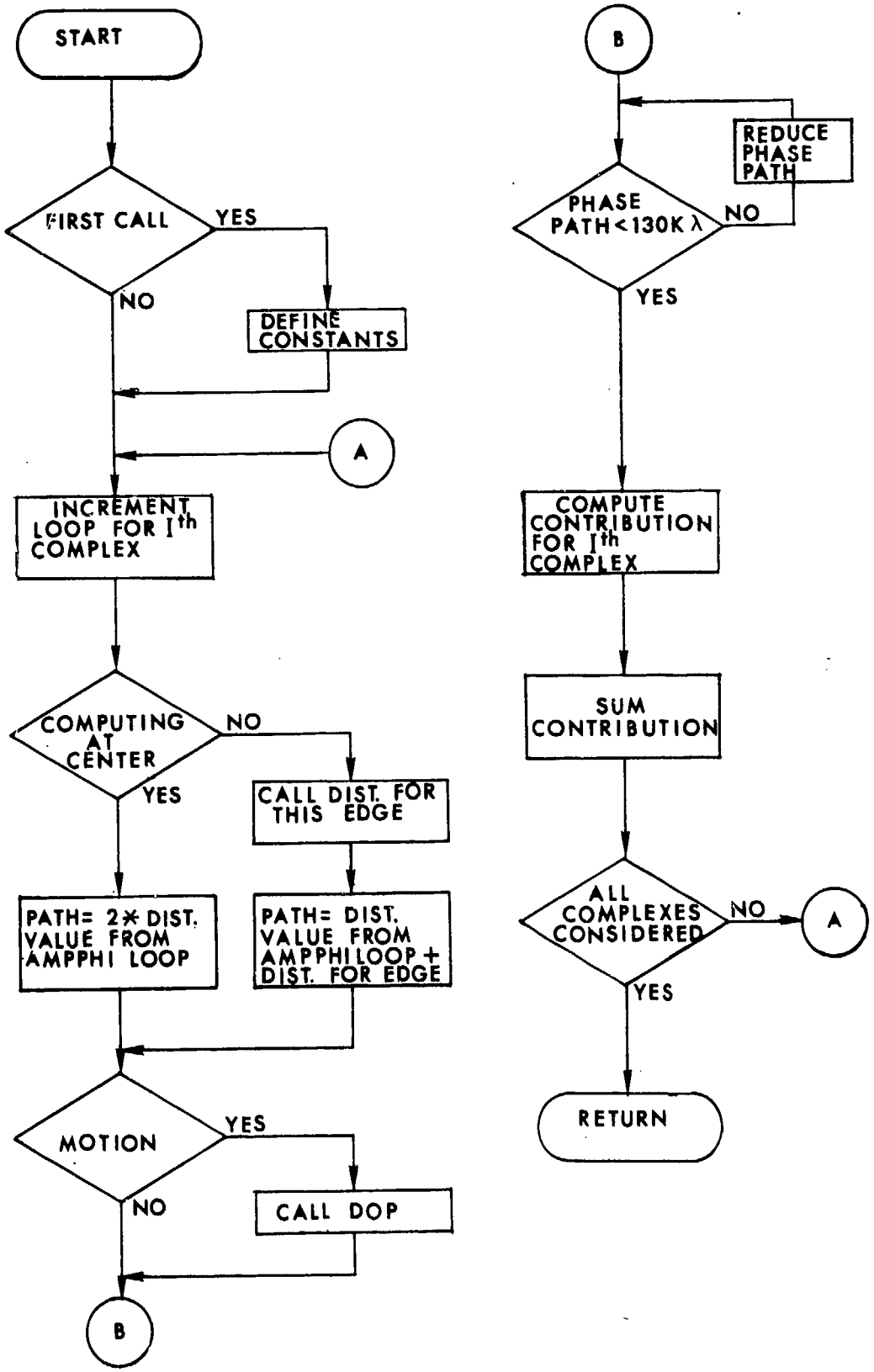

Fig. B-3.--Flowchart of subroutine SIGNAL.

```
      SUBROUTINE SIGNAL(L,K,DX,DY,PTH)
C
C     THIS SUBROUTINE COMPUTES THE TOTAL RECEIVED
C     SIGNAL FROM A GROUP OF SCATTERING COMPLEXES.
C     PROVISION IS MADE FOR DOPPLER DUE TO MOTION
C     OF COMPLEXES.
C
      IMPLICIT REAL*8 (D)
      REAL*8PTH(100)
      COMMON/COM1/AZ(100),EL(100),RD(100),NO(100),
     1 ROLL,PITCH,YAW
      COMMON/COM2/AZM,ELV,RG,AMP(100),PHI(100),AMPL(100)
      COMMON/COM3/DCONV,DWAVE,DPTH,DPHI,I
      COMMON/COM4/N,WAVE,CONV,RM
C
      IF((L+K).GT.2) GO TO 70
      DREDU=3.6E7/(WAVE*CONV)
      DPMAX=1.3D0*DREDU
      DCONV=CONV
      DWAVE=WAVE
      DRM=RM
C
C     BEGIN COMPUTATION OF TOTAL RECEIVED SIGNAL
 70   DX=0.
      DY=0.
      DO 80 NN=1,N
      I=NO(NN)
C
C     FIND PATH OF PROPAGATION ASSOCIATED WITH COMPLEX
      IF(L.EQ.1) GO TO 72
      CALL DIST(AZM,ELV,RG,AZ(I),EL(I),RD(I),DPTH)
      GO TO 73
 72   DPTH=PTH(I)
C
C     MODIFY PHASE TO INCLUDE DOPPLER, IF REQUIRED
 73   DPHI=PHI(I)
      IF((ROLL+PITCH+YAW).GT.0.) CALL DOP
      DPATH=PTH(I)+DPTH-2.D0*DRM
      PATH1=DPATH
C
C     REDUCE PATH TO LESS THAN 130,000 LAMBDA
 77   IF(DPATH.LT.DPMAX) GO TO 78
      DPATH=DPATH-DREDU
      GO TO 77
C
C     FIND RECEIVED SIGNAL
 78   E=AMP(I)/20.
      DAMPL=(10.**E)/PATH1
```

Fig. B-4.--Listing of subroutine SIGNAL.

```
      AMPL(NN)=DAMPL
      DPHSE=(DPHI/DCONV)-(DWAVE*DPATH)
      DX1=DAMPL*DCOS(DPHSE)
      DY1=DAMPL*DSIN(DPHSE)
      DX=DX+DX1
80    DY=DY+DY1
      RETURN
      END
```

Fig. B-4.--Listing of subroutine SIGNAL, continued.

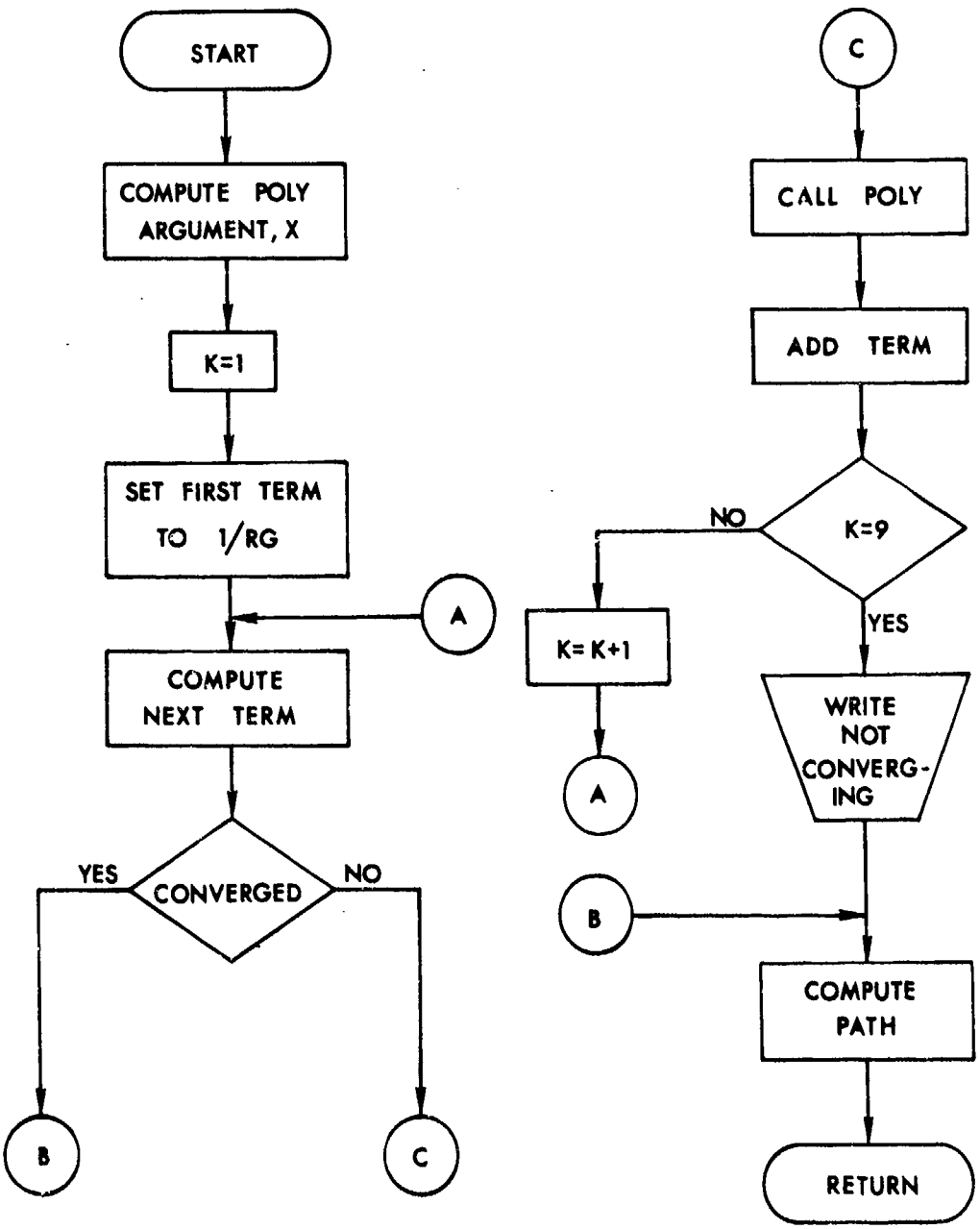

Fig. B-5.--Flowchart of subroutine DIST.

```
      SUBROUTINE DIST(AZM,ELV,RG,AZI,ELI,RDI,DPATH)
C
C     THIS SUBROUTINE COMPUTES THE 1-WAY PATH BETWEEN
C     THE FIELD POINT WITH SPHERICAL COORDINATES
C     (RG,ELV,AZM) AND THE POINT WITH COORDINATES
C     (RDI,ELI,AZI).
C
        IMPLICIT REAL*8 (D)
        DAZ=AZM
        DEL=ELV
        DRG=RG
        DAI=AZI
        DEI=ELI
        DDI=RDI
C
        DX=DCOS(DEL)*DCOS(DEI)+DSIN(DEL)*DSIN(DEI)
     1    *DCOS(DAZ-DAI)
C
        DS=1.D0/DRG
        DO 50 K=1,9
        DR=DDI**K/DRG**(K+1)
        IF(DR.LT.1.D-20) GO TO 10
        CALL POLY(K,DX,DP)
        DS=DS+DR*DP
 50     CONTINUE
        WRITE(6,600)
 600    FORMAT(1H0,'SERIES NOT CONVERGING')
 10     DPATH=1.D0/DS
        RETURN
        END
```

Fig. B-6.--Listing of subroutine DIST.

```
      SUBROUTINE POLY(L,DX,DP)
C
C     THIS SUBROUTINE COMPUTES THE LEGENDRE POLYNOMIAL
C     OF ORDER L AND ARGUMENT DX.
C
      IMPLICIT REAL*8 (D)
      GO TO (1,2,3,4,5,6,7,8,9),L
 1    DP=DX
      GO TO 10
 2    DP=5.D-1*(3.D0*DX**2-1.D0)
      GO TO 10
 3    DP=5.D-1*(5.D0*DX**3-3.D0*DX)
      GO TO 10
 4    DP=1.25D-1*(3.5D1*DX**4-3.D1*DX**2+3.D0)
      GO TO 10
 5    DP=1.25D-1*(6.3D1*DX**5-7.D1*DX**3+1.5D1*DX)
      GO TO 10
 6    DP=6.25D-2*(2.31D2*DX**6-3.15D2*DX**4
     1    +1.05D2*DX**2-5.D0)
      GO TO 10
 7    DP=6.25D-2*(4.29D2*DX**7-6.93D2*DX**5
     1    +3.15D2*DX**3-3.5D1*DX)
      GO TO 10
 8    DP=7.8125D-3*(6.435D3*DX**8-1.2012D4*DX**6
     1    +6.93D3*DX**4-1.26D3*DX**2+3.5D1)
      GO TO 10
 9    DP=7.8125D-3*(1.2155D4*DX**9-2.574D4*DX**7
     1    +1.8018D4*DX**5-4.62D3*DX**3+3.15D2*DX)
 10   CONTINUE
      RETURN
      END
```

Fig. B-7.--Listing of subroutine POLY.

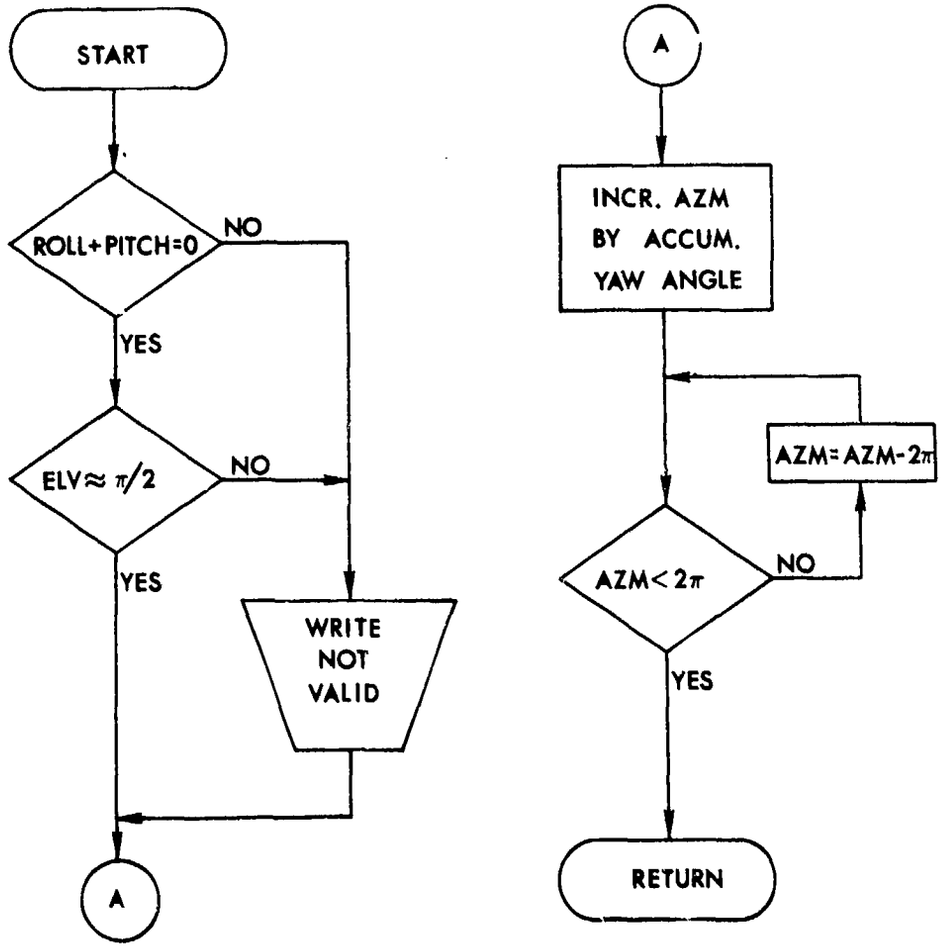

Fig. B-8.--Flowchart of subroutine MOTION.

```
      SUBROUTINE MOTION(T,AZM,ELV,ROLL,PITCH,YAW)
C
C     THIS SUBROUTINE CHANGES THE ASPECT ANGLE TO
C     ACCOUNT FOR TARGET MOTION.  IT IS VALID ONLY FOR
C     ROTATION ABOUT THE Z-AXIS (YAW) AND IS RESTRICTED
C     TO ASPECT ANGLES IN THE ELV = 90DEG PLANE.
C
      IF((ROLL+PITCH).NE.0.)WRITE(6,200)
      IF(ELV.GT.1.576.OR.ELV.LT.1.565)WRITE(6,200)
  200 FORMAT(1H0,28HMOTION CALLED WHEN NOT VALID)
C
      AZM=AZM+YAW*T
      DO 5 J=1,20
      IF(AZM.LT.6.2831853) GO TO 6
      AZM=AZM-6.2831853
    5 CONTINUE
    6 CONTINUE
      RETURN
      END
```

Fig. B-9.--Listing of subroutine MOTION.

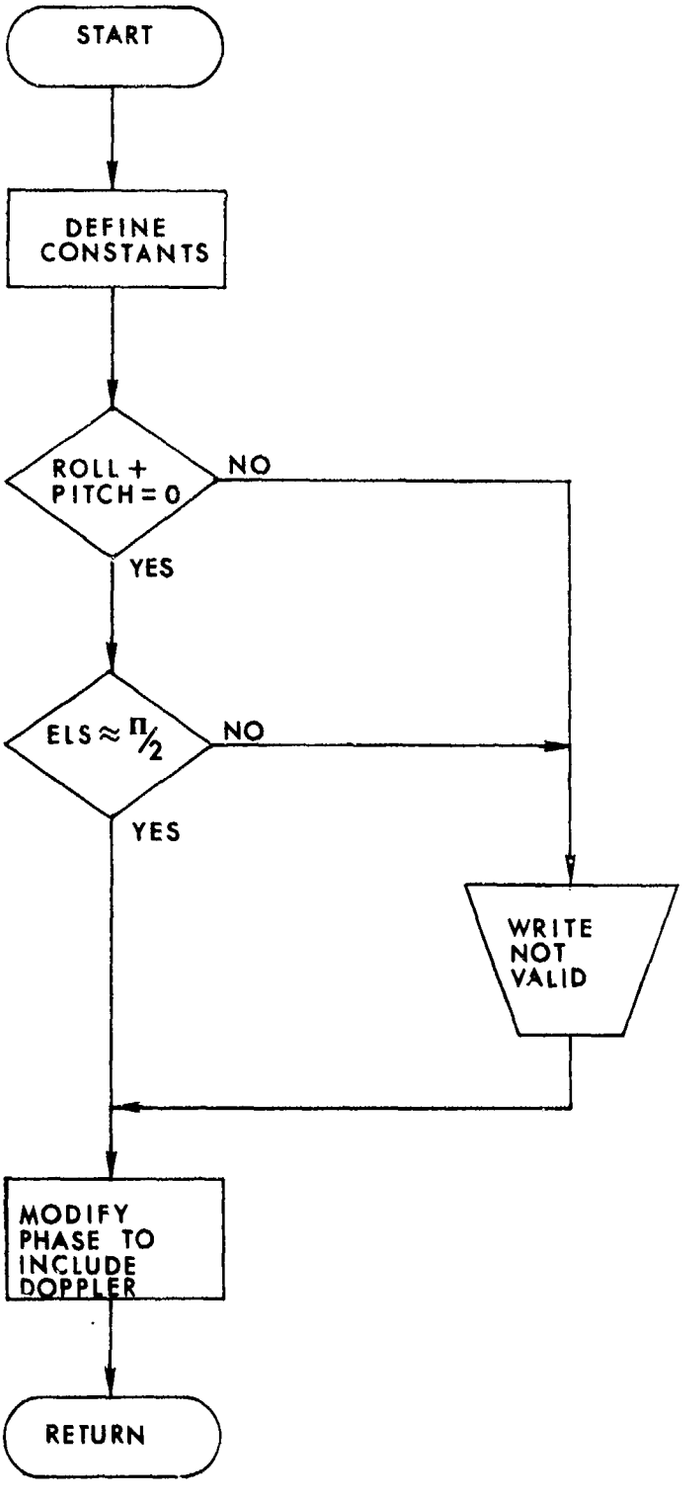

Fig. B-10.--Flowchart of subroutine DOP.

```
      SUBROUTINE DOP
C
C     THIS SUBROUTINE INCLUDES DOPPLER SHIFTS INTO THE
C     PHASE FROM A GIVEN COMPLEX.  IT IS VALID ONLY
C     FOR A ROTATION ABOUT THE Z-AXIS (YAW) AND IS
C     RESTRICTED TO ASPECT ANGLES IN THE ELV = 90DEG
C     PLANE.
C
      IMPLICIT REAL*8(D)
      COMMON/COM1/AZ(100),EL(100),RD(100),NO(100),
     1 ROLL,PITCH,YAW
      COMMON/COM3/DCONV,DWAVE,DPATH,DPHI,I
      COMMON/COM5/AZS(100),ELS(100)
C
      IF((ROLL+PITCH).NE.0.)WRITE(6,200)
      IF(ELS(I).GT.1.575.OR.ELS(I).LT.1.565)WRITE(6,200)
  200 FORMAT(1HO,'DOP CALLED WHERE NOT VALID')
C
      DYAW=YAW
      DI=RD(I)
      DAZI=AZ(I)
      DAZS=AZS(I)
      DPHI=DPHI-((DPATH*DYAW*DCONV*DWAVE*DI
     1     *DSIN(DAZI-DAZS))/3.D8)
      RETURN
      END
```

Fig. B-11.--Listing of subroutine DOP.

```
      SUBROUTINE OUTPUT(K,T,EAZ,EEL,ER,A,P,AMPL)
C
C     THIS SUBROUTINE WRITES THE PROGRAM RESULTS INTO
C     MAGNETIC DISK STORAGE.
C
      REAL LAMBDA
      COMMON/COM1/DUM(400),ROLL,PITCH,YAW
      COMMON/COM4/N,WAVE,CONV,RM
      COMMON/COM6/ICNT,JK
      COMMON/COM7/IDCON,L,LAMBDA,DIA
      DIMENSION AMPL(100)
      IF(K.GT.1) GO TO 10
C
C     WRITE PARAMETERS
      NUMBER=1
      WRITE(8)NUMBER,IDCON,L,JK,RM,LAMBDA,DIA,ROLL,
     1 PITCH,YAW
      WRITE(6,205)
C
C     WRITE A LINE OF RESULTS
 10   WRITE(8)T,EAZ,EEL,P,A,(AMPL(J),J=1,4)
      WRITE(6,204)T,EAZ,EEL,ER,A,P,(AMPL(J),J=1,4)
      IF(K.EQ.1001) END FILE 8
 204  FORMAT(1H ,F9.3,2F10.4,F9.3,7E13.4)
 205  FORMAT(1H ,4X,4HTIME,4X,3HEAZ,7X,3HEEL,3X,
     1 'TOT ANG ERR',5X,'AMP',10X,'PHASE')
      RETURN
      END
```

Fig. B-12.--Listing of typical subroutine OUTPUT.

```
      SUBROUTINE TRAJ(L,T,RG,ELV,AZM,CONV)
C
C     TRAJECTORY NO.11
C
C     THIS SUBROUTINE GENERATES A SET OF FIELD
C     COORDINATES, AS A FUNCTION OF TIME, WHICH DESCRIBE
C     A DESIRED TRAJECTORY
C
      L=11
      RG=4650.-3.75*T
      AZM=45./CONV+ATAN2(150.*SIN(6.2832*(RG-900.)/
     1 3750.),RG)
      ELV=90./CONV+ATAN2(50.0*SIN(6.2832*(RG-900.)/
     1 3750.),RG)
      RETURN
      END
```

Fig. B-13.--Listing of typical subroutine TRAJ.

```
      SUBROUTINE AMPPHI(I,AZS,ELS,AMP,PHI)
C
C     AMPPHI DATA SOURCE NO. 99
C
C     THIS SUBROUTINE SYNTHESIZES AMP AND PHASE VALUES
C     FOR COMPLEXES 20, 21, 22, AND 23
C
      COMMON/COM4/N, WAVE,CONV,RM
      COMMON/COM6/ICNT,JK
      IF(ICNT.NE.0) GO TO 89
      JK=99
      RM=0.
      ICNT=1
      PI=180./CONV
      GO TO 88
 89   CALL ROUND(AZS,ELS,AZ,EL)
      K=I-19
      GO TO (5,10,15,15),K
 5    A=(SIN(EL)*SIN(AZ)*COS(360.*AZ))**2
      PHI=180.*COS(720.*AZ)
      GO TO 20
 10   A=(.9*SIN(EL)*SIN(AZ)*COS(720.*AZ))**2
      PHI=180.*COS(360.*AZ)
      GO TO 20
 15   IF(ABS(AZ).LE.PI/2.)A=(SIN(EL)*COS(AZ)
     1 *COS(360.*AZ))**2
      IF(ABS(AZ).GT.PI/2.) A=0.
      PHI=180.*COS(720.*AZ)
 20   IF(A.EQ.0.) A=1.E-50
      AMP=10.*ALOG10(A)
 88   CONTINUE
      RETURN
      END
```

Fig. B-14--Listing of typical subroutine AMPPHI.

```
      SUBROUTINE ROUND(A,E,AZ,EL)
C
C     THIS SUBROUTINE ROUNDS, TO THE NEAREST 'R', THE
C     VARIABLES A AND E.  THE RESULTS ARE AZ AND EL.
C
C     THE DESIRED ROUNDING FACTOR, IN RADIANS, IS
C     PUNCHED INTO THE NEXT CARD
      R=.01745
      IF(R.EQ.0.) GO TO 90
      E=-1.-AINT(ALOG10(R))
      FACT=10.**E
      RND=R*FACT
      AZ=ABS(A)*FACT
      AZ=RND*AINT((AZ/RND)+.5)
      AZ=SIGN((AZ/FACT),A)
      EL=ABS(E)*FACT
      EL=RND*AINT((EL/RND)+.5)
      EL=SIGN((EL/FACT),E)
      GO TO 91
 90   AZ=A
      EL=E
 91   CONTINUE
      RETURN
      END
```

Fig. B-15.--Listing of subroutine ROUND.

Unclassified
Security Classification

DOCUMENT CONTROL DATA - R&D

(Security classification of title, body of abstract and indexing annotation must be entered when the overall report is classified)

1. ORIGINATING ACTIVITY *(Corporate author)*
Engineering Experiment Station
Auburn University
Auburn, Alabama 36830

2a. REPORT SECURITY CLASSIFICATION
Unclassified

2b. GROUP

3. REPORT TITLE
Final Report
Volume II: The Determination of Glint for a Complex Radar Target

4. DESCRIPTIVE NOTES *(Type of report and inclusive dates)*
Final Report

5. AUTHOR(S) *(Last name, first name, initial)*
Sims, Robert J. and Graf, Edward R.

6. REPORT DATE	7a. TOTAL NO. OF PAGES	7b. NO. OF REFS
24 July 1969	145	43

8a. CONTRACT OR GRANT NO.	9a. ORIGINATOR'S REPORT NUMBER(S)
DA-01-021-AMC 14525(Z) b. Project,Task,Work Unit Nos. c. DOD ELEMENT d. DOD SUBELEMENT	9b. OTHER REPORT NO(S) *(Any other numbers that may be assigned this report)*

10. AVAILABILITY/LIMITATION NOTICES

11. SUPPLEMENTARY NOTES	12. SPONSORING MILITARY ACTIVITY
	Future Missile Systems Div. and U.S. Army Missile Command.

13. ABSTRACT

The unclassified glint literature is described and discussed, with particular emphasis on applications of diversity. A computer-implemented model based upon the concept of coherent summation of contributions from independent scattering complexes is developed. The application of the model is illustrated using synthesized scattering patterns. Data processing techniques for frequency and space diversity are investigated with the model. The results indicate a significant reduction in RMS glint error is possible by the appropriate utilization of diversity techniques.

DD FORM 1 JAN 64 1473

Unclassified
Security Classification

Unclassified

Security Classification

14. KEY WORDS	LINK A		LINK B		LINK C	
	ROLE	WT	ROLE	WT	ROLE	WT
Glint, Glint Error, Computer Glint Model, Diversity Effects on Glint						

INSTRUCTIONS

1. ORIGINATING ACTIVITY: Enter the name and address of the contractor, subcontractor, grantee, Department of Defense activity or other organization *(corporate author)* issuing the report.

2a. REPORT SECURITY CLASSIFICATION: Enter the overall security classification of the report. Indicate whether "Restricted Data" is included. Marking is to be in accordance with appropriate security regulations.

2b. GROUP: Automatic downgrading is specified in DoD Directive 5200.10 and Armed Forces Industrial Manual. Enter the group number. Also, when applicable, show that optional markings have been used for Group 3 and Group 4 as authorized.

3. REPORT TITLE: Enter the complete report title in all capital letters. Titles in all cases should be unclassified. If a meaningful title cannot be selected without classification, show title classification in all capitals in parenthesis immediately following the title.

4. DESCRIPTIVE NOTES: If appropriate, enter the type of report, e.g., interim, progress, summary, annual, or final. Give the inclusive dates when a specific reporting period is covered.

5. AUTHOR(S): Enter the name(s) of author(s) as shown on or in the report. Enter last name, first name, middle initial. If military, show rank and branch of service. The name of the principal author is an absolute minimum requirement.

6. REPORT DATE: Enter the date of the report as day, month, year, or month, year. If more than one date appears on the report, use date of publication.

7a. TOTAL NUMBER OF PAGES: The total page count should follow normal pagination procedures, i.e., enter the number of pages containing information.

7b. NUMBER OF REFERENCES: Enter the total number of references cited in the report.

8a. CONTRACT OR GRANT NUMBER: If appropriate, enter the applicable number of the contract or grant under which the report was written.

8b, 8c, & 8d. PROJECT NUMBER: Enter the appropriate military department identification, such as project number, subproject number, system numbers, task number, etc.

9a. ORIGINATOR'S REPORT NUMBER(S): Enter the official report number by which the document will be identified and controlled by the originating activity. This number must be unique to this report.

9b. OTHER REPORT NUMBER(S): If the report has been assigned any other report numbers *(either by the originator or by the sponsor)*, also enter this number(s).

10. AVAILABILITY/LIMITATION NOTICES: Enter any limitations on further dissemination of the report, other than those imposed by security classification, using standard statements such as:

(1) "Qualified requesters may obtain copies of this report from DDC."

(2) "Foreign announcement and dissemination of this report by DDC is not authorized."

(3) "U. S. Government agencies may obtain copies of this report directly from DDC. Other qualified DDC users shall request through

_____."

(4) "U. S. military agencies may obtain copies of this report directly from DDC. Other qualified users shall request through

_____."

(5) "All distribution of this report is controlled. Qualified DDC users shall request through

_____."

If the report has been furnished to the Office of Technical Services, Department of Commerce, for sale to the public, indicate this fact and enter the price, if known.

11. SUPPLEMENTARY NOTES: Use for additional explanatory notes.

12. SPONSORING MILITARY ACTIVITY: Enter the name of the departmental project office or laboratory sponsoring *(paying for)* the research and development. Include address.

13. ABSTRACT: Enter an abstract giving a brief and factual summary of the document indicative of the report, even though it may also appear elsewhere in the body of the technical report. If additional space is required, a continuation sheet shall be attached.

It is highly desirable that the abstract of classified reports be unclassified. Each paragraph of the abstract shall end with an indication of the military security classification of the information in the paragraph, represented as *(TS), (S), (C), or (U).*

There is no limitation on the length of the abstract. However, the suggested length is from 150 to 225 words.

14. KEY WORDS: Key words are technically meaningful terms or short phrases that characterize a report and may be used as index entries for cataloging the report. Key words must be selected so that no security classification is required. Identifiers, such as equipment model designation, trade name, military project code name, geographic location, may be used as key words but will be followed by an indication of technical context. The assignment of links, rules, and weights is optional.

Unclassified

Security Classification